TARGETED CHEMOTHERAPY: TRASTUZUMAB TAILORED DOCETAXEL LOADED PLGA NANOPARTICLES FOR HER2 POSITIVE BREAST CANCER

A Thesis Submitted to the College of Graduate Studies and Research

in Partial Fulfillment of the Requirements for the

Degree of Master of Science

in the College of Pharmacy and Nutrition, University of Saskatchewan

Saskatoon, Saskatchewan, Canada

By

Sams Mohammad Anowar Sadat

PERMISSION TO USE

In presenting this thesis in partial fulfillment of the requirements for a postgraduate degree from the University of Saskatchewan, I agree that the Libraries of this University may make it freely available for inspection. I further agree that permission for copying this thesis in any manner, in whole or in part, for scholarly purposes may be granted by the professor who supervised my thesis work or, in their absence, by the Head of the Department or the Dean of the College in which my thesis work was done. It is understood that any copying, publication or use of this thesis or parts thereof for financial gain shall not be allowed without my written permission. It is also understood that due recognition shall be given to me and to the University of Saskatchewan in any scholarly use which may be made of any material in my thesis. Requests for permission to copy or make any other use of material in this thesis in whole or in part should be addressed to:

Dean of the College of Pharmacy & Nutrition

University of Saskatchewan

Saskatoon, Saskatchewan, Canada

ABSTRACT

This study was designed to explore the rationale of using trastuzumab (TmAb) tailored docetaxel (Doc) loaded poly-D, L-lactide-co-glycolide (PLGA) nanoparticles (NPs) to target the human epidermal receptor-2 (HER2) receptors of breast cancer cells. Utilizing emulsification solvent evaporation technique, pre-activated drug loaded NPs were prepared by embedding a homo bi-functional spacer, bis(sulfosuccinimidyl) suberate (BS3) non-covalently onto the NP surface. Freeze-dried pre-activated NPs were then decorated with TmAb followed by one step covalent attachment method. Prepared NPs were characterized for size, surface charge, polydispersity index (PDI), drug loading, drug entrapment efficiency, and antibody (Ab) quantification. All the results after physicochemical characterization were found in a desired range. The covalent attachment between TmAb and BS3 embedded NPs was confirmed by both Fourier transform infrared (FTIR) spectroscopy and Sodium Dodecyl Sulfate-Polyacrylamide Gel Electrophoresis (SDS-PAGE). Quantitative assay was performed to measure the amount of TmAb attached per mg of NPs.

In vitro cell uptake studies were evaluated for fluorescent coumarin-6 (Coum-6) dye instead of drug loaded into the PLGA NPs with flow cytometry and confocal microscopy. Higher cellular uptake was resulted for Ab decorated NPs in both cell types which support the potential use of this formulation strategy as a targeted chemotherapeutic drug delivery system against HER2 positive breast cancer. Cell uptake of Coum-6 loaded NPs of different formulations was also observed after preincubation of both cell lines to investigate the targeting efficiency

of the TmAb. Preincubation of HER2 overexpressed SKBR-3 cells with TmAb demonstrated a significant reduction in cellular uptake of Coum-6 loaded TmAb modified NPs.

The level of HER2 expression was assessed for the targeted NPs comparing other NP formulations, free Doc, filtered TmAb, and Herceptin® by flow cytometry, Western blot, and fluorescence microscopy. Relative HER2 expression levels were observed for all treatment groups, however HER2 expression was lower after treating the cells with TmAb modified Doc loaded NPs.

To explore the possible reasons of reduced HER2 expression and chemotherapeutic responses, cell viability and apoptosis study were considered after treating both cell lines with the formulations. Apoptosis studies revealed the chemotherapeutic responses for different formulations to the HER2 overexpressed and moderate expressed cell lines.

ACKNOWLEDGEMENTS

At first, I would like to acknowledge the close guidance and all the supports of my supervisor Dr. Azita Haddadi. I would also like to thank the members of my advisory committee, Dr. Adil Nazarali and Dr. Ed Krol. I thank Dr. Nazarali for providing me the help for improving my writing. I also thank all of my colleagues; Sheikh Tasnim Jahan, Pedram Rafiei, Mehran Yarahmadi for their kind support whenever needed. I also acknowledge the help for using fluorescence microscope that I got from Dennis Okello who is doing his MSc in Dr. Nazarali's lab. Finally, I would like to thank my friend, Sayem Miah who helped me to do the Western blot studies and confocal studies. Now, Sayem is doing his PhD at Biochemistry under the supervision of Dr. K. Erique Lukong. I would also like to acknowledge the help from Dorota Rogowski (Technician, Core Equipment Facility) and Deborah Michel (Research Technician) whenever needed.

DEDICATION

This thesis is dedicated to all my friends and family. In particular, I would like to dedicate this thesis to my parents; Mohammad Abdus Salam and Salma Akter, my wife; Sheikh Tasnim Jahan and my only beloved daughter; Alina Zafreen whose constant supports and love have been my inspiration.

TABLE OF CONTENTS

LIST OF TABLES

LIST OF FIGURES

LIST OF ABBREVIATIONS

Ab	Antibody
ADCC	Antibody dependent cell mediated or cellular cytotoxicity
BCA	Bicinchoninic acid
BS3	Bis-sulfosuccinimidyl suberate
CLSM	Confocal laser scanning microscopy
Doc	Docetaxel
ECD	Extracellular domain
ECM	Extracellular matrix
EE	Entrapment efficiency
EGF	Human epidermal growth factor
EPR	Enhanced permeability and retention
FACS	Fluorescence activated cell sorting
Fcγ	Fc-gamma
FDA	Food and Drug Administration
HER	Human epidermal growth factor receptor
mAb	Monoclonal antibody
MDR	Multiple drug resistance
MFI	Mean Fluorescent Intensity
NHS	N-hydroxy succinimide
NK	Natural killer
NP	Nanoparticle
PBS	Phosphate buffer solution

PDI	Poly dispersity index
PLGA	Poly(d-lactic co-glycolic acid)
PVA	Polyvinyl alcohol
SD	Standard deviation
SDS-PAGE	Sodium Dodecyl Sulfate-Polyacrylamide Gel Electrophoresis
TAA	Tumor associated antigens
Tg	Glass transition temperature
TmAb	Trastuzumab
VEGF	Vascular endothelial growth factor
ZP	Zeta potential

1. INTRODUCTION

Cancer remains one of the most ominous diseases that is complex and difficult to treat. Conventional chemotherapies have been widely used to treat cancerous diseases along with other therapies although they are limited due to unavoidable side-effects (1). In recent years, chemotherapeutic drug loaded biodegradable nanoparticles (NPs) have been found with substantial potential to offer some model solution for the main limitations of conventional chemotherapies such as non-specificity, multiple drug resistances. Nevertheless, the reduced localization and insufficient selectivity of drug loaded NPs for desired tumor cells were reported with inadequate efficacies for effective chemotherapeutic responses. To overcome the limitations, targeted chemotherapy has been well accepted concept to design an effective targeted drug delivery system which can carry the chemotherapeutic agent to desired tumor cells without affecting normal healthy cells.

Overexpression of certain proteins called tumor antigens often takes place for some cancers' progression. HER2 is one of those tumor antigens which have been reported with overexpression in 25-30% of all breast cancer types in women (2). In addition, the overexpression of HER2 is a key pathological biomarker to diagnose early stage breast cancer. Targeting such tumor antigens with a suitable ligand has been reported most often in the literature for the development of ideal targeted drug delivery systems for HER2 positive breast cancer.

FDA approved humanized mAb; Trastuzumab (Herceptin®) (TmAb) is clinically recommended option for treating the HER2 overexpressed breast cancer. In some cases, enhanced synergistic clinical effects of TmAb have been reported while using with the first-line chemotherapy for metastatic breast cancer (3). Hence, the arrangement for combination of TmAb and chemotherapeutic agents utilizing nano-drug delivery system for treating HER2 positive breast cancer has been proposed as reasonable means of targeted chemotherapy. To achieve this goal, docetaxel (Doc) has become a most common chemotherapeutic drug of choice for breast cancer due to some benefits over the other taxans members (4). In addition, biodegradable US FDA approved PLGA NPs have been emerged as an effective drug delivery system for use in humans (5). The purpose of using polymeric NPs for designing of targeted chemotherapy have been well reported for three major reasons namely; a) the large surface area of NPs for functionalization convenience, b) controlled therapeutic efficacy, and c) the ease capacities to load most anti-cancer drugs (6). However, practical tailoring of receptor specific ligand to the surface of drug loaded PLGA NPs has not been established with perfect progression.

To achieve the predicted ligand-receptor binding for NPs depot into the tumor cell, surface functionalization of NPs with ligand is a required condition. To execute this pre-requisite condition, several processes have been adduced to conjugate the ligand to the NPs with or without using cross linking agents (7). There are mainly two types of cross linking agents such as homo-bi-functional and hetero-bi-functional agents that can be used depending on the reactive group at the end of the spacer arm that is required. A homo-bi-functional spacer, bis-sulfosuccinimidyl suberate (BS3) has been used to develop a cross link between Ab and NPs by

forming covalent amide bond. Utilizing emulsification and solvent evaporation technique, BS3 was pre-embedded onto the surface of NPs before the covalent attachment (8). The reaction mechanism involves the release of terminal sulpho-NHS group from both end sides of the spacer to form an amide bond between the carboxylic group of BS3 and the lysine group of TmAb. This covalent amide bond formation is a simple one step stable attachment process without any modification of either spacer or targeting Ab.

Moreover, targeted tumor cell specific chemotherapeutic delivery using NPs has grown in importance since the cytotoxic drugs can concentrate only in the cancer cells which subsequently yield enhanced therapeutic effects with reduced side effects. Upon attachment of targeted ligand of NPs to the specific tumor antigen of cell, the particles can thus, ideally, are internalized into the cells through uptake and keep the chemotherapeutic payload away from plasma exposure. Therefore, the chemotherapeutic drug inside the NPs can be released inside the cell membrane through endosomal or lysosomal degradation. As a result, releasing the drug throughout the cell cytoplasm is able to kill the desired tumor cell and stop further tumor proliferation.

2. LITERATURE REVIEW

2.1. Overview: HER2 overexpressed breast cancer

In most cases, cancer takes place when genetic material is damaged or altered. This genetic alteration causes abnormal activities and unregulated proliferation of cells in the body. For rapid proliferation, cancerous cells require more nutrient supply than normal cells. Being in competition for sufficient nutrient supply, normal cells get displaced by the tumor cells resulting in uncontrolled cell division (9). Cancer remains one of the most prevalent and predominant diseases causing death. More than 10 million people per year are diagnosed with cancer disease worldwide (10). Breast cancer is rated as the second leading cause of cancer deaths among all invasive cancers in women (11) (12). Around 25-30% of all types of breast cancers are found to be associated with the overexpression of one of the epidermal growth factor receptors HER2. HER2 is a key biomarker for the pathogenesis of earlier stage breast cancer and exhibits an opportunity to design anticancer based targeted drug delivery system (13). However, no specific symptoms are notable at the initial stages of breast cancer in women and HER2 screening test is one of the common diagnosis processes to identify the disease (14).

2.2. Conventional therapies for breast cancer

Currently surgery, radiation therapy, hormone therapy, immunotherapy and chemotherapy are well established as common effective treatment options to tackle

the overall breast cancer. However, these traditional cancer therapies have a number of drawbacks and limitations (15). Research has been successful in developing treatment options with antibodies that impede breast cancer cell growth (16, 17). Chemotherapy is a more common breast cancer therapy where cytotoxic drugs interfere with the cellular processes in a nonspecific manner (18). However, normal healthy tissues are inevitably exposed to these chemotherapeutic agents leading to adverse drug effects (19). Poor bioavailability of high molecular weight chemotherapeutic agents and multiple drug resistance are two of the most important drawbacks of chemotherapy (20). Inefficient and non-selective drug delivery can lead to the development of drug resistance. Additionally drug entry (influx and efflux), metabolic alteration, drug sequestration or repossession, disruption of apoptotic pathways, alteration of signal transduction pathways, microenvironment and activation of DNA repair mechanisms are also responsible for the manifestation and development of drug resistance (21). To overcome these limitations, more effective site-specific drug delivery systems need to be developed, which can significantly improve the efficacy of the therapeutic agent with minimal toxicity. To advance research towards this goal, nanotechnology has attracted considerable attention from the researchers to establish the synthesis of nano scale biodegradable drug carriers that can specifically target tumor sites (22).

2.3. Role of HER2 in targeting

The transmembrane HERs play a key role in transmission of cell signals regulating cell growth and proliferation. This receptor family is comprised of four homologous members including HER1, HER2, HER3 and HER4. Among these,

only HER2 does not have an identifiable ligand for its extracellular domain (23). The HER2 receptor (also known as Neu, ErbB2, CD340 or cluster of differentiation 340, p185 or 185-kDa plasma membrane phosphoprotein) is a transmembrane glycoprotein encoded by ErbB2 gene on the long arm of chromosome-17 in humans (24). Structurally, HER2 has three parts including the N-terminal cysteine rich extracellular domain (ECD), a single α-helix transmembrane lipophilic domain and an intracellular tyrosine kinase domain in cytoplasmic sites (25). HER2 receptor's dimerization depends on the binding of selective ligands with its ECD while a conformational change occurs. As a result of dimerization, this conformational change activates the cytoplasmic catalytic function, which in turn autophosphorylates the tyrosine residues within the cytoplasmic domain of the receptor. The induced autophosphorylation initiates a complex variety of signal transduction pathways (figure-2.1) (26-28).

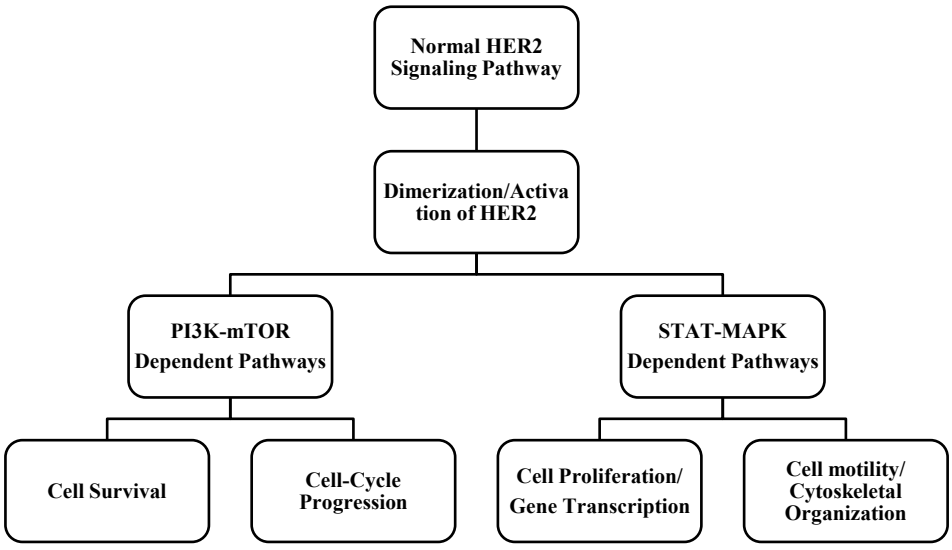

Figure-2.1: HER2 signaling pathways (26-28)

Although HER2 regulates cell development stages in normal cells, signaling of HER2 through various pathways stimulates cell proliferation and blood vessel growth to nourish tumor angiogenesis as well as to induce metastasis. The common mechanism of HER2 protein overexpression due to increased HER2 protein synthesis is associated with HER2 gene amplification and transcriptional dysregulation. This overexpressed HER2 protein concentration results in the activation of HER2 dimerization in the absence of ligand binding leading to uncontrolled cell proliferation and tumorigenic transformation (29). During normal cell growth, HER2 receptor is expressed at normal levels; but in cancerous cells, overexpression of HER2 receptors occurs. This overexpression facilitates free ligands to bind with excessive HER2 receptors to become preferential heterodimers for other HER receptors. These 'preferential' heterodimers have long survival on the cell surface, which induces enhanced transduction signaling and high malignant survival growth (30). Monoclonal antibodies (mAb) have been employed as an effective active targeted therapy since these antibodies can specifically recognize the overexpressed HER2 positive tumor cells and internalize through receptor mediated endocytosis (13, 31).

2.4. Strategic principles of targeting HER2 receptor

For effective cancer treatment with minimum side effects, anticancer drugs have to localize at selective tumor cells without losing its therapeutic properties during the systemic circulation and thus able to kill the tumor cells without interfering with the normal cells. Ideally, the principle of targeted anti-cancer therapy is based on active targeting (32). Cellular recognition in molecular level is

able to target the tumor cell actively by ligand-receptor, antigen-antibody interactions, and aptamers. Active targeting of therapeutic drug can be accomplished by coupling drug or nano-carrier with cell specific targeting moiety. These targeting moieties consist of specific affinity for the receptors or antigens on the cell surface. The level of such antigen expression can be employed as a tool to differentiate between tumor and normal cells (33). However, to formulate more effective tumor specific delivery system, some important factors should be optimized carefully such as –

i) the receptor or antigen on the surface of cell should be entirely expressed on the tumor cells rather than normal cells,
ii) expression on all the targeted tumor cells should be consistent,
iii) the receptor or antigen on the cell surface should not be shed into the systemic circulation.

In addition, selecting suitable targeting ligand is a major criterion to achieve the maximum internalization property of targeted conjugates after binding to the target cells. Internalization mechanism is defined as the process of high accumulation of drug into the tumor cells after recycling of the receptor or antigen back onto the cancer cells for second round of drug transport by binding with the same new receptor targeted conjugates (9) (34) (35).

Active targeting through ligand-receptor interaction includes some possible pathways such as lectin-carbohydrate interaction, transferrin receptor, folate receptor, human epidermal growth factor (EGF) receptor, and finally peptide

receptor (36). A mitogenic protein of human body is well known as EGF receptor associated with cellular mechanism such as cell division, transcription, and growth. Expression of one EGF receptor (HER2) occurs on the surface of tumor cells 100 times more than normal cells, which is more pronounced marker for a variety of human cancers such as lung, prostate, and breast cancer. Drug delivery system conjugated by anti-HER2 ligand can be an effective way for targeting cancer cell (37) (38). However, body can distinguish such drug carrier-conjugates as foreign substances, which are taken by the liver and spleen from the blood stream through reticulo-endothelial system (RES) (39). In order to escape the mononuclear phagocytosis, surface functionalization and enhanced hydrophilicity of nano drug carriers can be considered as the primary requirements. Because, the enhanced half-life of the nano-carriers during the systemic circulation is prerequisite for maximum binding between the specific cell surface receptors and the ligands of NPs towards active localization (40) (41) (42). In addition, NP attached humanized mAb can be distinguished as body's own components to hide the NPs from RES.

2.5. Components for designing HER2 targeted anticancer drug loaded NP

An ideal anti-HER2 receptor specific targeted anticancer drug loaded NP can be designed by combining the following components as described in the figure-2.2.

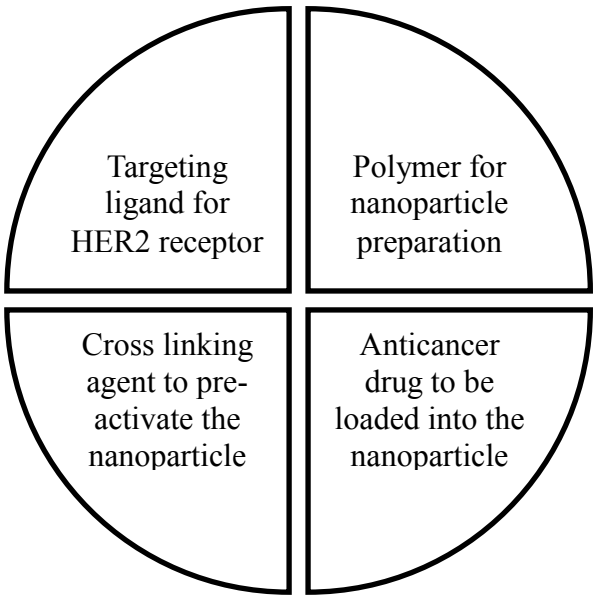

Figure-2.2: Different components for designing anti-HER2 targeted cytotoxic drug loaded carrier

2.5.1. Targeting ligand: Trastuzumab

A number of monoclonal antibodies have already been approved by FDA for targeted cancer treatment which can be utilized to target respective EGF ligand. To identify and target the antigenic epitope on the ECD of HER2 receptor, a humanized IgG1 mAb named Trastuzumab (TmAb) has been well exhibited as the primary HER2 receptor blocker, derived from murine mAb 4D5 (43). A number of possibilities have already been established to define the mechanism of actions how TmAb works to inhibit the tumor angiogenesis and tumor cell proliferation (figure-2.3) (44).

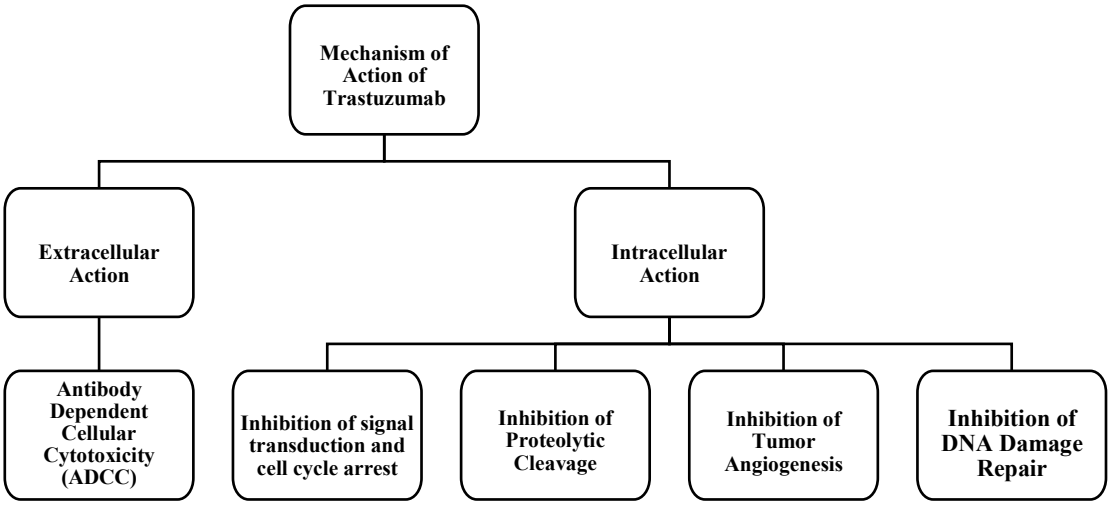

Figure-2.3: Mechanism of action of TmAb (44)

An open configuration exhibits on the ECD of HER2 receptor which is always available for the dimerization with itself (homo-dimerization) and with other HER family member receptors (hetero-dimerization). TmAb is able to bind with C-terminal portion of ECD-IV alike other mAbs (45). F_{ab} region of TmAb is thought to bind the membrane surface antigens of target cells while the F_c region of the mAb is free to be recognized by the $F_{c\text{-}gamma}$ ($F_{c\gamma}$) receptors of the immune effector cells like natural killer (NK) cells. Upon binding, NK cells release cytokines and cytotoxic materials to lyse the target cell by stimulating the apoptosis process. This is called Ab dependent cell mediated or cellular cytotoxicity (ADCC) which is the extracellular mechanism of action of TmAb (46).

The regulatory proteins of cells control the cell cycle development and apoptosis, which can be functionally interrupted due to HER2 overexpression or mutation. In HER2 overexpressed condition, cell signaling through both PI3K-mTOR and STAT-MAPK dependent pathways are subjected to be enhanced. Thus, both tumor cell's proliferation and survival get stimulated by regulating cyclin-

dependent kinase inhibitor and by inhibiting apoptosis process (47) (48). TmAb hinders the dimerization or activation of HER2 which consequences the inhibition of cell cycle arrest and the decreased signaling through both PI3K-mTOR and STAT-MAPK dependent signaling pathways (49) (50) (51) (52) (53) (54).

Due to proteolytic cleavage, ligand free tyrosine kinase HER2 receptor causes the release of ECD and phosphorylated p95 (a truncated membrane bound HER2 fragment with M_r~95000). In HER2 overexpressed breast cancers, p95 is concomitant with the positive lymph nodal metastasis (55). TmAb blocks both basal and activated HER2 ectodomain cleavages, which thereby stop the phosphorylation of p95 (56).

Tumor cells secret some important growth factors such as vascular endothelial growth factor (VEGF), transforming growth factor-α to induce angiogenesis for their own growth and proliferation. In breast cancer, both HER2 overexpression and VEGF manifestation are inter-related. Treatment with TmAb significantly reduces volume and width of blood vessel which ultimately down regulates the HER2 overexpressed tumor growth. Vasculature permeability is also decreased with TmAb therapy (57).

Conventional anticancer therapies are associated with various types of drawbacks. Cellular DNA damage is one of the important drawbacks of them. In damaged cells, activation of cells' respond is required to repair damaged DNA, process of cell cycle arrest and apoptosis. To repair such damaged gene, HER2 mediated signal transduction pathways play an important role (58) (59). Blocking of this HER2 mediated signal transduction pathways by TmAb can lead the inhibition

of repairing conventional anticancer therapy induced DNA damages as well as tumor cell growth (60) (61).

2.5.2. PLGA NP

Nanotechnology is now an advanced field of interest for various applications (62). Thus, polymeric NP is a significant output of modern nanotechnology practice. Most chemotherapeutical drugs are toxic and hydrophobic in nature which requires adequate dilution for slow infusion into the body. To overcome these limitations, biocompatible and biodegradable polymeric NPs can be employed as a suitable drug carriers (63).

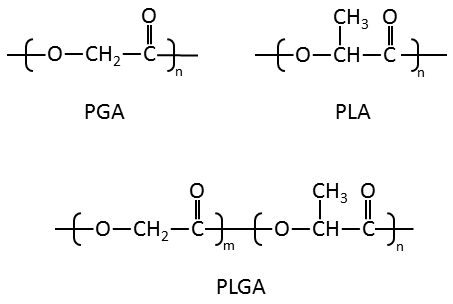

Figure-2.4: Composition of PLGA polymer

PLGA is now a widely studied biodegradable co-polymer under required applications for effective anticancer drug delivery. PLGA breaks down into two endogenous metabolite monomers (lactic acid and glycolic acid) upon hydrolysis of its ester linkage within the body (figure-2.4) (64). The main regulatory agencies like US FDA and European Medicine Agency (EMA) approved PLGA for numerous drug delivery systems to apply in human because of the biocompatibility, swelling behavior, easy preparation techniques, mechanical strength, and limited systemic

toxicity (5) (65). PLGA is a hydrophobic molecule in nature, which facilitates the easy incorporation of most anticancer drugs (6). Targeted drug delivery with enhanced half-life can be achieved by the surface functionalization with different purpose based various functional groups (66). Vast surface area of PLGA NPs is an attractive feature to control the release kinetics, drug loading capacity and administration route, which can regulate the degradation of drug into the body (67). To optimize targeted therapeutic delivery, preparation of PLGA NPs can be carried out by various available methods such as emulsification solvent evaporation, nano-precipitation, polymerization, self-assembly, ionic gelation, salting out etc. However, the preparation methods are dependent on the necessity of its purpose and type of drug to be loaded into the NPs (68) (69) (70).

2.5.3. Docetaxel: A choice of cytotoxic drug for HER2 overexpressed breast cancer

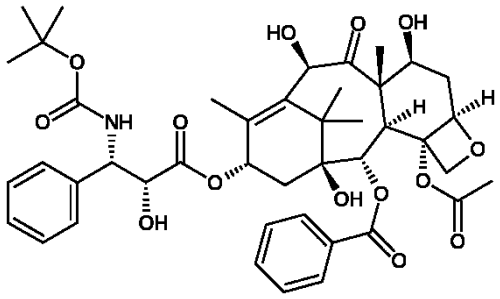

Figure-2.5: Chemical structure of Docetaxel (60)

Among all anti-neoplastic classes of drug, the taxans family gained substantial consideration as a versatile and clinically useful class of anticancer drugs. Being a member of taxans family, Doc is now widely used chemotherapeutic agent (figure-2.5) (71). Exclusively in breast cancer, Doc has been comprehensively used

for trialed over the past decades due to its prolong half-life (11-19 hours), wide volume of distribution, enhanced binding affinity with tissues, less toxicity and some advantages over other taxans members. Cellular microtubule networking is necessary for interphase as well as mitotic functions, which are interrupted by Doc more potentially than other anti-neoplastic drugs (72) (4). Doc leads to the stabilization of microtubules, since it can bind with the free tubulin and thus inhibits the microtubule depolymerization (73). Despite the successive mechanism, Doc is reported with relative side effects such as enhanced neutropenia, fatigue, leucopenia, stomatitis, alopecia, edema, and diarrhea (74) (75). In addition, Doc is associated with poor water solubility and systemic cytotoxicity mostly due to broad spectrum administration (76). Such limitations can be minimized by selective tumor cell targeting using nano-carriers such as polymeric NPs, which carry the drug to the specific desired cell environment to inhibit infected cell replication. For specific binding to receptor of targeted cell surface, functionalization of the nano-carriers is an essential prerequisite part, which involves the requirement of selective mAb conjugation with or without appropriate spacer.

2.5.4. Cross linking agent to functionalize the NP surface

The concept behind the surface functionalization of NPs is to deliver the cytotoxic agents after binding with uniquely expressed or overexpressed receptors of target cells, which allows subsequent penetration and accumulation of therapeutic drugs into the cells (77). For successful Ab-NP conjugation, spacer or cross linker can act as an important utility bridge (102). However, no perfect progression is available to control the desired ligand cross linked with PLGA NPs for required

targeting effects. Because, most of the ligand-NP conjugation processes using spacer has been demonstrated as a self-assembling processes (78). Conjugation between the HER2 specific ligand and PLGA NP can be carried out following several attachment approaches. Spacer can be homobifunctional and heterobifunctional which depends on its reactive group at the end of the spacer arm.

Figure-2.6: Chemical structure of BS3

Homobifunctional spacer, bis-sulfosuccinimidyl suberate (BS3) is reported as an effective cross linker between Ab and NPs followed by the formation of amide linkage (8). In brief, BS3 is an eight-carbon spacer, which consists of two terminal hydrophilic sulfonyl groups at the end of its carboxylic moieties, which are to be oriented around the surface of NPs. Amide bond between the carboxylic groups of BS3 and the lysine groups of Ab is to be formed upon relieving the terminal sulpho-NHS group from both terminal ends of the spacer (figure-2.6). The mechanism of this crosslinking is a simple one step stable and reproducible attachment process without any modification of the spacer and antibody. In addition, using such spacer has been found with no steric hindrance in earlier study (8) (79).

3. PURPOSE OF PROJECT

3.1. Purpose

The primary purpose of this research is to formulate and characterize an ideal Doc loaded PLGA NPs functionalized with the TmAb and to observe its *in vitro* effects in breast cancer cells. Afterwards, *in vivo* experitments could be done in HER2 overexpressed tumor bearing mice.

3.2. Rationale

The rationale of this research focuses on overcoming the current challenges related to conventional chemotherapy for cancer patients. Because most of the anticancer drugs after clinical use are associated with some limitations such as poor solubility profile, multiple drug resistances, short half-life, and instability. In most cases, the exposure of chemotherapeutic agents to the normal healthy cells results in severe side effects due to nonspecific broad spectrum administration. Sometimes, these drawbacks result in the discontinuation of many potential anticancer drugs in the very early stage from the market. To overcome these drawbacks, nanotechnology offers many new dimensions in targeted drug delivery systems to improve both therapeutic efficacies of these anticancer drugs and tumor imaging by early detection. Taking the advantages of nano-drug delivery system to overcome the existing limitations of conventional chemotherapy, this experimental design has

been considered to develop a perfect NP formulation in respect to targeted drug delivery system for HER2 positive breast cancer.

3.3. Hypothesis

The following hypotheses have been assumed to establish a targeted chemotherapy for HER2 overexpressed breast cancer:

1. Docetaxel can be loaded into the PLGA polymeric NPs successfully followed by emulsification solvent evaporation technique.
2. A humanized monoclonal antibody (Trastuzumab) can be covalently attached with the homobifunctional cross linking agent (BS3) embedded on PLGA NP surface (figure-3.1).
3. Presence or absence of HER2 specific ligand on NP surface can differentiate the degree of cell uptake of Coumarin-6 (instead of docetaxel) loaded NPs in both HER2 overexpressed (SKBR-3) and moderate expressed (MCF-7) breast cancer cells.
4. Compared to unmodified NPs, Trastuzumab modified docetaxel loaded PLGA NPs can efficiently inhibit the HER2 receptor expression which will stop further proliferation breast cancer cells (SKBR-3 and MCF-7) (figure-3.2).

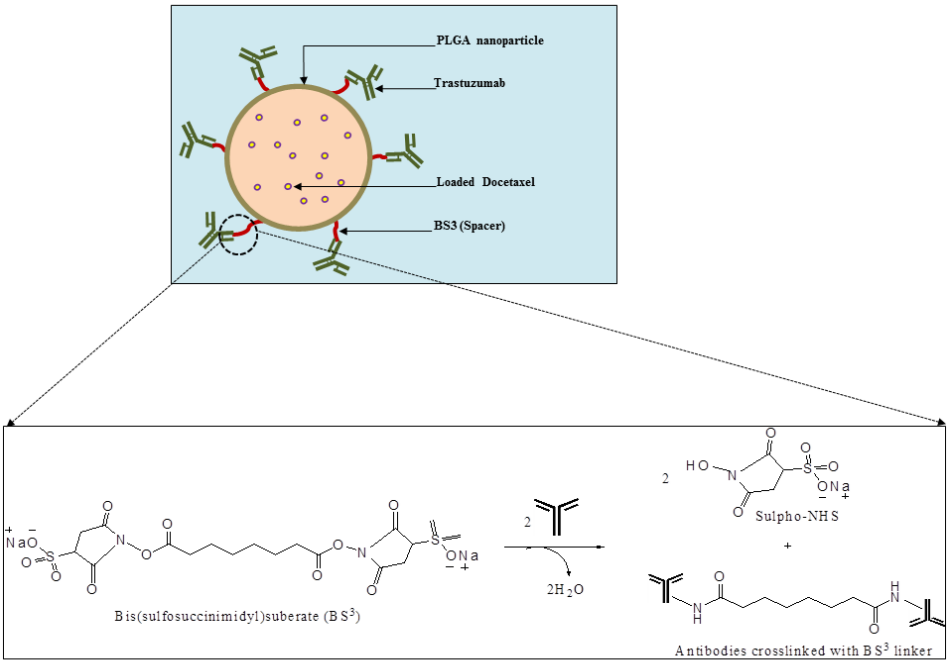

Figure-3.1: Graphical representation of TmAb modifed Doc loaded PLGA NP and the covalent attachment mechanism between TmAB and BS3 pre-embedded onto the NP surface

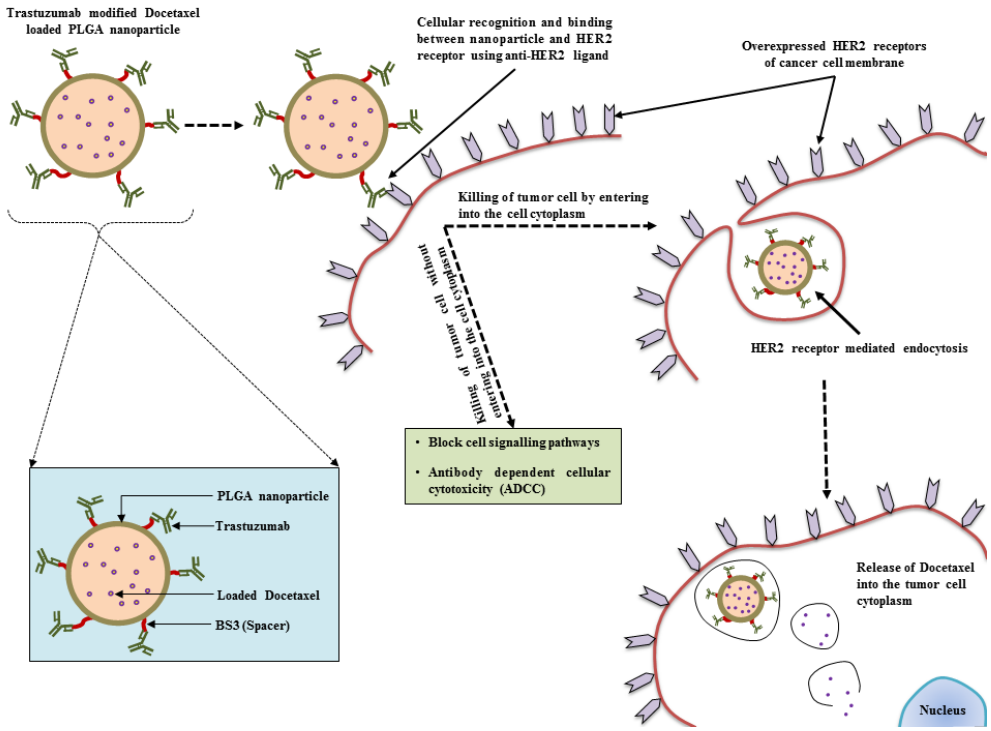

Figure-3.2: Graphical representation for the predicted fate of TmAb modifed Doc loaded PLGA NP to breast cancer cells

3.4. Objectives

Targeted chemotherapy is aimed to avoid broad spectrum distribution of available chemotherapeutic drugs into the whole body. Towards this goal, this study has been designed primarily to establish docetaxel loaded modified PLGA NPs functionalized with trastuzumab which can be able to target overexpressed HER2 receptors of breast cancer cells. In this regard, the following primary objectives have been considered:

1. Development of trastuzumab modified docetaxel loaded PLGA NPs.
2. Physicochemical characterization of trastuzumab modified docetaxel loaded PLGA NPs in terms of size, polydispersity index, zeta potential.
3. Quantification of drug loading and drug entrapment efficiency.
4. Quantification of trastuzumab attached with the docetaxel loaded pre activated PLGA NPs.
5. Identification of the covalent bond between trastuzumab and BS3 embedded on the PLGA NPs.
6. Assessment of cell uptake by coumarin-6 loaded nano-formulations (instead of docetaxel).
7. Evaluation of HER2 expression of breast cancer cells (SKBR-3 and MCF-7) after treating the nano-formulations.
8. Assessment of cell viability and toxicity after treating the nano-formulations with breast cancer cells (SKBR-3 and MCF-7).

4. MATERIALS AND METHODS

4.1. Materials

Ester terminated PLGA (inherent viscosity 0.15-0.25 dl/g) were purchased from LACTEL, Birmingham polymers (USA). Trastuzumab (Herceptin®) was from Genentech (a member of the Roche group). Docetaxel was purchased from LC Laboratories, USA. Polyvinyl alcohol (PVA), BS3, BCA protein assay kit, 0.25% Trypsin-EDTA solution and Fetal Bovine Serum were purchased from Sigma-Aldrich, USA. SKBR-3 and MCF-7 cell lines were purchased from ATCC, USA. Hyclone DMEM/High Glucose medium, Hyclone McCoy's 5A medium, BCA Protein Assay-Reducing Agent Compatible, Bovine Gamma Globulin (BGG) Standards from Thermo Fisher Scientific Inc., Canada. Analytical grade solvent; ethyl acetate was used.

4.2. Methods

4.2.1. Preparation of NPs

Oil in water (O/W) emulsification solvent evaporation technique has been applied to prepare Doc loaded ester-terminated PLGA NPs (80). At first, ethyl acetate was considered as the organic solvent to prepare the oil phase. A weighed amount of drug and 65 mg of PLGA co-polymer were dissolved into 1 ml of solvent (ethyl acetate). 2.2 % polyvinyl alcohol (PVA) solution was considered as the

aqueous phase. A weighted amount of BS3 was added into PVA solution to prepare NPs for covalent attachment (8). Then drug and co-polymer (dissolved in the solvent) consisting oil phase was transferred drop-wise to aqueous phase and this mixture was then primarily emulsified by using micro tip probe-sonicator. Therefore, the primarily emulsified mixture was transferred drop-wise into a beaker for 1 hr gentle stirring to remove the organic solvent by evaporation. After removal of organic solvent, the NP suspension was subjected for centrifugation to recover only Doc loaded NPs. To remove the residual of PVA completely from the precipitate, the NPs were washed and re-suspended twice with distilled water followed by centrifugation at 4° C (25,000 rpm, 25 mins). Finally, suspended NPs were freeze-dried for 48 hrs to obtain dried and fine powder (81). And then the dried NPs were stored at -20° C (82).

4.2.2. TmAb conjugation process

4.2.2.1. Physical adsorption

A weighted amount of BS3 excluded plain or drug loaded ester ended freeze-dried PLGA NPs was added into phosphate buffer saline (PBS) in a small vial. Then varying amounts of TmAb were added into the small vial for physical adsorption and kept for 1 hr continuous stirring in room temperature to reduce the chance of any aggregation among the NPs (8) (83). Recovery of surface modified NPs was followed by washing and centrifugation at 4° C (18,000 rpm, 15-20 mins) twice (7).

4.2.2.2. Covalent conjugation

Covalent conjugation method is same as physical adsorption method. Only

exception is the presence of BS3 in the NP formulations that act as spacer to form covalent amide bond with the antibody.

4.2.3. Size analysis, surface charge and yield of preparation

To investigate the size, size distribution, poly-dispersity index (PDI), and zeta potential (ZP), the NPs were suspended in water. Size and size distribution measurement of both modified and unmodified NPs were carried out through Malvern Zetasizer (84). The measurement was performed for the NPs before and after freeze-drying (85). And mean value and standard deviation (SD) from the data were also assessed. The measurements were conducted at 25° C and average of four samples was reported. The recovery or yield of the NPs was measured using the following equation:

$$\text{Yield (\%)} = \frac{\text{Weight of obtained NPs}}{\text{Initial weight of polymer, drug, and other ingredients}} \text{ X } 100$$

4.2.4. Drug loading and entrapment efficiency by mass spectrometry

Mass spectrometer has been used to quantitatively determine the amount of Doc present in the samples throughout the study following an extraction procedure, previously established in our laboratory (86). Quantitation procedure was performed on corresponding Doc and internal standard MRM graphs using Analyst software version 1.6.

4.2.4.1. Sample preparation

A stock solution of Doc (100 µg/ml) in methanol was prepared. Working

solution of 3.9, 7.8, 15.6, 31.2, 62.5, 125, 250, 500, 1000, 2000, 4000, 8000, and 16,000 ng/ml concentrations were prepared by serial dilution of the stock solution in methanol. For internal standard, a stock solution of paclitaxel 100 µg/ml in methanol was also prepared.

4.2.4.2. Preparation of standards, controls and test samples

To prepare polymer-free standards (Doc in methanol), 10 µl of internal standard along with 1 ml of working solution (3.9-1000 ng/ml) were transferred into 2 ml tubes and vortexed. Polymer-free controls were prepared as such to obtain 100, 200, 400, and 800 ng/ml Doc concentrations. To prepare standard samples of NP formulations, 10 µl of internal standard along with 1 ml of working solution 125-16,000 ng/ml for PLGA NPs was transferred into 2 ml tubes and vortexed. The solvent was then evaporated and 5 mg plain (drug-free) NPs were added to the tube. Concentration set of 1250, 2500, 5000, and 10,000 ng/ml was used to prepare quality control samples of PLGA NPs. This is while 625, 1250, 2500, and 5000 ng/ml concentration set was used to prepare quality control samples of PLGA NPs. 10 µl of internal standard was added to control samples of PLGA NPs and vortexed. The solvent was evaporated and 5 mg plain NPs was added to the tube. To prepare test samples, 10 µl of paclitaxel solution was added to 2 ml tubes along with 5 mg of drug loaded PLGA NPs. Standard, control, and test samples were extracted twice with acetone.

4.2.4.3. Drug extraction

Doc was extracted from PLGA NPs to prepare the samples for mass

spectrometric analysis. In brief, 1 ml acetone was added to 5 mg drug-loaded NPs to dissolve both polymer and drug. The mixture was vortexed for 30 secs and subjected to bath sonication for 30 mins. Then it was centrifuged for 20 mins at 20,000 rpm. The supernatant was separated and preserved. The precipitate was then dissolved in acetone and the same procedure was repeated. Obtained supernatants from the first and second centrifugation step were mixed and evaporated. 1 ml methanol was added to the residue, vortexed for 30 secs and centrifuged for 20 mins at 20,000 rpm. Doc was then quantified in supernatant using mass spectrometry method. Finally, drug loading and encapsulation efficiency (EE) were calculated using the following equation:

$$\text{Docetaxel loading } (w/w) = \frac{\text{Amount of loaded Docetaxel } (\mu g)}{\text{Amount of polymer (mg)}}$$

$$\text{Encapsulation efficiency } (\%) = \frac{\text{Amount of loaded drug (mg)}}{\text{Initial amount of drug used (mg)}} \text{ X } 100$$

4.2.5. Determination of TmAb amount attached on the NPs

The micro-bicinchoninic acid protein assay kit-reducing agent compatible (BCA-RAC) and bovine gamma globulin (BGG) standards were used as per protocol to determine the amount of TmAb conjugated with per mg of drug loaded NPs (7). The amount of Ab attachment was determined using indirect method from the unbound Ab present in the collected supernatant during washing steps. For assay procedure, the supernatant of unmodified NPs was used as blank standard. As per instruction followed by BCA protein assay kit procedure, 96 wells plate was used to quantify the unbound Ab amount. Absorbance of the samples was measured at 562

nm in BioTek Microplate Reader using Gen5 data analysis software. By plotting the absorbance found from the assay versus concentration of the standard solution (bovine gamma globulin), a standard curve was yielded (81). The calculation of the Ab attachment and the attachment efficiency were done using the following equations:

$$\text{Trastuzumab attached (per mg of NPs) (w/w)} = \frac{\text{Amount of TmAb attached (μg)}}{\text{Amount of NPs (mg)}}$$

$$\text{Attachment efficiency (\%)} = \frac{\text{Amount of TmAb per mg of NPs (μg)}}{\text{Initial amount of TmAb used per mg of NPs (μg)}} \text{ X } 100$$

4.2.6. Identification of the covalent bond between TmAb and BS3 (embedded into NPs)

4.2.6.1. Fourier Transform Infrared (FTIR) spectroscopy

Infrared (IR) spectra of NPs were recorded on a Bruker IFS 66v/S Fourier Transform Spectrometer (Bruker Optics, Billerica, MA) in the mid-IR range at the Canadian Light Source, University of Saskatchewan, Canada. All samples were mixed with spectroscopic grade potassium bromide (KBr) and mulled to prepare pellets. The spectra were taken for KBr pellets in the range of 4000 – 400 cm^{-1} in absorbance mode.

4.2.6.2. Sodium Dodecyl Sulfate-Polyacrylamide Gel Electrophoresis (SDS-PAGE)

For the analysis of structural integrity, TmAb was extracted from the modified NPs by adding 0.5 ml ethyl acetate into 5 mg of NPs to be dissolved.

Maintaining 1:4 ratio, distilled water was added to the dissolved solution and then vortexed at 1400 rpm for 15 mins. Two distinct phases were resulted upon centrifugation of the solution at 12000 rpm for 10 mins. 5 ml syringe was used to extract the water phase to quantify the concentration of TmAb followed by earlier mentioned assay procedure (87) (88). Mini-Protean® TGX™ Gel 7.5% was used to run SDS-PAGE under non-reduced and denatured conditions as per the protocol from Bio-Rad Laboratories (Canada) Ltd. Exactly, 15 µl of each samples of 1µg/µl TmAb concentration was loaded per well. The gel was stained with Coomassie Brilliant Blue R-250 staining solution (Bio-Rad, Canada) for 3 hrs and later de-stained with de-staining solution (Bio-Rad, Canada) for whole night gently at room temperature in a shaker.

4.2.7. Cell culture

SKBR-3 and MCF-7 breast cancer cell lines were considered as the positive detection of HER-2 over and moderate expression respectively (89). These cells were routinely cultured in the respective medium consisting 10% fatal bovine serum (FBS) and 1% penicillin (100 IU/ml)-streptomycin (100 µg/ml) solution followed by ATCC guideline. Routine cell culture was carried out in the incubator with a set temperature of 37° C in humidified atmosphere containing 5% CO_2. The harvesting of cells from culture plates was performed using 0.25% trypsin-EDTA solution.

4.2.8. Quantification of Coumarin-6 (Coum-6) in NPs

To quantify the amount of Coum-6 in NPs, the particles were dissolved in methanol and kept overnight in dark. Then the fluorescence intensity was measured

at the emission wavelength of 505 nm using a fluorescent spectrophotometer with a microplate reader (90).

4.2.9. Cellular uptake

4.2.9.1. Flow cytometry analysis

4.2.9.1.1. Cellular uptake without TmAb pre-incubation

$1.5x10^5$ cell cells were plated in each well of 6 wells suspension culture plate with culture medium and kept for 24 hrs in the incubator. 0.5 mg of Coum-6 loaded both unmodified and modified NPs were incubated with both cell lines for 24 hrs. After incubation, cells were washed twice with 2% ice cold FBS containing PBS. 0.25% trypsin-EDTA solution was used to harvest the adherent cells from the plate. After centrifugation, cells were washed with FACS buffer twice prior to be analyzed using flow cytometry (91).

4.2.9.1.2. Cellular uptake after TmAb pre-incubation

To explore the binding efficacy of TmAb to HER2 receptor, the respective cell types of varying HER2 expression levels were preincubated with TmAb before treating the cells with TmAb modified and unmodified Coum-6 loaded NPs. In brief, $1.5x10^5$ MCF-7 and SKBR-3 cells were seeded in each 6 well plates and were kept in the respective culture mediums for overnight. The next day, cells were treated with TmAb (1 µg/µl concentration) for 30-45 mins into the incubator (92). Followed by 30-45 mins of pre-incubation, cells were then treated with plain [NP (Coum-6)], physically TmAb attached [NP (Coum-6)-TmAb] and covalently attached [NP (Coum-6)-BS3-TmAb] Coum-6 loaded NPs at 0.25 mg/ml concentration into the

incubator for overnight. After incubation of cells with different NPs, cells were harvested following the same procedures as stated above to measure the cell uptakes using flow cytometry.

4.2.9..2. Confocal laser scanning microscopy

In order to visualize the binding and internalization into the cells, confocal laser scanning microscopy (CLSM) was employed for both cell types. Briefly, coverslips were kept in each well of 6 wells plate prior to plate the cells for NP treatments. The condition of cell culture and treatments with different Coum-6 loaded NPs were the same as stated in the cellular uptake without TmAb pre-incubation section. In the day of sample preparation, coverslips of adhered cells were washed twice with ice-cold PBS and fixed with 4% paraformaldehyde for 25 mins. After that, the fixed cells were washed twice again with ice-cold PBS and the nuclei of the cells were counterstained with gold anti-fade reagent with DAPI (4', 6-diamidino-2-phenylindole) prior to subject under the confocal microscope.

4.2.10. Measurement of HER2 expression

4.2.10.1. Flow cytometry analysis

$1.5x10^5$ cells were plated in each well of 6 wells suspension culture plate with culture medium and kept for 24 hrs in the incubator. For the treatment of cells, same concentration of TmAb attached with NPs was considered as the standard. Different NP formulations were incubated with both cell lines for different time points. After incubation at different time points, cells were washed twice with 2% ice cold FBS containing PBS. 0.25% trypsin-EDTA solution was used to harvest the

adherent cells from the plate. After centrifugation, cells were washed with PBS and then stained with FITC conjugated anti-HER2 Ab which was purchased from BD Bioscience, Canada. After incubation with labeled Ab, ice cold FACS buffer was used to wash unbound labeled Ab from the cells twice prior to flow cytometric analysis.

4.2.10.2. Western blot analysis

Protein was isolated from both cell types after NP treatment by lysis with sample buffer and then to ensure equal amount of loading on gel, protein concentration was assayed using the BCA protein assay kit. For different types of NP formulations, HER2 expressions of both cell types were analyzed following previously described Western Blot analysis method (89) (93) (94).

4.2.10.3. Fluorescence microscopic analysis

Glass coverslips were kept in each well of 6 wells plate. $1.5x10^5$ cells were plated in each well of 6 wells plate with culture medium and kept for 24 hrs in the incubator. For the treatment of cells, a weighted amount of TmAb and drug loaded TmAb modified NPs were considered after refreshing cells with new media. After 48 hrs of incubation, samples were washed with ice-cooled PBS and fixed with ice-cooled 2% paraformaldehyde for 20 mins. After 2 times washing, cells were treated with anti-HER2 FITC Ab at room temperature for 45 mins and washed 2 times again to remove unbound labeled Ab from the cells before sampling with DAPI to counterstain the nucleus. Fluorescence images were obtained using Olympus fluorescence microscope with 40X objective lens.

4.2.11. Cell viability and toxicity studies

The impact of different NPs formulations on HER2 overexpressed (SKBR-3) and HER2 moderate expressed (MCF-7) breast cancer cells was evaluated by using Annexin V-FITC/Propidium Iodide (PI) staining according to the protocol provided by BD biosciences. In details, $1x10^6$ cells were plated in each well of 6 wells plate with culture medium and kept for 24 hrs in the incubator. In the next day, media was refreshed and treated with the same formulations with same conditions as stated in the HER2 expression measurement section for 48 hrs. After the treatment, cells were washed twice with cold PBS and then resuspended cells in 1x binding buffer [0.1 M Hepes/NaOH (pH 7.4), 1.4 M NaCl, and 25 mM $CaCl_2$]. Then 10µl of cells ($1x10^5$) suspension was transferred into a 5 ml culture tube. For staining the cells, 5µl Annexin V-FITC and 5µl PI were added with gentle shaking and kept for 15 mins incubation at room temperature in dark milieu. 400 µl of 1x binding buffer was added to each tube before subjecting for the flow cytometry analysis. Untreated unstained cells, untreated cells stained with Annexin V-FITC, untreated cells stained with PI, and untreated cells stained with both Annexin V-FITC and PI were considered as control standards. The basal level of apoptotic and dead cells was considered for the untreated cell population stained with Annexin V-FITC and PI. Subtraction of the apoptotic or necrotic percentage for untreated cells from that of treated cells was considered to be the percentage of cells being induced to undergo apoptosis or necrosis due to the treatments.

4.2.12. Statistical analysis

Data were analyzed by descriptive statistics, calculating the mean and

standard deviation (mean ± SD) for continuous variables. The paired student's t-test has been considered to evaluate the differences between modified versus un-modified NPs. The level of significance is set to $p<0.05$.

5. RESULTS AND DISCUSSIONS

5.1. Size, PDI, and ZP

Size, PDI, and ZP measurements of the NP formulations are important considerations prior to *in vitro* and *in vivo* experiments. All the prepared NPs were characterized in terms of size, PDI, ZP expressed as mean ± SD. One-way ANOVA analysis of variance and Newman-Keuls multiple comparison test were performed to demonstrate statistical differences at α level of 0.05 using the software GraphPad Prism 5 for Windows. The characterizations were performed considering different conditions including before and after freeze-drying, and TmAb attachment with the NPs.

5.1.1. Plain NPs (without Doc)

5.1.1.1. Plain NPs freeze-dried with no cryoprotectant

Table-5.1 shows the data for all the plain NPs, which did not have any drug and freeze-dried with no cryoprotectant.

Table-5.1: Size, PDI and ZP of plain NPs without drug and freeze-dried with no cryoprotectant (n=10)

NPs	Before freeze-drying			After freeze-drying		
	Mean Z-Ave (nm) ± SD	**Mean PdI ± SD**	**Mean ZP (mV) ± SD**	**Mean Z-Ave (nm) ± SD**	**Mean PdI ± SD**	**Mean ZP (mV) ± SD**
Plain	158.8±5.6	0.20±0.03	-5.4±1.1	344.1±56.1	0.54±0.11	-14.7±3.4
Plain+BS3	136.7±8.2	0.12±0.02	-5.5±0.7	330.1±71.6	0.46±0.12	-18.5±7.9

The mean size of plain NPs without incorporation of drug and BS3 was found to be 158.8±5.6 nm, whereas mean size of BS3 containing plain NPs was measured to be 136.7±8.2 nm before freeze-drying. This result indicates a slightly lower average particle size after BS3 inclusion in the plain NP formulation before freeze-drying. Freeze-drying was found to increase the particle size of NPs that was confirmed by the high PDI. The ZP values also shifted towards more negative after freeze-drying.

5.1.1.2. Plain NPs freeze-dried with cryoprotectant

Table-5.2 summarizes the data for plain NPs using cryoprotectant (10% sucrose). When cryoprotectant was present in the formulation, the mean size of NPs before freeze-drying was found to be 148.1±6.8 nm and 132.3±3.9 nm for plain NPs and NPs containing BS3, respectively.

Table-5.2: Size, PDI and ZP of plain NPs without drug and freeze-dried with 10% cryoprotectant (n=10)

NPs	Before freeze-drying			After freeze-drying		
	Mean Z-Ave (nm) ± SD	**Mean PdI ± SD**	**Mean ZP (mV) ± SD**	**Mean Z-Ave (nm) ± SD**	**Mean PdI ± SD**	**Mean ZP (mV) ± SD**
Plain+10% Suc	148.1±6.8	0.13± 0.03	-10.6±2.2	242.9±11.4	0.16± 0.02	-10.7±1.7
Plain+BS3+10% Suc	132.3±3.9	0.12± 0.02	-13.2±4.8	228.6±7.2	0.17 ± 0.03	-4.8±2.3

From table-5.2, it can be concluded that average particle size and PDI values of plain NPs were improved having reduced range before and after freeze-drying but no significant change was observed for surface charge of the NPs.

5.1.1.3. Plain NPs formulations with different amounts of BS3

Different amounts of BS3 ranging from 1.5 mg to 9 mg were used to prepare BS3 containing plain NPs to investigate the covalent binding efficiency of NPs to TmAb. Table-5.3 shows the mean particle size, PDI and ZP data for the BS3 containing NPs freeze-dried with and without cryoprotectant.

Table-5.3: Size, PDI and ZP of plain NP formulations with different amounts of BS3 (n=3)

NPs	Before freeze-drying			After freeze-drying		
	Mean Z-Ave (nm) ± SD	Mean PdI ± SD	Mean ZP (mV) ± SD	Mean Z-Ave (nm) ± SD	Mean PdI ± SD	Mean ZP (mV) ± SD
Plain	158.8±5.6	0.20±0.03	-5.4±1.1	344.1±56.1	0.54±0.11	-14.7±3.4
Plain+10% Suc	148.1±6.8	0.13±0.03	-10.6±2.2	242.9±11.4	0.16±0.02	-10.7±1.7
Plain+BS3 (1.5mg)	136.7±8.2	0.12±0.02	-5.5±0.7	330.1±71.6	0.46±0.12	-18.5±7.9
Plain+BS3 (1.5mg)+10% Suc	132.3±3.9	0.12±0.02	-13.2±4.8	228.6±7.2	0.17±0.03	-4.8±2.3
Plain+BS3 (3mg)	131.1±3.9	0.17±0.02	-14.6±0.5	375.8±106.5	0.51±0.23	-13.3±9.6
Plain+BS3 (3mg)+10% Suc	139.8±6.1	0.14±0.01	-10.4±0.3	227.5±47.9	0.19±0.05	-15.6±2.5
Plain+BS3 (6mg)	129.8±4.1	0.13±0.01	-19.6±0.5	375.7±162.1	0.26±0.19	-14.8±5.5
Plain+BS3 (6mg)+10% Suc	142±4.8	0.12±0.01	-18.1±0.9	274.1±18.3	0.30±0.14	-9.9±1.7
Plain+BS3 (9mg)	139.5±3.6	0.13±0.01	-18.5±0.5	311.8±144.8	0.36±0.12	-14.1±2.4
Plain+BS3 (9mg)+10% Suc	131.6±2.2	0.11±0.01	-14.4±0.6	278.8±56.1	0.24±0.14	-12.3±0.7

Table-5.3 shows that using cryoprotectant in the formulation improved the particle size and PDI after freeze-drying although no statistical correlation could be made. Surface charge of the BS3 containing plain formulations with 10% cryoprotectant were observed to be less than -20mV. However, ZP values showed a more negative trend by increasing the amount of BS3 in NPs.

5.1.2. Doc loaded NP formulations

5.1.2.1. Effect of different Doc concentrations in NP formulations with no BS3

Doc concentrations of 0.75 mg/ml to 3 mg/ml were initially used to prepare the drug loaded NPs using cryoprotectant as summarized in table-5.4. Particle sizes of Doc loaded NP formulations without BS3 were in range from 133.6±3.6 to 141.1±3.8 before freez-drying and from 202.3±3.6 to 235.6±15.2 after freeze-drying. The ZP values of these formulations varied from -13.7±3.8 to -17.6±4.4 befrore freeze-drying and -5.4±1.1 to -7.8±1.9 after freeze-drying. The obtained PDI values were below 0.15 and 0.25 before and after freeze-drying, respectively.

Table-5.4: Size, PDI and ZP of Doc (different concentrations) loaded NP formulations without BS3, freeze-dried with cryoprotectant (n=3)

NPs	Before freeze-drying			After freeze-drying		
	Mean Z-Ave (nm) ± SD	Mean PdI ± SD	Mean ZP (mV) ± SD	Mean Z-Ave (nm) ± SD	Mean PdI ± SD	Mean ZP (mV) ± SD
Plain+10% Suc	148.1±6.8	0.13±0.03	-10.6±2.3	242.9±11.4	0.16±0.02	-10.7±1.7
0.75 mg/ml Doc+10% Suc	141.1±3.8	0.12±0.03	-13.7±3.8	235.6±15.2	0.23±0.02	-5.4±1.1
1.5 mg/ml Doc+10% Suc	135.4±5.1	0.14±0.03	-14.2±1.3	302.1±8.5	0.19±0.01	-6.8±4.9
3 mg/ml Doc+10% Suc	133.6±3.6	0.14±0.02	-17.6±4.4	202.3±3.6	0.21±0.01	-7.8±1.9

A lower trend for average size range was found while increasing Doc concentration in drug loaded NP formulations when compared with that of the plain NPs. In BS3 free Doc loaded NP formulations, the surface charges were moved towards more negative with the increase of drug concentration used to prepare the NPs. After freeze-drying the drug-loaded formulations with cryoprotectant, the

surface charges shifted towards less negative compared to before freeze-drying. However, no significant differences were found after statistical analysis.

5.1.2.2. Effect of different Doc concentrations in NP formulations with BS3

Table-5.5 summarizes the data for BS3 included NP formulations containing Doc with various concentrations from 0.75 mg/ml to 3 mg/ml. The mean size of BS3 containing drug-loaded formulation was found in a range from 131.0±5.7 nm to 144.1±3.8 nm in the presence of 10% cryoprotectant, before freeze-drying. The size range after freeze-drying was found to be from 279.5±6.9 nm to 309.4±7.6 nm. The ZP values of these formulations varied from -12.9±1.9 to -17.1±2.5 befrore freeze-drying and -4.6±0.5 to -8.1±3.6 after freeze-drying. In fact, PDI values were found to be similar for all cryoprotectant-containing formulations before and after freeze-drying.

Table-5.5: Size, PDI and ZP of Doc (different concentrations) loaded BS3 included NP formulations freeze-dried with no cryoprotectant (n=3)

NPs	Before Freeze Drying			After Freeze Drying		
	Mean Z-Ave (nm) ± SD	**Mean PdI ± SD**	**Mean ZP (mV) ± SD**	**Mean Z-Ave (nm) ± SD**	**Mean PdI ± SD**	**Mean ZP (mV) ± SD**
Plain+BS3+10% Suc	132.3±3.9	0.12±0.02	-13.2±6.2	228.6±7.2	0.17±0.03	-4.8±2.3
0.75 mg/ml Doc+BS3+10% Suc	144.1±3.8	0.10±0.03	-12.9±1.9	279.5±6.9	0.19±0.02	-4.6±0.5
1.5 mg/ml Doc+BS3+10% Suc	135.0±5.5	0.14±0.04	-18.0±3.1	231.9±18.9	0.27±0.05	-7.9±3.4
3 mg/ml Doc+BS3+10% Suc	131.0±5.7	0.13±0.04	-17.1±2.5	309.4±7.6	0.19±0.02	-8.1±3.6

Similar trend of decreasing size of Doc loaded NPs was also observed with increasing the initial concentration of drug used in the BS3 included formulations. PDI values for the BS3 containing formulations and NPs without BS3 followed the similar trend. It indicates that BS3 inclusion as cross linking agent in the formulations may not affect the size distribution profile of this NP formulation strategy. In addition, surface charges of the BS3 containing drug loaded NP formulations were observed to be slightly more negative compared to the formulations with no BS3 before freeze-drying.

5.1.3. Effect of TmAb attachment to the NP formulations

Table-5.6 represents the physicochemical characteristics of TmAb modified NPs considering both methods of TmAb attachment: physical adsorption and covalent conjugation compared to the plain NPs. All the formulations in table-5.6 were freeze-dried with 10% cryoprotectant. Particle size ranges of TmAb modified NP formulations were from 313.4±12.8 to 374.3±57.3. PDI values of the NP formulations were found to be below 0.5 after TmAb conjugation. Surface charge of TmAb modified NPs was in range between + 3.2±0.5 mV and + 4.3±0.3 mV.

After TmAb conjugation with NPs, a significant increase in the average hydrodynamic diameter (300 - 450 nm) was observed. No significant change in terms of PDI values was shown after TmAb functionalization. Most importantly, a significant change in surface charge was observed for the NPs after TmAb attachment which shifted towards positive to nearly neutral. This indicates the presence of positively charged Ab on the NP surface.

Table-5.6: Size, PDI and ZP of TmAb modified Doc (different concentrations) loaded BS3 (1.5 mg) included NP formulations compared to BS3 excluded plain NPs, TmAb modified BS3 excluded plain NPs (n=10). All the NP formulations were freeze-dried with 10% cryoprotectant

Formulations	Before TmAb Conjugation			After TmAb Conjugation		
	Mean Z-Ave (d.nm) ± SD	Mean PdI ± SD	Mean ZP (mV) ± SD (mV)	Mean Z-Ave (d.nm)± SD	Mean PdI ± SD	Mean ZP (mV) ± SD (mV)
NP	148.1±6.9	0.13±0.03	-10.6±2.2	262.80±63.18*[a]	0.24±0.10[a]	-4.7±0.3*[a]
TmAb-NP	148.1±6.9	0.13±0.03	-10.6±2.2	362.30±70.73*	0.40±0.04	3.5±0.5*
TmAb-BS3-NP	145.1±4.8	0.12±0.05	-11.5±1.4	374.25±57.29*	0.33±0.15	4.3±0.3*
TmAb-BS3-Doc(0.75)-NP	131.0±5.7	0.13±0.04	-17.1±2.5	368.40±39.36*	0.38±0.24	4.1±0.6*
TmAb-BS3-Doc(1.5)-NP	135.0±5.5	0.14±0.04	-18.0±3.1	313.40±12.76*	0.25±0.06	3.2±0.5*
TmAb-BS3-Doc(3)-NP	144.1±3.9	0.10±0.03	-12.9±1.9	317.40±24.76*	0.44±0.12	4.1±0.4*

Formulation details

NP : Plain PLGA NP without Doc

TmAb-NP : TmAb attached plain NP with no BS3 (physical adsorption)

TmAb-BS3-NP : TmAb covalently attached with BS3 of plain NP

TmAb-BS3-Doc(0.75)-NP : Doc (0.75 mg/ml; initial concentration) loaded TmAb attached BS3 containing NP (covalent attachment)

TmAb-BS3-Doc(1.5)-NP : Doc (0.1.5 mg/ml; initial concentration) loaded TmAb attached BS3 containing NP (covalent attachment)

TmAb-BS3-Doc(3)-NP : Doc (3 mg/ml; initial concentration) loaded TmAb attached BS3 containing NP (covalent attachment)

* Statistically different from the nano-formulations before TmAb attachment

[a] Without TmAb attachment (for control) but maintained in same condition alike TmAb attachment

5.2. Drug loading and entrapment efficiency

Doc was used as a model drug and loaded into the PLGA NPs at various initial concentrations ranging from 0.75mg/ml to 3 mg/ml. In addition to the previously mentioned physicochemical characterization, the Doc loaded formulations were also assessed for their degree of drug loading and drug entrapment efficiency using mass spectrometry analysis.

5.2.1. Doc loaded NP formulations with no BS3

Doc concentrations of 0.75 mg/ml to 3 mg/ml were used to incorporate into the NPs, which were freeze-dried with 10% cryoprotectant. Table-5.7 summarizes the EE (%), drug loading (%), µg of drug/mg NPs, and µg of drug/mg NPs (theoretical) for all the NP formulations with no BS3 incorporation.

Table-5.7: Drug loading, EE (%) of the Doc (different concentrations) loaded BS3 excluded NP formulations freeze-dried with 10% cryoprotectant (n=3)

NPs	Drug Loading (µg/mg of NPs)	EE (%)	Yield (%)
0.75 mg/ml Doc+10% Suc	1.89±0.36	16.40±3.14	51.67±2.30
1.5 mg/ml Doc+10% Suc	4.02±0.02	17.42±0.09	46.01±8.66
3 mg/ml Doc+10% Suc	7.01±1.11	15.17±2.41	57.67±10.1

EE was measured to be in a range from 15.17±2.41 % to 17.42±0.09 % and the recovery of NPs after freeze-drying (yield) ranging from 46.01±8.66 % to 57.67±10.10 %. Amount of drug per mg of NPs (loading) was calculated to be in a range from 1.89±0.36 µg to 7.01±1.11 µg. Among the drug loaded formulations without BS3, drug concentration of 3 mg/ml demonstrated the lowest EE and 1.5 mg/ml showed the highest EE. Loading was calculated to be the highest for 3 mg/ml

and lowest for 0.75 mg/ml drug concentration. The yield of NP preparation was assessed to be below 50% for drug concentration of 1.5 mg/ml, however, the differences were not statistically significant.

5.2.2. Doc loaded NP formulations with BS3

To evaluate the effect of BS3 inclusion in drug loading, Doc concentrations of 0.75 mg/ml to 3 mg/ml were used to load into the BS3 containing NP formulations using cryoprotectant. Table-5.8 shows the EE (%), drug loading (%), µg of drug/mg NPs, and µg of drug/mg NPs (theoretical) for all the NP formulations with BS3.

Table-5.8: Drug loading, EE (%) of the Doc (different concentrations) loaded BS3 included NP formulations freeze-dried with 10% cryoprotectant (n=3)

NPs	Drug Loading (µg/mg of NPs)	EE (%)	Yield (%)
0.75 mg/ml Doc+BS3+10% Suc	3.11±0.15	26.98±1.30	42.33±3.21
1.5 mg/ml Doc+BS3+10% Suc	3.31±0.52	15.64±0.55	51.67±8.08
3 mg/ml Doc+BS3+10% Suc	7.13±0.89	15.44±1.94	52.33±10.69

Table-5.8 shows that EE was found in a range from 15.44 ± 1.94 % to 26.98 ± 1.30 % with the yield of NPs after freeze-drying varried from 42.33±3.21 % to 52.33±10.69 %, respectively. Around 3.11±0.15 µg/mg to 7.13±0.89 µg/mg of the drug was loaded into NPs depending on the initial concentration of the drug used. Lowest EE was reported with the NP formulation with drug concentration of 3 mg/ml and hightest EE was found with the drug concentration of 0.75 mg/ml. However, higher loading was found for for the NP formulations with 3 mg/ml drug concentration and lowest was for 0.75 mg/ml drug concentration. The concentration

of 0.75 mg/ml after freeze-drying the NPs showed the lowest yield of NP preparation, which was less than 50 %.

Figure-5.1 and figure-5.2 represent the the statistical analysis after one-way ANOVA analysis of variances based on the results of drug loading per mg of NPs and drug EE in table-5.7 and table-5.8. NP formulation of 0.75 mg/ml drug concentration was found with statistically moderate significant difference between same drug concentration groups (with and without BS3). But, no statistically significant differences were found between the other drug loaded NP formulations of similar drug concentration groups. Similar trend was also observed for the drug EE of all Doc loades NP formulations.

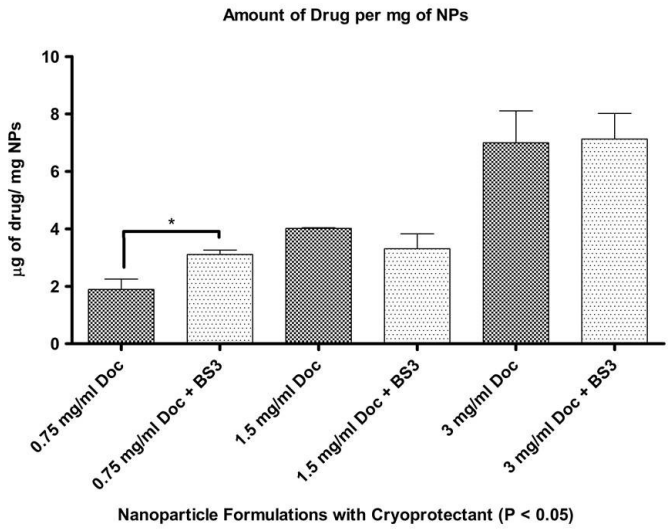

Figure-5.1: Comparative drug loading of Doc loaded NP formulations with different drug concentrations (n=3). 10% cryoprotectant was used in all the formulations. The statistical significances between the groups were represented by indicating the encompassed lines with the number of (*) sign. The level of significance was set to $p < 0.05$ (one-way ANOVA followed by Tukey's multiple comparison test method). Each bar represents the mean % ± SD (n=4)

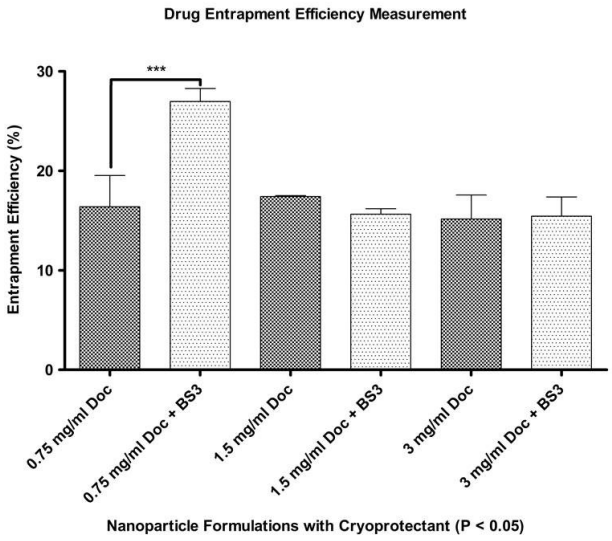

Figure-5.2: Comparative drug loading efficiency of NP formulations with different drug concentrations (n=3). 10% cryoprotectant was used in all the formulations. The statistical significances between the groups were represented by indicating the encompassed lines with the number of (*) sign. The level of significance was set to $p < 0.05$ (one-way ANOVA followed by Tukey's multiple comparison test method). Each bar represents the mean % ± SD (n=4)

Compare to theoretical amount of drug to be loaded per mg of NPs, practically loaded amount of drug into the NPs was found very low. The loaded amount of drug into the NPs and EE were found correlated where the increase in initial drug concentration resulted with reduced EE and vice versa.

5.3. TmAb quantification

Both physically adsorption (without BS3) and covalent attachment (with BS3) methods were employed to conjugate TmAb with the NPs. The desired NP formulations for TmAb modification were evaluated for their level of TmAb attachment.

5.3.1. Effect of different amounts of BS3 in the plain NP formulations with constant amount of Ab

To measure the efficiency of NPs for TmAb binding, different BS3 amounts were incorporated to prepare the plain NPs. A constant amount of TmAb was used for all the formulations. Table-5.9 shows the comparative TmAb attachment per mg of NPs, when Tm Ab is attached by physical absorption (TmAb-NP) or covalent conjugation (TmAb-BS3-NP). No significant increase in TmAb attachment was observed with increasing BS3 amounts in the formulations.

Table-5.9: Comparative amounts of TmAb attachment and binding efficiency after incubation of same amount of TmAb to the different amounts of BS3 in the NP formulations freeze-dried with 10% cryoprotectant (n=10)

NP formulations	TmAb attached/mg of NPs (µg) ±SD	TmAb attachment efficiency (%)* ±SD
TmAb-NP	5.93±0.64	47.41±5.14
TmAb-BS3(1.5)-NP	7.19±0.80	57.47±3.21
TmAb-BS3(3)-NP	4.86±0.71	38.87±5.67
TmAb-BS3(6)-NP	1.71±0.38	13.67±3.02
TmAb-BS3(9)-NP	3.49±0.77	27.94±6.12

$* \text{ TmAb attachment efficiency (\%)} = \left(\frac{\text{Ab attached per mg of NP}}{\text{Initial amount of Ab used}}\right) \text{X } 100$

* Fixed amount of TmAb treated per mg of NPs = 12.5µg
* TmAb is physically absorbed to the NPs (TmAb-NP)
* Various amounts of BS3 used to prepare NPs ranges from 1.5 to 9mg (TmAb-BS3-NP)
* Condition for the TmAb attachment: 4°C

Higher TmAb attachment efficiency was found when a lowest amount of BS3 was used in the formulation although comparible attachment efficiency was observed between adsorption and covalent conjugation.

5.3.2. Effect of different amounts of TmAb and BS3 on the plain NP formulations

In order to optimize the TmAb modified NPs, different TmAb amounts were considered to incubate with the different amounts of BS3 containing plain NPs. Table-5.10 shows the comparative TmAb attachment amount and attachment efficiency per mg of NPs.

Table-5.10: Comparative amounts of TmAb attachment and binding efficiency after incubation of different amounts of TmAb to the different amounts of BS3 in the NP formulations freeze-dried with 10% cryoprotectant (n=10)

NP formulations	TmAb attached/mg of NPs (µg) ±SD	TmAb attachment efficiency (%)* ±SD
TmAb(125)-NP	2.67±0.31	42.94±5.01
TmAb(125)-BS3(1.5)-NP	3.07±0.23	47.94±3.72
TmAb(250)-BS3(3)-NP	5.82±0.29	46.57±2.32
TmAb(500)-BS3(6)-NP	10.93±0.62	43.71±2.48
TmAb(500)-BS3(9)-NP	11.46±0.65	45.85±2.58

$* \text{ TmAb attachment efficiency } (\%) = \left(\frac{\text{Ab attached per mg of NP}}{\text{Initial amount of Ab used}}\right) \text{X } 100$

* Various amount of TmAb treated per mg of NPs ranges from 125µg to 500ug

* Various amounts of BS3 used to prepare NPs ranges from 1.5mg to 9mg

* Condition for the Ab attachment 4°C

5.3.3. Effect of various conjugation conditions for attaching TmAb to the Doc-loaded NPs

In order to obtain an optimum TmAb attachment efficiency, two types of

conjugation conditions were also considered such as 4°C and room temperature. Table-5.11 shows the comparative TmAb attachment amount and efficiency to the NPs.

Table-5.11: Comparative amounts of TmAb attachment and binding efficiency after incubation of fixed amount of TmAb to the fixed amount of BS3 in the Doc loaded NP formulations freeze-dried with 10% cryoprotectant (n=10)

NP formulations	TmAb attached per mg of NP (µg) ±SD		TmAb attachment efficiency (%)* ±SD	
	At 4°C	At room temperature	At 4°C	At room temperature
TmAb-NP	6.32±1.34	14.09±1.46	29.50±6.26	46.95±4.88
TmAb-(1.5)BS3-NP	6.66±1.12	19.12±1.14	31.06±5.21	63.73±3.79
TmAb-(1.5)BS3-Doc(0.75)-NP	4.16±1.18	11.02±1.1	19.39±5.51	36.73±5.70
TmAb-(1.5)BS3-Doc(1.5)-NP	3.39±1.22	8.42±1.95	15.83±5.70	28.06±6.51
TmAb-(1.5)BS3-Doc(3)-NP	3.77±1.20	12.05±1.39	17.61±5.62	40.17±4.63

$* \text{ TmAb attachment efficiency (\%)} = \left(\frac{\text{Ab attached per mg of NP}}{\text{Initial amount of Ab used}}\right) \text{X } 100$

* Amount of TmAb treated per mg of NPs = 30µg

* Amount of BS3 used to prepare NPs = 1.5 mg

Although covalent method showed higher attachment efficiency with drug free NPs than adsorption method, however it was not equially potential to attach in case of drug loaded NPs in both incubation conditions. However, the percentage of TmAb attachment efficiency was found higher at room temperature incubation condition. Considering room temperature as a standard condition to attach TmAb with all NP formulations, no significant difference was observed after assaying TmAb attachment levels.

5.4. Identification of the covalent bond between TmAb and BS3 (embedded into NPs)

After attaching TmAb with NPs covalently, it is important to confirm the structural integrity of targeting ligand as well as the chemical conjugation. This is an essential factor in order to get maximum targeting efficiency. To confirm the covalent bond and structural integrity of TmAb modified NPs, two experiments were designed such as FTIR spectroscopy and SDS-PAGE.

5.4.1. Identification of covalent bond with FTIR

A marked peak at the wavelength of 1750 cm^{-1} elicits the presence of a carbonyl bond (C=O stretching vibration) which represents the characteristic of PLGA (95). Ideally, at the wavelength of near 1640 cm^{-1}, an amide bond (C=N stretching vibration) can be identified for the presence of the covalent conjugation between PLGA NPs and Ab. According to figure-5.3(A), a clear peak spectra at the wavelength of 1650 cm^{-1} represents the presence of covalent amide bond for the TmAb modified PLGA NP, which corresponds to another C=O stretching bond on both components. However, this corresponding stretching bond does not allow to draw a concrete conclusion for the covalent conjugation of the NPs (96). In addition, the presence of N-H stretching at the wavelength of 3400 cm^{-1} shows comparatively higher intensity for the modified NPs than the plain and unmodified NPs. This stretched peak spectrum can be considered to differentiate TmAb modified NPs from the unmodified one. Figure-5.3(B) represents the secondary derivative for the spectrums in figure-5.3(A) to visualize the peak for claimed amide bond (black spectra) more closely which was different from other two spectrums.

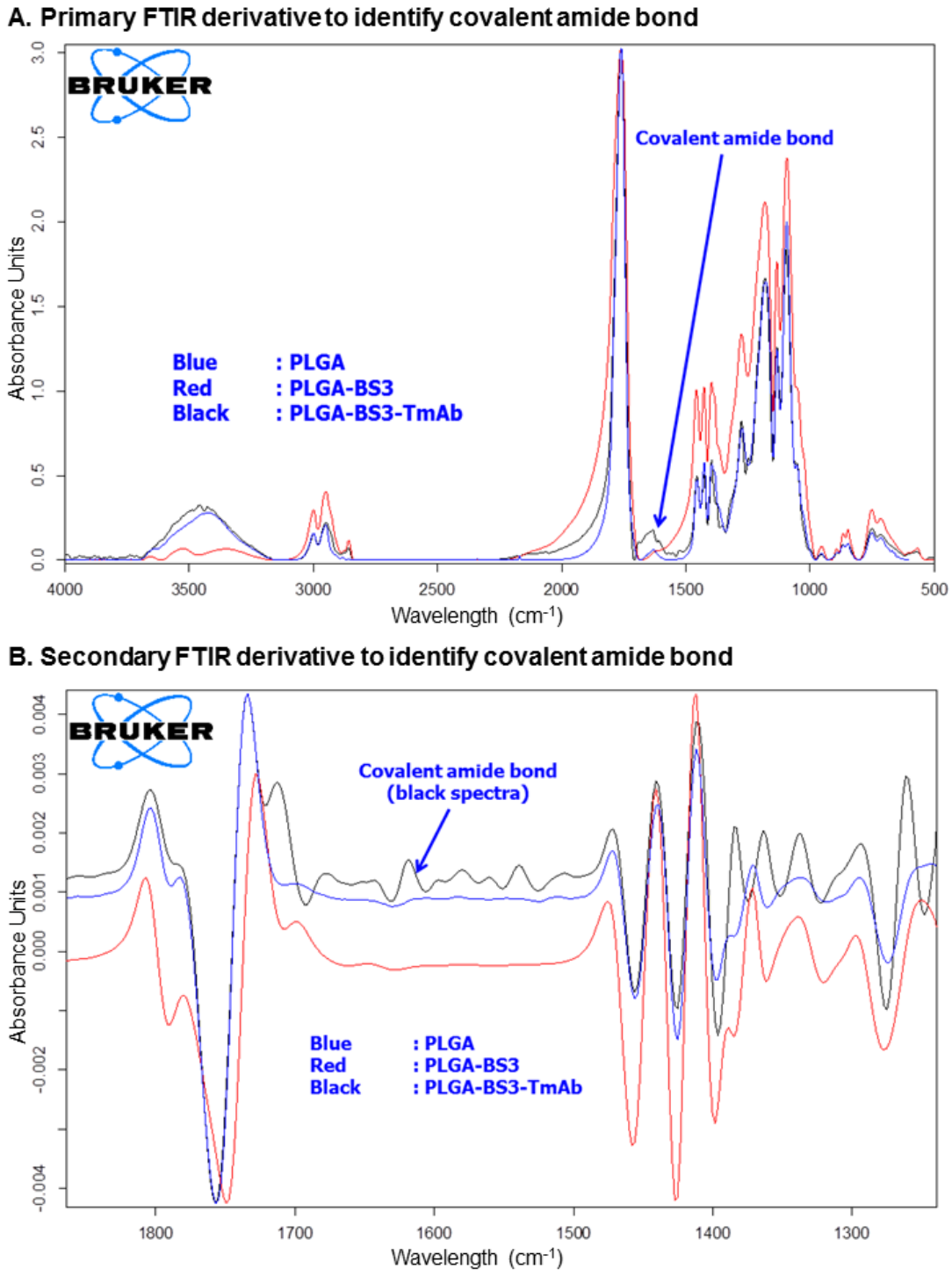

Figure-5.3: Primary and secondary FTIR derivative spectra of (a) 0.15 Ester terminated PLGA NPs without BS3 (green), (b) BS3 containing 0.15 Ester terminated PLGA NPs (blue) and (c) BS3 containing 0.15 Ester terminated TmAb modified PLGA NPs (red). Data is represented in absorbance units versus wavelength (cm^{-1})

5.4.2. Identification of covalent bond with SDS-PAGE

To confirm the covalent conjugation between TmAb and BS3 linked NPs, SDS-PAGE study was also designed. As a protein, TmAb may turn into inactive state during conjugation with pre-activated NPs due to agglomeration or denaturation. To analyze the structural integrity and stability of TmAb, SDS-PAGE experiment was carried out after proper extraction from the functionalized NPs.

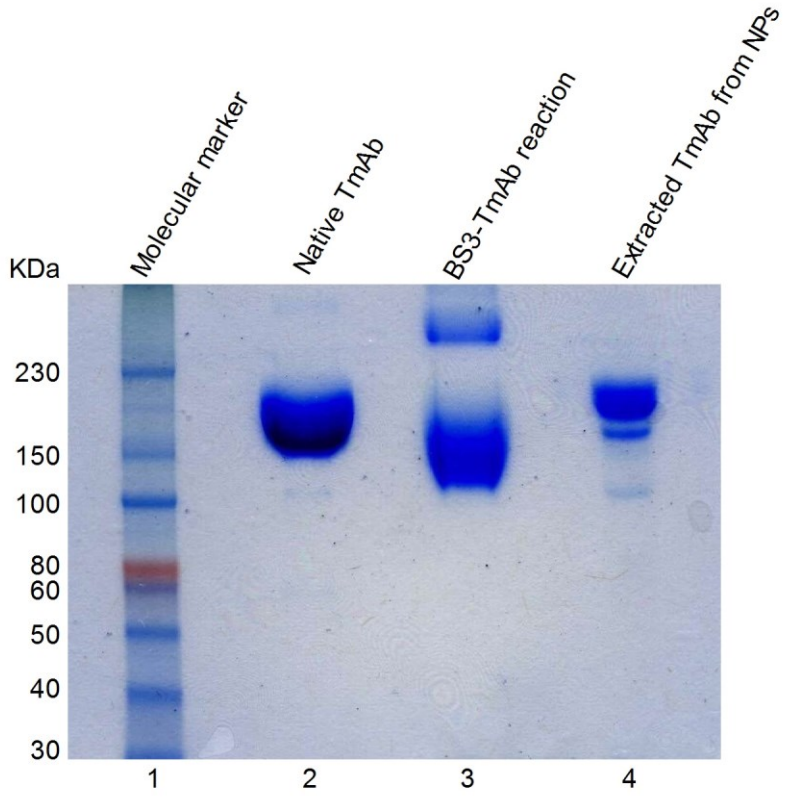

Figure-5.4: SDS-PAGE for covalent bond between TmAb and BS3 linked NPs: Lane 1 is for the molecular marker (Color Plus Prestained Protein Ladder); Lanes 2 to 4 are for native TmAb, BS3-TmAb reaction, and extracted TmAb from NPs respectively

Figure-5.4 shows the SDS-PAGE analysis for native TmAb, reaction between and TmAb, and extracted TmAb under non-reduced and denatured condition as the molecular weight of the mAb is quite high (148 kDa). From the figure-5.4, it can be concluded that TmAb remains similar after conjugated with NPs

(lane-2 and lane-4). To confirm the covalent bond between BS3 and TmAb, lane-3 shows two separate bands. One band of those reflects the same as native TmAb confirming the unreacted TmAb with BS3 in presence of phosphate buffer saline (PBS) and the other band (top, lane-3) is above 230 kDa since both arms of homo-bi-functional cross-linker successfully reacted with TmAb to increase the molecular weight. Thus the confirmation of covalent reaction between mAb and cross-linker validates the feasibility of formulating targeted chemotherapeutic drug delivery system for HER2 overexpressed breast cancer.

5.5. Quantification of Coum-6 in NPs

To quantify the amount of Coum-6 in plain NP formulations, the dye loaded NPs were dissolved in methanol and kept overnight in dark place. Then the fluorescence intensity was measured at the emission wavelength of 505 nm using a fluorescent spectrophotometer with a micro-plate reader.

5.5.1. Standard curve for Coum-6

A concentration range from 1µg/ml to 100µg/ml was used to prepare the standard curve of Coum-6 in an organic solvent, methanol. A micro-plate reader containing fluorescence spectrophotometer (Biotek's Synergy Gen 5) was used to measure the fluorescence intensity of the samples. The excitation and emission wavelength were 443 nm and 505 nm, respectively. Figure-5.5 shows the standard curve of Coum-6 in methanol. Table-5.12 shows the loading and EE of Coum-6 using the respective standard curve.

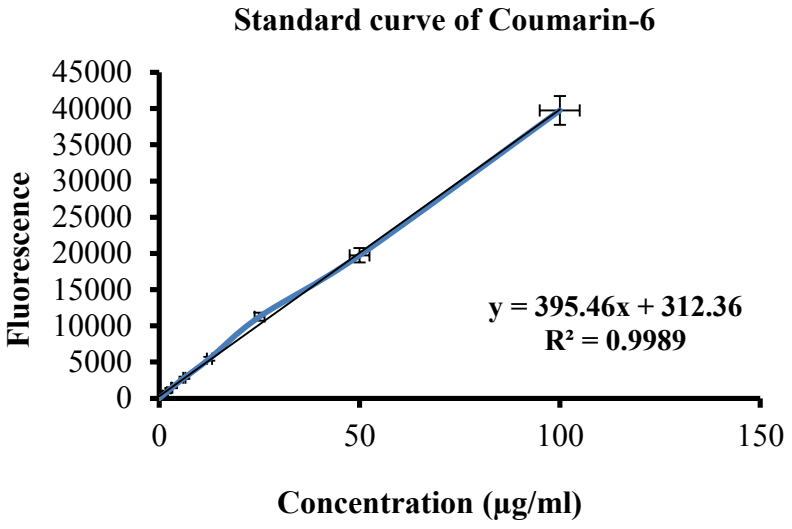

Figure-5.5: Standard curve of Coum-6

5.5.2. Coum-6 loading and EE into the plain NP formulations

Table-5.12: Coum-6 loading and EE for different formulations

NP formulations	Coum-6 loading (μg/mg)±SD	EE of Coum-6 (%)±SD
NP (Coum-6)	19.21±1.05	83.23±1.89
TmAb-NP (Coum-6)	20.23±1.78	81.13±2.66
TmAb-BS3-NP (Coum-6)	22.13±1.74	75.35±1.37

To simulate the internalization efficiency of drug loaded targeted NPs, Coum-6 loaded targeted NPs were considered. Coum-6 loading per mg of NPs was found in a range from 19.21±1.05 μg/mg to 22.13±1.74 μg/mg with EE range from 75.35±1.37% to 83.23±1.89%. Similar loading tendency was observed in Doc loaded NPs. However, the loading and EE of Coum-6 into the PLGA NPs were found comparatively higher than the drug loaded NP formulations.

5.6. Uptake study

Cell uptake of NPs was evaluated in two cell lines: MCF-7 (HER2 moderate expressing) and SKBR-3 (HER2 overexpressing). Flow cytometry experiments and CLSM were conducted to observe the uptake effects. In addition, dot plots and histograms were represented to show the difference in NPs uptake for non-targeted and targeted Coum-6 loaded plain NPs.

5.6.1. Uptake study by flow cytometry

5.6.1.1. Cellular uptake without pre-incubation with TmAb

5.6.1.1.1. Coum-6 loaded NPs uptake in MCF-7 cells

Uptake of NPs by MCF-7 cells was conducted utilizing Coum-6 loaded NPs. The detector was selected based on the absorption/emission wavelength of Coum-6 dye. The experiments were repeated four times using the same setting with a minimal adjustment. Figure-5.6 shows the dot plots and histograms for the untreated MCF-7 cells and treated MCF-7 cells with Coum-6 loaded plain NPs, TmAb modified NPs and BS3 containing TmAb modified NPs. Only 1.5% gated population was accounted to have fluorescence in the untreated cell group. A gate was used to accumulate the signal of fluorescence from 10,000 cell population. This number was selected based on flow cytometry experiment done in our previous studies and other papers. A shift in fluorescence is evident from the histograms.

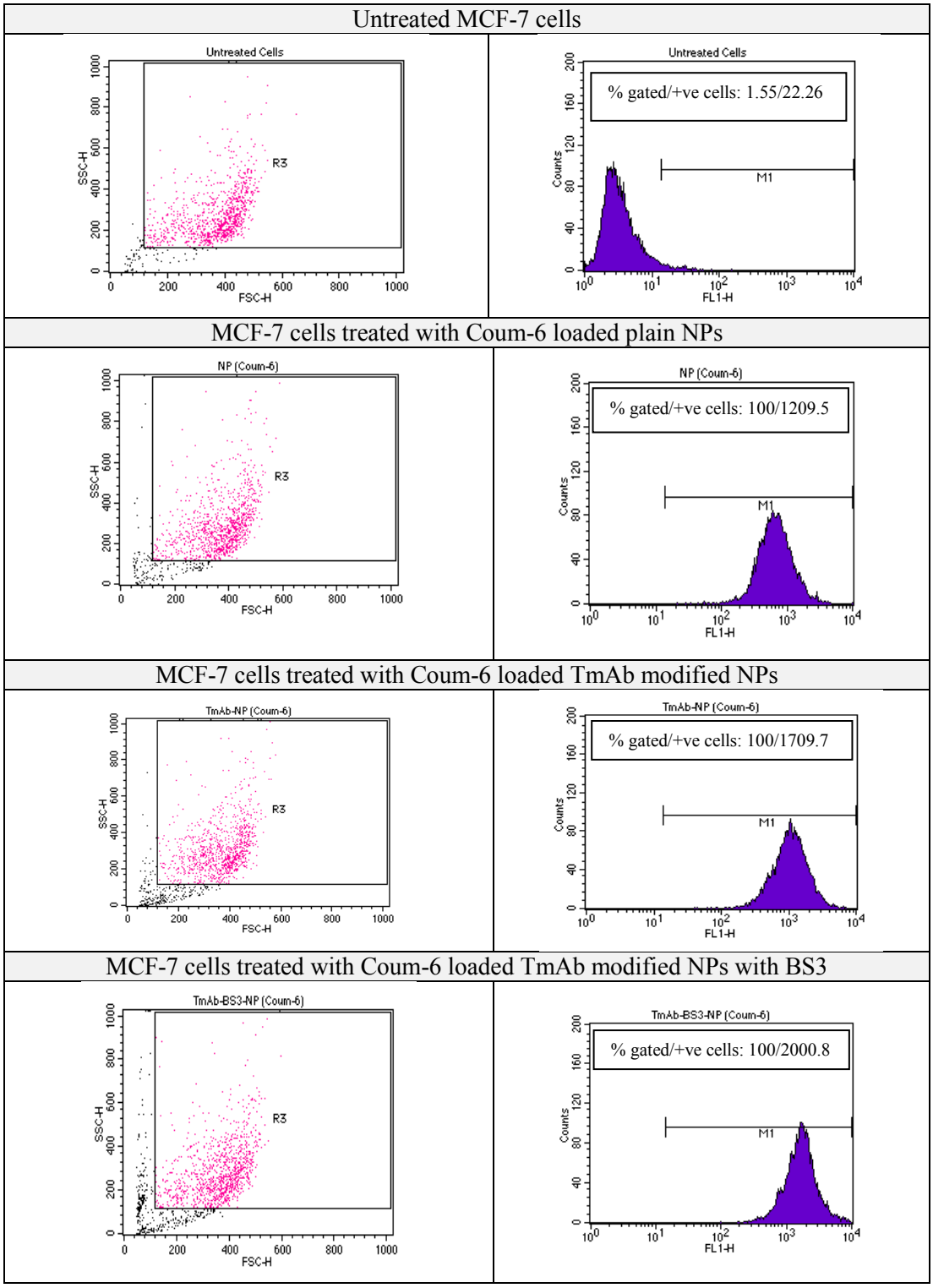

Figure-5.6: Dot plots and histograms for untreated MCF-7 cells and treated MCF-7 cells with Coum-6 loaded loaded plain NPs, TmAb modified NPs and BS3 containing TmAb modified NPs (n=4)

The difference between untreated and treated MCF-7 cells was more prominent, when the graphs obtained from the histograms were overlapped in the figure-5.7. A comparative difference in uptake can be visualized from the diagram.

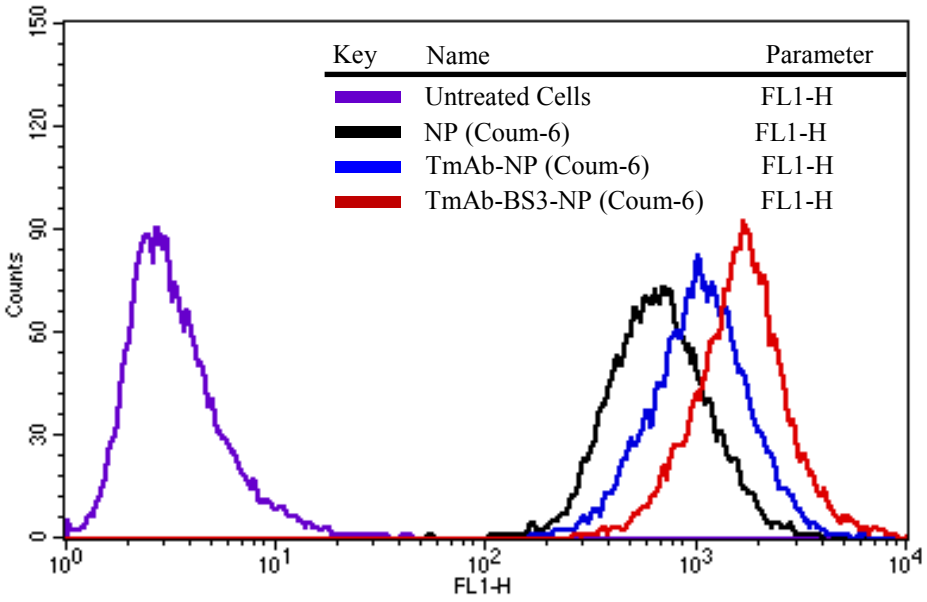

Figure-5.7: Overlayed histogram for untreated MCF-7 cells and the MCF-7 cells treated with Coum-6 loaded unmodified plain NPs, TmAb modified NPs, BS3-TmAb modified NPs (n=4)

For TmAb modified Coum-6 loaded NPs, significant shifts in fluorescence were found which is comparatively higher than that of plain Coum-6 loaded NP formulations. Also, covalently attached TmAb showed better uptake by the MCF-7 cells as indicated in figure-5.7 (redline histogram).

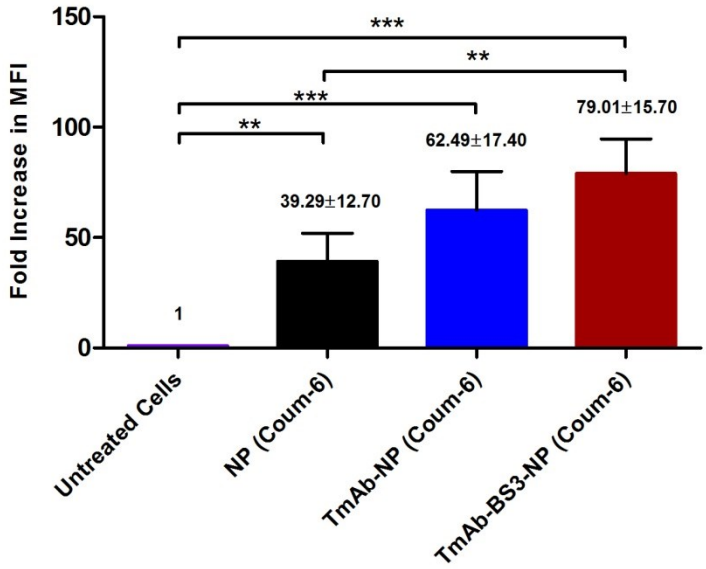

Figure-5.8: Bar diagram indicating the fold increase of MFI for untreated MCF-7 cells and the MCF-7 cells treated with Coum-6 loaded unmodified plain NPs, TmAb modified NPs, BS3-TmAb modified NPs. Fold increase was calculated considering MFI of untreated cells as control. The statistical significances between the groups were represented by indicating the encompassed lines with the number of (*) sign. The level of significance was set to $p < 0.05$ (one-way ANOVA followed by Tukey's multiple comparison test method). Each bar represents the mean % ± SD (n=4)

The fold increase in mean fluorescence intensity (MFI) is shown in figure-5.8. The difference in MFI indicates that Coum-6 loaded NPs were taken by cells. Figure-5.8 represents that the plain NPs showed 39.29±12.7 fold increase in uptake when compared with untreated cells. When TmAb was present in the formulation, the uptake increased 62.49±17.4 and 79.01±15.7 folds for TmAb-NPs and TmAb-BS3-NPs, respectively.

5.6.1.1.2. Coum-6 loaded NPs uptake in SKBR-3 cells

Figure-5.9 shows the dot plots and histograms for the untreated SKBR-3 cells and treated SKBR-3 cells with Coum-6 loaded plain NPs, TmAb modified NPs and BS3 containing TmAb modified NPs, respectively.

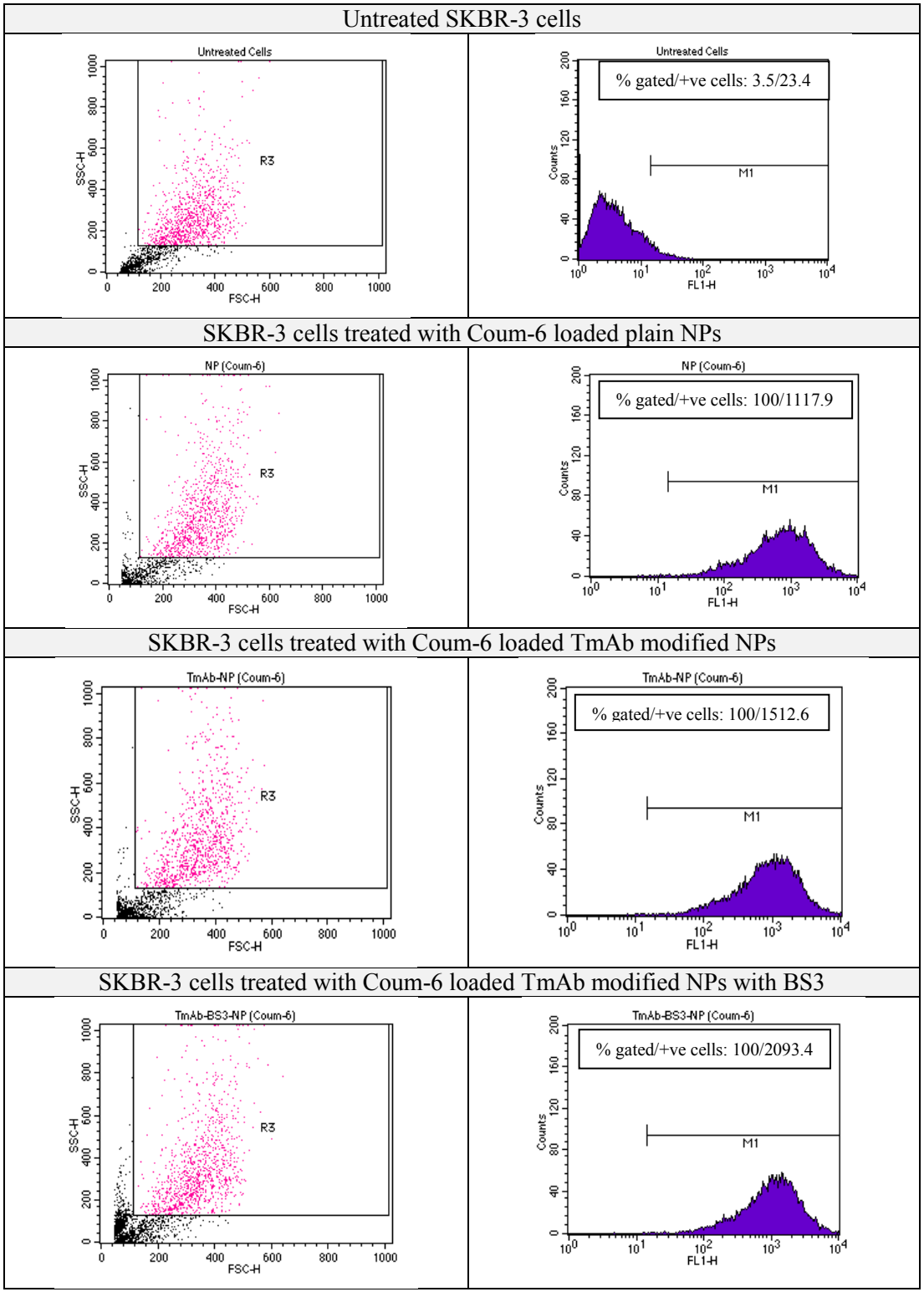

Figure-5.9: Dot plots and histograms for untreated SKBR-3 cells and treated SKBR-3 cells with Coum-6 loaded loaded plain NPs, TmAb modified NPs and BS3 containing TmAb modified NPs (n=4)

Following the treatment of SKBR-3 cells with Coum-6 loaded different NP formulations, a shift in the fluorescence was observed. Untreated cells showed an auto-fluorescence with the MFI of 2.34, which was accounted as the background (figure-5.9). An MFI value above background was considered the fluorescence. The uptake of plain and modified NPs showed significant difference in fluorescence intensity. Shifts in the fluorescence with TmAb modified NPs were significantly notable after treating with SKBR-3 cells. The uptake of covalently attached TmAb modifie Coum-6 loaded NPs by SKBR-3 cells was prominent compared to unmodified and physically TmAb attached NPs.

Overlaying the histograms as shown in figure-5.10 further clarifies the justification of formulating targeted NPs as opposed to non-targeted. Similar trend for the shifts in fluorescence was observed as found with the treatment of NPs in of MCF-7 cells. However, the MFI found with SKBR-3 cells was comparatively higher in comparison to the MFI observed for MCF-7 cells.

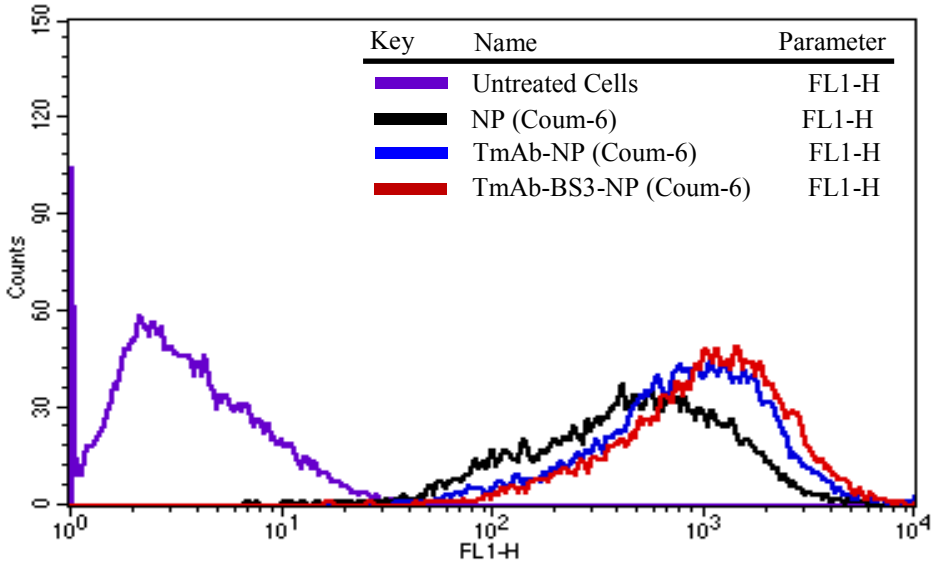

Figure-5.10: Overlayed histogram for untreated SKBR-3 cells and the SKBR-3 cells treated with Coum-6 loaded unmodified plain NPs, TmAb modified NPs, BS3-TmAb modified NPs (n=4)

Figure-5.11 shows the relative fold increase in MFI for the untreated SKBR-3 cells, Coum-6 containing plain NPs, TmAb modified NPs, BS3-TmAb modified NP treatment groups. The TmAb modified formulations showed higher fold increase in MFI compared to the plain NPs. The fold increase in MFI for plain NPs were 47.77±14.01. Whereas, the fold increase in MFI for the TmAb modified NPs, BS3-TmAb modified NPs were 64.64±20.21 and 89.47±34.4 times, respectively.

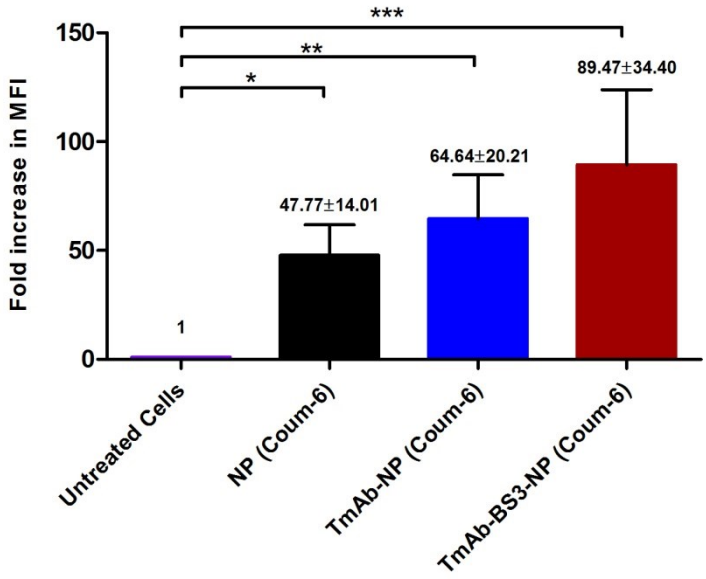

Figure-5.11: Bar diagram indicating the fold increase of MFI for untreated SKBR-3 cells and the SKBR-3 cells treated with Coum-6 containing plain NPs, TmAb modified NPs, BS3-TmAb modified NPs. Fold increase was calculated considering MFI of untreated cells as control. The statistical significances between the groups were represented by indicating the encompassed lines with the number of (*) sign. The level of significance was set to $p < 0.05$ (one-way ANOVA followed by Tukey's multiple comparison test method). Each bar represents the mean % ± SD (n=4)

In case of both celly types before TmAb preincubation, covalently TmAb modified NPs showed the derscernable shifts in fluorescence compared to unmodified NPs as well as physically adsorbed TmAb modified NPs. However, covalent attachment of the ligand to the NPs was not found to significantly improve the cellular uptake in comparison to the NPs that were physically attached with the ligand.

5.6.1.2. Cellular uptake after TmAb preincubation

5.6.1.2.1. Coum-6 loaded NPs uptake in TmAb preincubated MCF-7 cells

In this experiment, HER2 moderate expressed MCF-7 cells were incubated with TmAb before treatment with different types of Coum-6 loaded NPs and then continued as stated above. Figure-5.12 represents the comparative fold increases in

MFI for TmAb preincubated untreated MCF-7 cells and the preincubated cells treated with Coum-6 containing plain NPs, TmAb modified NPs, BS3-TmAb modified NPs. After 24 hrs incubation with respective NPs, non-specific cell uptake of TmAb free Coum-6 loaded NPs was reported with 46.72±6.02 folds increase in MFI for MCF-7 cells which was found in similar range as reported with same NPs uptake without TmAb preincubation. However, treatment with TmAb modified Coum-6 loaded NPs showed a slight reduction in uptake for the physically adsorbed (62.98±13.73 MFI) and covalently attached (68.46±8.49 MFI) TmAb modified coumarin-6 loaded NPs compared to the relative MFI found for the treatment gourps with no TmAb preincubation.

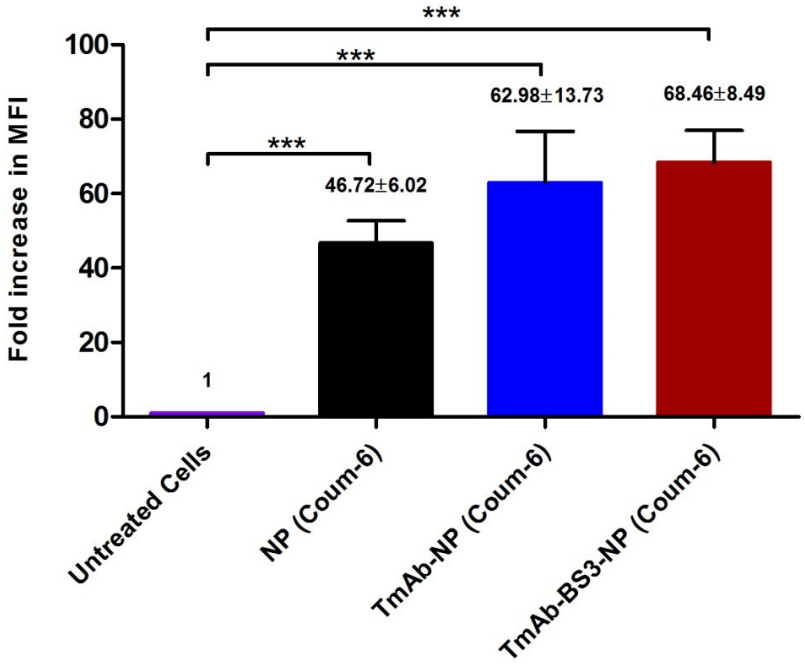

Figure-5.12: Bar diagram indicating the fold increase of MFI for TmAb preincubated untreated MCF-7 cells and the TmAb preincubated MCF-7 cells treated with Coum-6 containing plain NPs, TmAb modified NPs, BS3-TmAb modified NPs. Fold increase was calculated considering MFI of untreated cells as control. The statistical significances between the groups were represented by indicating the encompassed lines with the number of (*) sign. The level of significance was set to $p < 0.05$ (one-way ANOVA followed by Tukey's multiple comparison test method). Each bar represents the mean % ± SD (n=4)

5.6.1.2.2. Coum-6 loaded NPs uptake in TmAb preincubated SKBR-3 cells

Similarly, HER2 overexpressed SKBR-3 cells were preincubated with TmAb and then treated with different types of Coum-6 loaded NPs treatment. Figure-5.13 shows the relative fold increases in MFI for TmAb preincubated untreated SKBR-3 cells and the preincubated cells treated with different NPs.

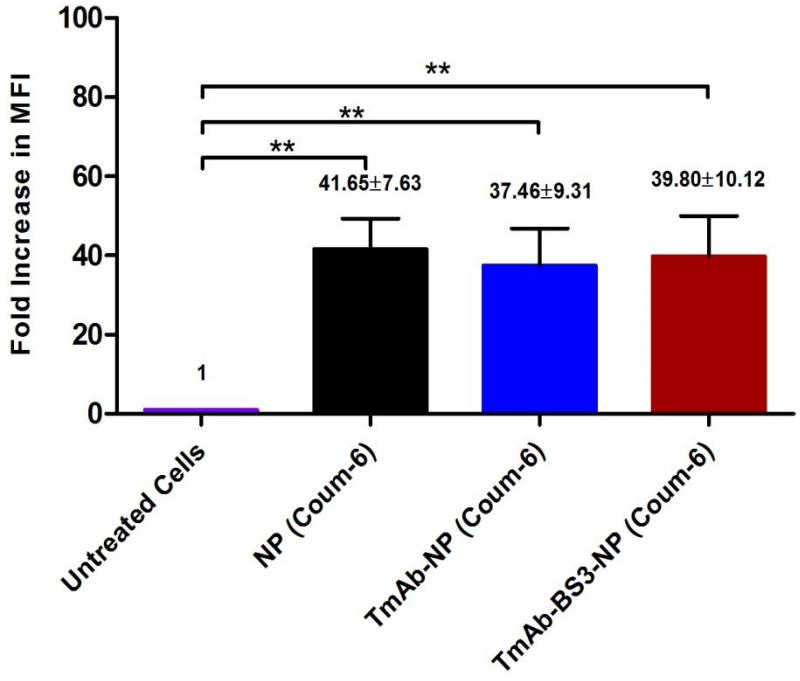

Figure-5.13: Bar diagram indicating the fold increase of MFI for TmAb preincubated untreated SKBR-3 cells and the TmAb preincubated SKBR-3 cells treated with Coum-6 containing plain NPs, TmAb modified NPs, BS3-TmAb modified NPs. Fold increase was calculated considering MFI of untreated cells as control. The statistical significances between the groups were represented by indicating the encompassed lines with the number of (*) sign. The level of significance was set to $p < 0.05$ (one-way ANOVA followed by Tukey's multiple comparison test method). Each bar represents the mean % ± SD (n=4)

Non-specific cell uptake of TmAb free Coum-6 loaded plain NPs was found with 41.65±7.63 folds increase for TmAb preincubated SKBR-3 cells after 24 hrs incubation which followed the similar range as reported with same NPs uptake without TmAb preincubation. However, fold increases in MFI for both [TmAb-NP

(Coum-6)] and [TmAb-BS3-NP (Coum-6)] were reduced significantly to 37.46±9.31 MFI and 39.80±10.12 MFI after preincubation of SKBR-3 cells with TmAb.

The fold increases in MFI for both [TmAb-NP (Coum-6)] and [TmAb-BS3-NP (Coum-6)] were reduced significantly after preincubation of HER2 overexpressed cells with TmAb after 24 h incubation. However, non-specific cell uptake of TmAb free Coum-6 loaded NPs in both cells was found in a similar range as reported with same NPs uptake without TmAb preincubation. In addition, HER2 moderate expressed cells showed comparatively higher uptake for modified NPs compared to HER2 overexpressed cell lines in both conditions. Finally in both cell types, the overall uptake of TmAb modified NPs was declined after TmAb preincubation except unmodified NPs. This indicates a lack of selective binding receptors that were already saturated by TmAb preincubation.

5.6.2. Uptake study by CLSM

The cellular uptake of NPs in MCF-7 and SKBR-3 cells was further investigated by CLSM to visualize the internalization of NPs into the cell cytoplasmic region and confirm the targeting efficiency of TmAb of the NPs. CLSM images provided actual scenario of cellular uptake for Coum-6 loaded PLGA NPs with and without TmAb conjugation in SKBR-3 and MCF7 cells after 24 hrs incubation. The nuclei of cells were stained blue with DAPI while the NPs consisted green fluorescence due to the emission produced by Coum-6 dye. Figure-5.14 listed all the merged images of both channels, where row-A and row-B represent the cellular uptake in SKBR-3 and MCF-7 cells, respectively after treating with Coum-6 loaded plain, physically, and covalently attached TmAb modified NPs.

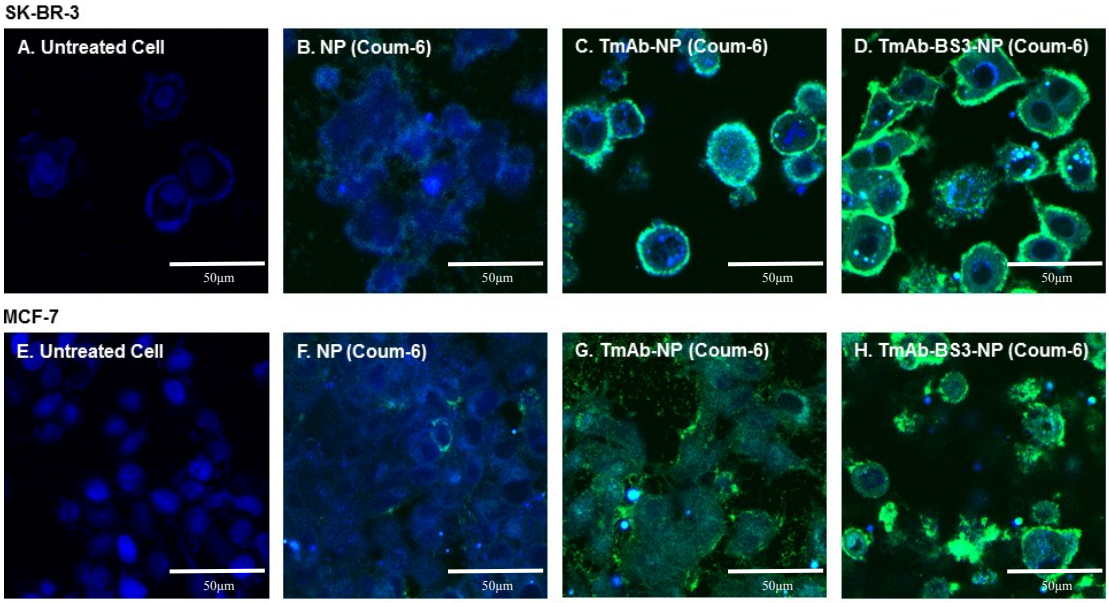

Figure-5.14: Representative overlapped CLSM images for the cellular uptake of fluorescent Coum-6 loaded NPs with and without TmAb conjugation comparing untreated cells. Upper (A, B, C, and D) and lower (E, F, G, and H) rows are for HER2 overexpressed SKBR-3 and HER2 moderate expressed MCF-7 cells respectively. Blue color represents the DAPI stained nuclei which are encompassed by green fluorescence for the groups treated with Coum-6 loaded NPs. All iImages' magnification objectives: A-Apochromal 63x/1.2 W corr.

5.7. HER2 Expression

To measure the amount of HER2 expression on HER2 dependent cells after treating with different formulations; flow cytometry, western blot and fluorescence microscopic studies were performed.

5.7.1. Flow cytometry study

The main purpose of staining all the cell groups with anti-HER2 FITC Ab was to quantify the amount of free HER2 receptor remaining on the cell surface after treatment with different formulations.

5.7.1.1. Effect of incubation time for treating the cells with different formulations

Incubation time for the treatment of cells with different formulations is an important parameter to evaluate the HER2 expression on the cells. Both cell types were treated with the formulations for 24 and 48 hrs.

5.7.1.1.1. HER2 expression in MCF-7 cells

Primarily, HER2 moderate expressed (MCF-7) cells were treated with TmAb modified plain NPs and various amounts of filtered TmAb for 24 and 48 hrs. Figure-5.15 shows the relative MFI of MCF-7 cells for different treatment groups according to the time of incubation. Similar expression levels for HER2 were observed after 24 hrs treatment. However, the level of HER2 expression was found to be higher after 48 hrs incubation compared to 24 hrs incubation with the formulations. In addition,

the treatment of cells with the formulations for 48 hrs were found to lower the HER2 expression compared to untreated cells that were stained with anti-HER2 FITC Ab.

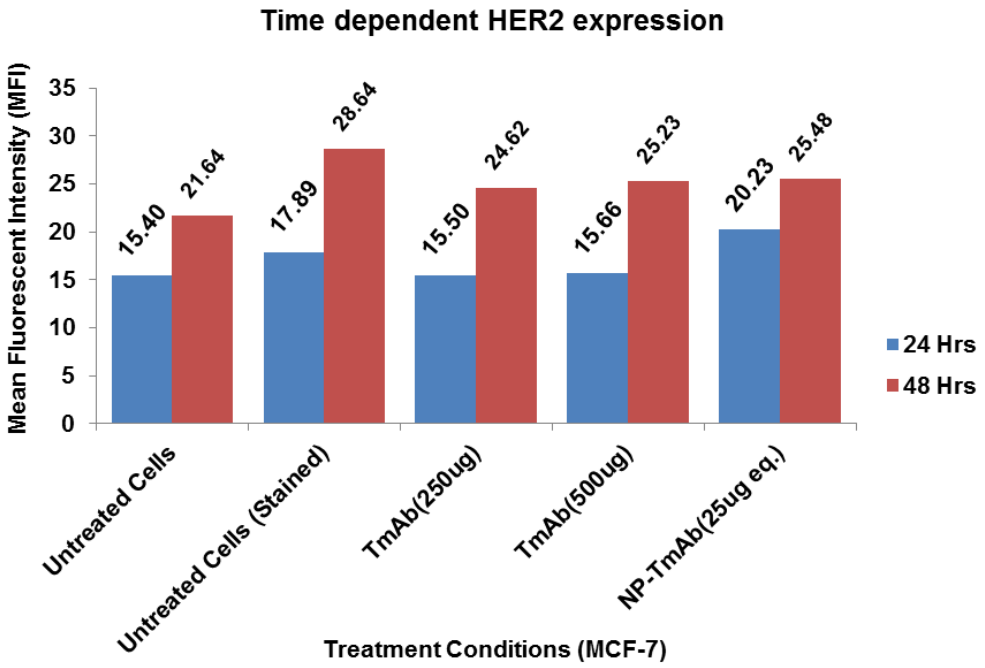

Figure-5.15: Time dependent HER2 expression of MCF-7 cells for different treatment groups (n=2)

5.7.1.1.2. HER2 expression in SKBR-3 cells

Following the same treatment conditions as MCF-7 cells, HER2 overexpressed SKBR-3 cells were also treated with different amounts of filtered TmAb and TmAb modified plain NPs for 24 and 48 hrs. As observed in figure-5.16, nearly similar HER2 expression levels were observed for different treatments after 24 hrs incubation. Higher HER2 expression levels were observed after 48 hrs incubation compared to 24 hrs. However, less HER2 expression was observed after 48 hrs treatments of cells with the formulations.

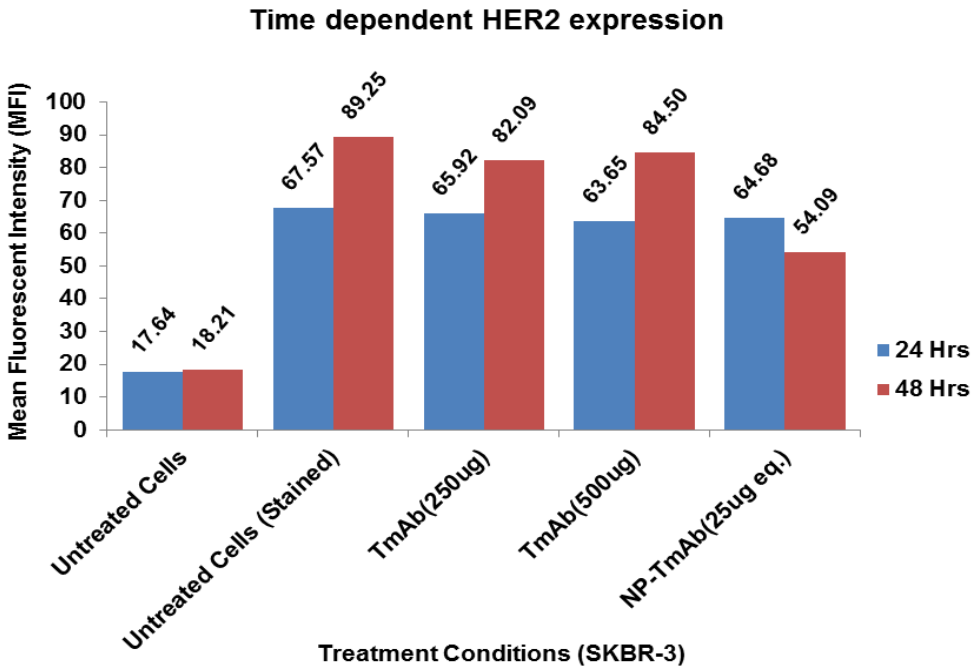

Figure-5.16: Time dependent HER2 expression of SKBR-3 cells for different treatment groups (n=2)

After time dependent HER2 expression experiments performed, it was observed that HER2 expression was increased by time in both cell types. In fact, the both cell types treated with different TmAb concentration were found higher after 48 hrs compared to 24 hrs. However, HER2 expression was found lower after 48 hrs treatment with TmAb modified plain NPs that was not found to be reduced after 24 hrs. Afterwards, I decided to continue with 48 hrs treatment of both cell types with other formulations.

5.7.1.2. Effect of different formulations after 48 hrs incubation

HER2 expression for both cell types was observed again for 48 hrs treatments with different NP formulations, filtered TmAb, free Doc, and Herceptin®.

In order to measure the effects of treating different formulations, dot plots and histograms were also considered.

5.7.1.2.1. HER2 expression in MCF-7 cells

Figure-5.17 shows the comparative dot plots and histograms for 48 hrs treatments of MCF-7 cells with different formulations comparing with the untreated groups. The detector was selected based on the absorption/emission wavelength of anti-HER2 FITC Ab. The experiments were repeated four times using the same setting with some minimum adjustment. $1.5x10^5$ live cells were initially considered for all the treatment groups. Less then 5% of gated population was considered for auto fluorescent of untreated unstained cells. Above that value the instrument counted the percentage of fluorescence as mean fluorescence intensity. All cell population without gate was accounted to have mean fluorescence intensity. The shift in fluorescence is evident from the diagrams.

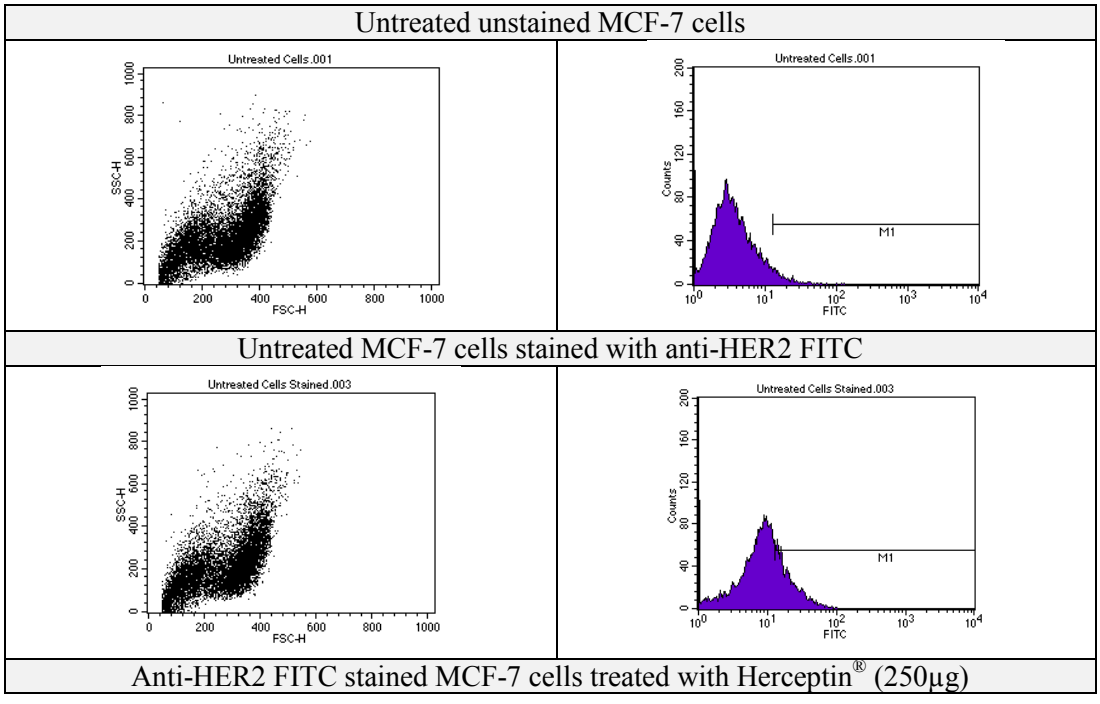

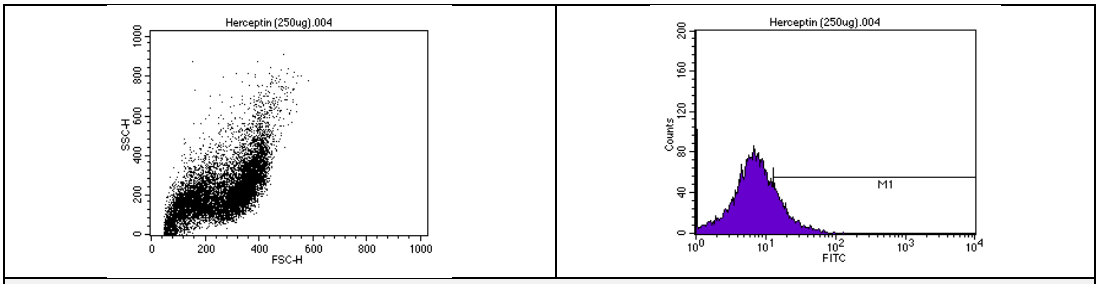

Anti-HER2 FITC stained MCF-7 cells treated with filtered TmAb (250µg)

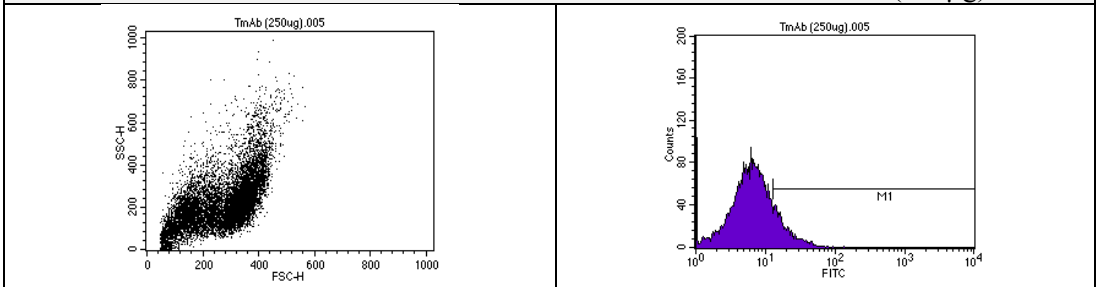

Anti-HER2 FITC stained MCF-7 cells treated with Doc (10µg)

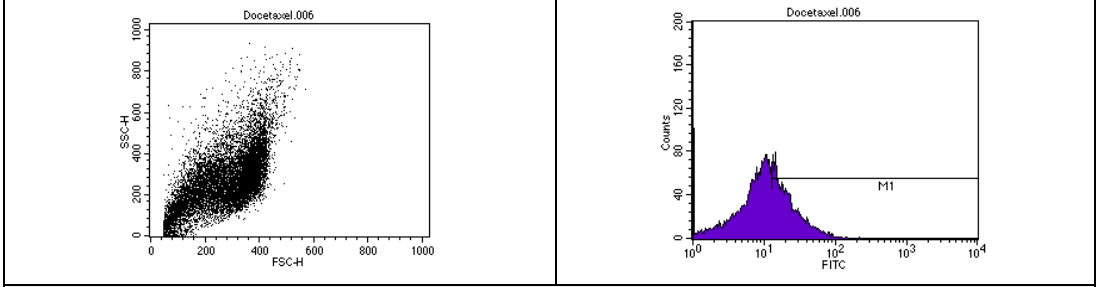

Anti-HER2 FITC stained MCF-7 cells treated with plain NPs [NP] (2mg)

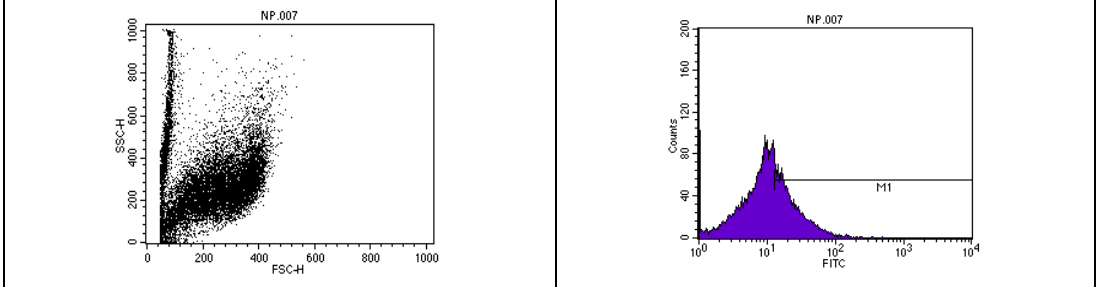

Anti-HER2 FITC stained MCF-7 cells treated with TmAb modified plain NPs [NP-TmAb (25µg equivalent)]

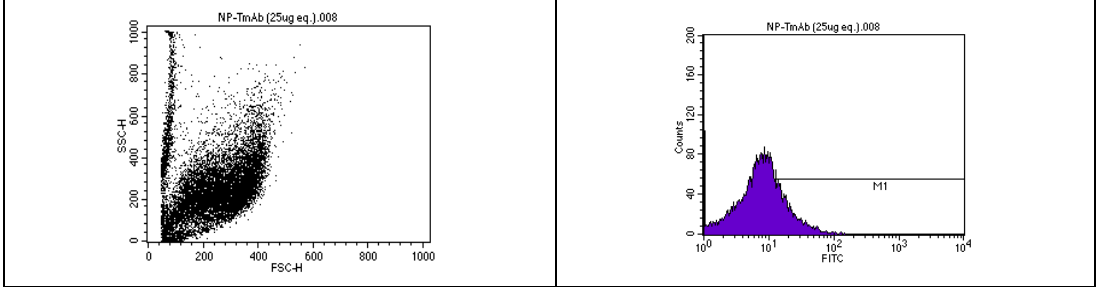

Anti-HER2 FITC stained MCF-7 cells treated with Doc loaded NPs (NP-Doc) (2mg)

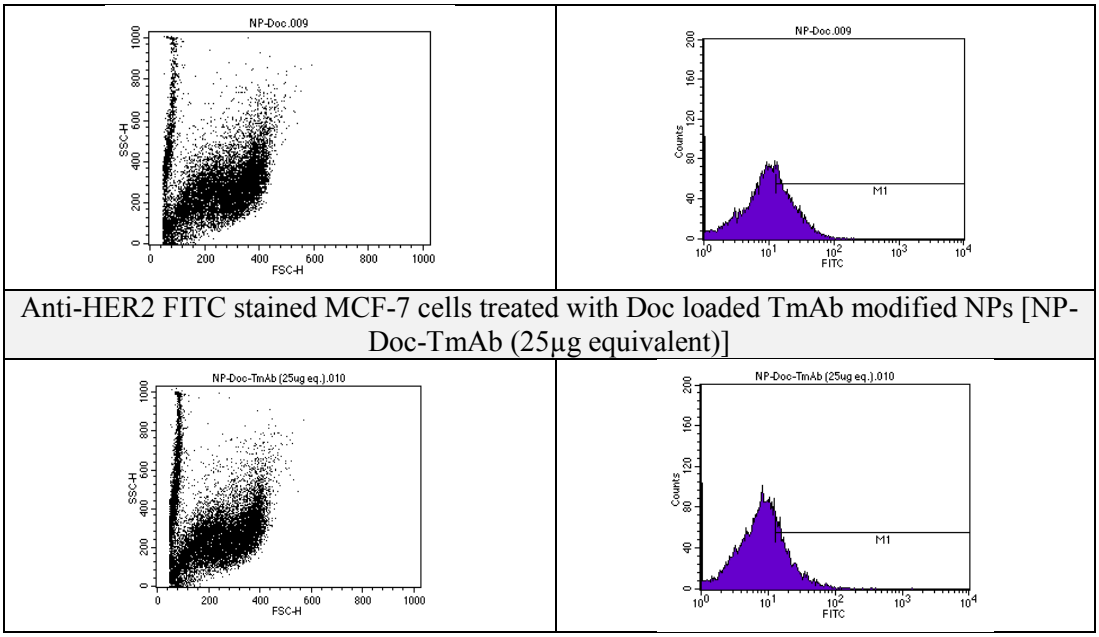

Figure-5.17: Dot plots and histograms for untreated unstained, untreated stained MCF-7 cells, and stained MCF-7 cells ater 48 hrs treatment with filtered TmAb, Herceptin®, Doc, and different NP formulations (n=4)

Figure-5.18 shows the comparative differences for percentage of fluorescent cells expressing HER2 and MFI for each cell after various treatments. Fluorescent cells percentage (red colored bars) indicated the number of events which showed the mean fluorescent intensity (blue colored bars) for HER2 expression.

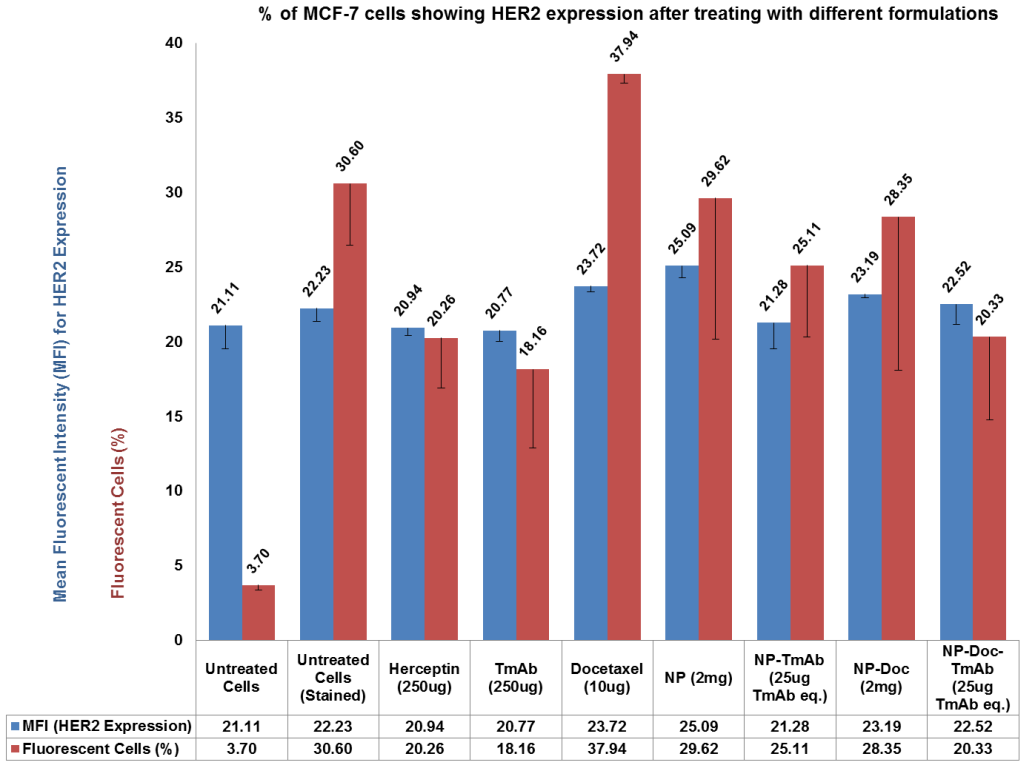

Figure-5.18: Relative % of MCF-7 cells showing HER2 expression after the treatment with different formulations (n=4)

In figure-5.18, only 3.7% untreated cells showed the auto fluorescence. When untreated cells were stained with anti-HER2 FITC Ab, 30.60% of untreated MCF-7 cells were found with 22.23 MFI for HER2 expressions as a control. Whereas, Doc loaded TmAb modified NPs showed 22.52 MFI for HER2 expressions with 20.33% positive cells among the total events. Relatively higher but insignificant HER2 expressions were found in case of the treatment with Doc (23.72 MFI), plain NPs (25.09 MFI) and Doc loaded unmodified NPs (23.19 MFI) but the percentage of respective fluorescent cells was found to be higher in comparison to that of other treatments. However, HER2 expression for TmAb modified drug free NPs (21.28 MFI) was found in similar ranges as observed in case of Herceptin® (20.94 MFI) and TmA (20.77 MFI).

5.7.1.2.2. HER2 expression in SKBR-3 cells

Figure-5.19 shows the comparative dot plots and histograms for 48 hrs treatment of SKBR-3 cells with different formulations comparing the untreated groups following the treatment conditions similar to MCF-7 cells.

Untreated unstained SKBR-3 cells	
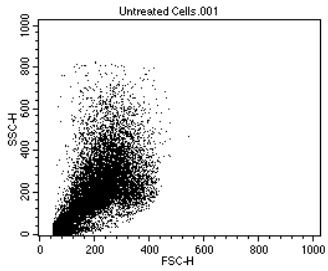	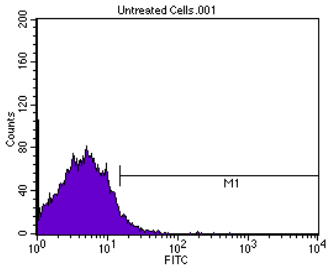
Untreated SKBR-3 cells stained with anti-HER2 FITC	
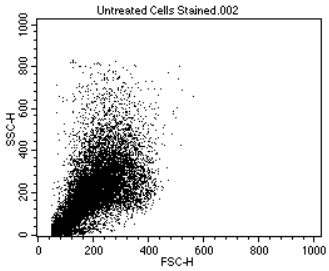	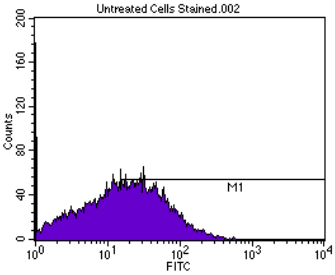
Anti-HER2 FITC stained SKBR-3 cells treated with Herceptin® (250µg)	
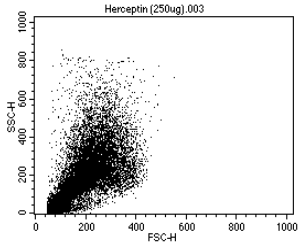	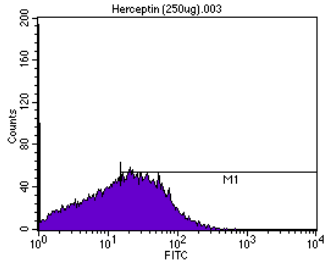
Anti-HER2 FITC stained SKBR-3 cells treated with filtered TmAb (250µg)	
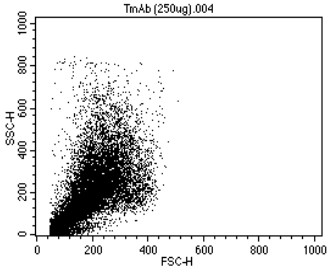	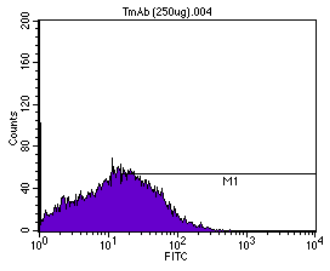
Anti-HER2 FITC stained SKBR-3 cells treated with Doc (10µg)	

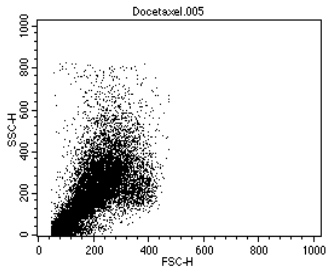

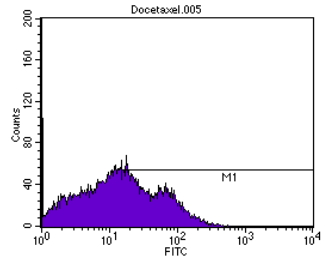

Anti-HER2 FITC stained SKBR-3 cells treated with plain NPs [NP] (2mg)

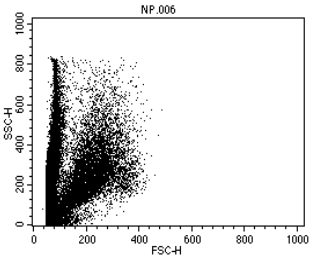

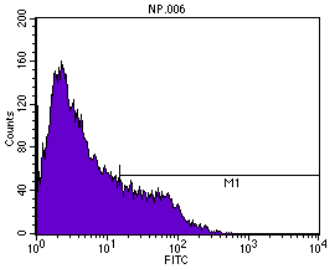

Anti-HER2 FITC stained SKBR-3 cells treated with TmAb modified plain NPs [NP-TmAb (25µg equivalent)]

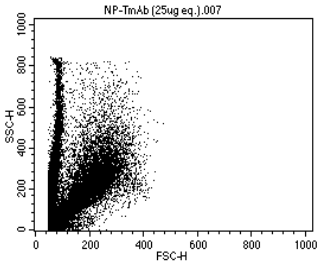

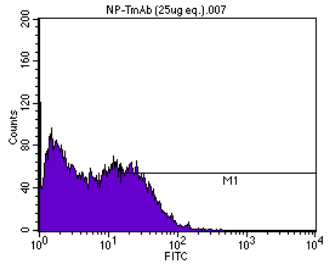

Anti-HER2 FITC stained SKBR-3 cells treated with Doc loaded NPs (NP-Doc) (2mg)

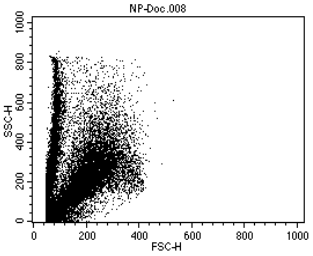

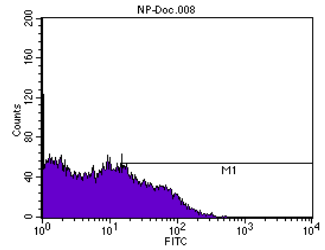

Anti-HER2 FITC stained SKBR-3 cells treated with Doc loaded TmAb modified NPs [NP-Doc-TmAb (25µg equivalent)]

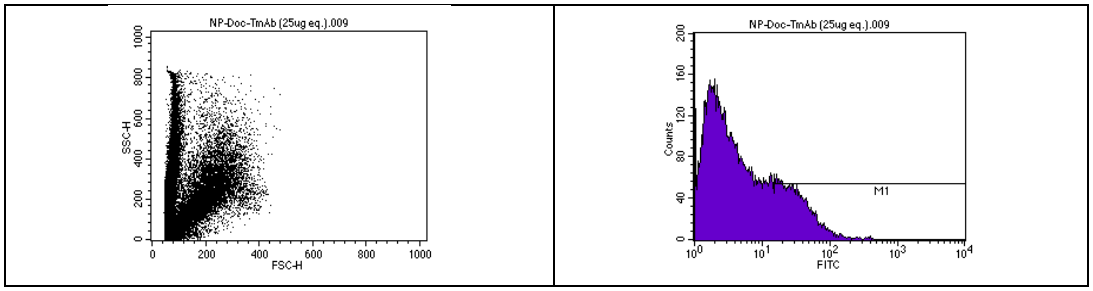

Figure-5.19: Dot plots and histograms for untreated unstained, untreated stained SKBR-3 cells, and stained SKBR-3 cells after 48 hrs treatment with filtered TmAb, Herceptin®, Doc, and different NP formulations (n=4)

Figure-5.20 shows the comparative differences for percentage of cells showing MFI for HER2 expression for all treatments. In figure-5.20, only 4.49% untreated cells showed the auto fluorescence (21.75 MFI). When untreated cells were stained with anti-HER2 FITC Ab, 68.41% of untreated SKBR-3 cells were found with 72.53 MFI for HER2 expressions as a control. Doc loaded TmAb modified NPs showed 48.62 MFI for HER2 expression with 22.12% positive cells among the total events. Relatively higher HER2 expressions along with high percentage of fluorescent cells were found for the cells treated with Herceptin® (63.15 MFI, 68.97 %), TmAb (59.89 MFI, 65.39 %), and Doc (60.76 MFI, 49.64 %) compared to plain NPs (49.58 MFI, 27.36 %), TmAb modified plain NPs (45.34 MFI, 34.38 %), Doc loaded unmodified NPs (59.64 MFI, 23.51 %), and Doc loaded TmAb modified NPs (48.62 MFI, 22.12 %).

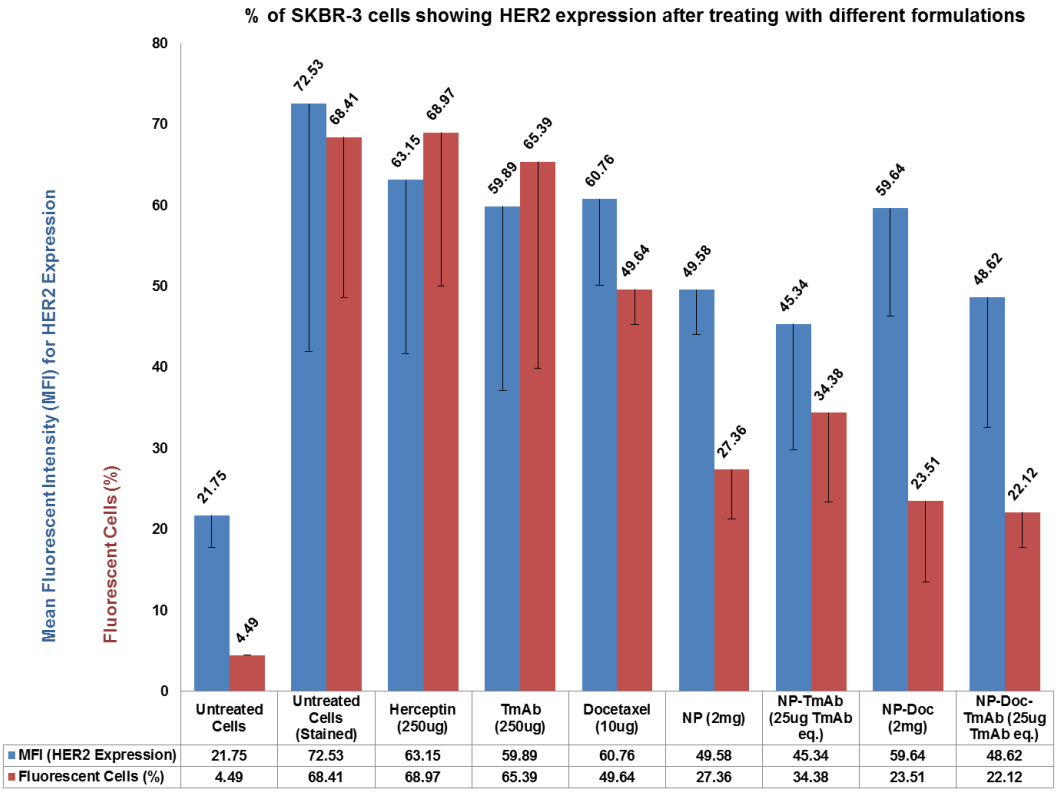

Figure-5.20: Relative % of SKBR-3 cells showing HER2 expression after the treatment with different formulations (n=4)

The overall flow cytometry studies indicate an enhanced ligand-receptor interaction with NP system depending on the variables. The HER2 overexpressed cell lines showed significant reduction of HER2 expression compared to that of HER2 moderate expressed cells types.

5.7.2. Western blot study

To verify the results from flow cytometry studies, the western blot experiment was considered to measure the relative HER2 protein expression levels after treating both cell types with same formulations maintaining similar conditions. Blotting membranes were incubated with the respective antibodies against HER2 and β-actin. Figure-5.21 shows the relative HER2 protein expression levels for both cell types.

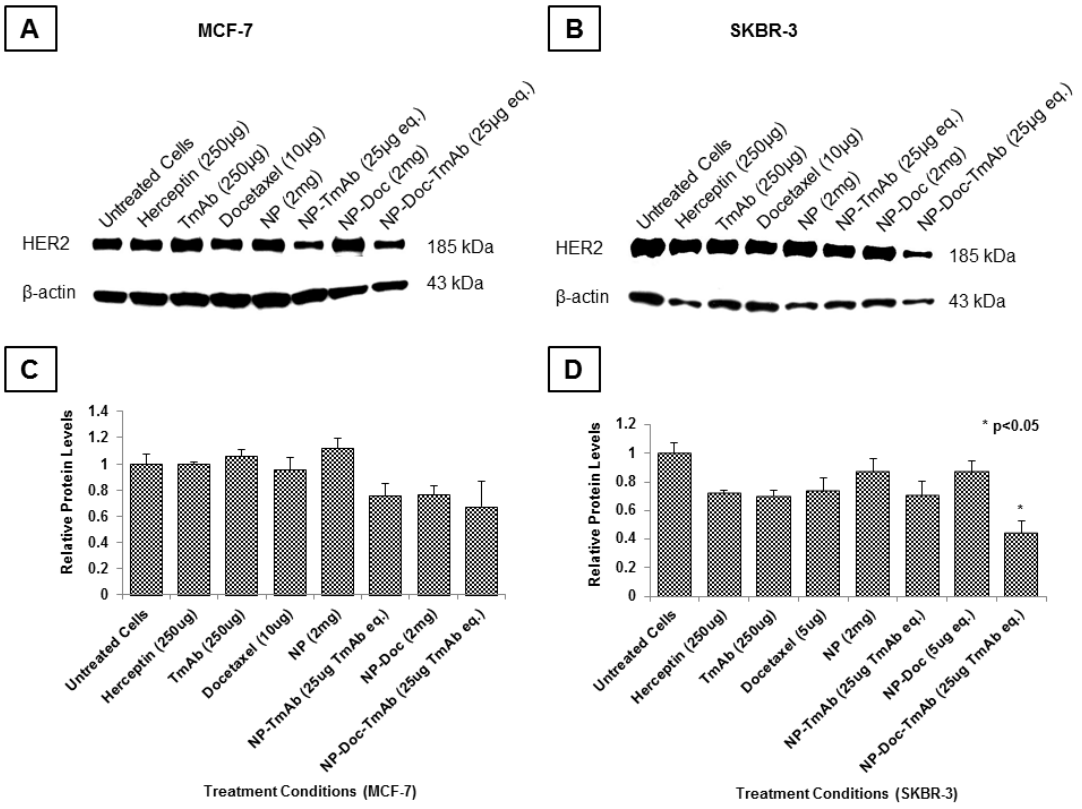

Figure-5.21: Comparison of HER2 expression levels of breast cancer cell lines in western blots. After treating both cell types with same formulations, 30µg and 40µg equivalent proteins were taken from the prepared lysates to load in each well/lane. β-actin levels were determined to ensure equal amount of loading. (A) and (B) are the quantitative HER2 protein expression of MCF-7 and SKBR-3 cells respectively. (C) and (D) represents the relative HER2 protein levels of both cell types which were measured using Image J software. The relative protein level of untreated cells was set as control. The statistical significances between the groups were represented by indicating the (*) sign. The level of significance was set to $p<0.05$ (one-way ANOVA followed by Tukey's multiple comparison test method). Each bar represents the mean % ± SD (n=3)

Almost similar HER2 expression trend was observed in Western blot studies as reportes in flow cytometry studies with both cell types. Although a declining trend for HER2 protein expression was observed for the treatment of modified drug loaded NPs in moderate expressed cells, a significant reduction in protein expression level was noted in HER2 overexpressed cells.

5.7.3. Fluorescence microscope study

To visualize the effects of Doc loaded TmAb modified NPs on HER2 expression levels of both cell types, fluorescence microscopic study was considered. To achieve this, only TmAb and Doc loaded TmAb modified NPs were treated with both cell types following same treatment conditions as maintained in flow cytometry and western blot experiments.

5.7.3.1. HER2 expression in MCF-7 cells

Fluorescence images in figure-5.22 are demonstrating the specificity of TmAb binding and chemotherapeutic response in MCF-7 cells.

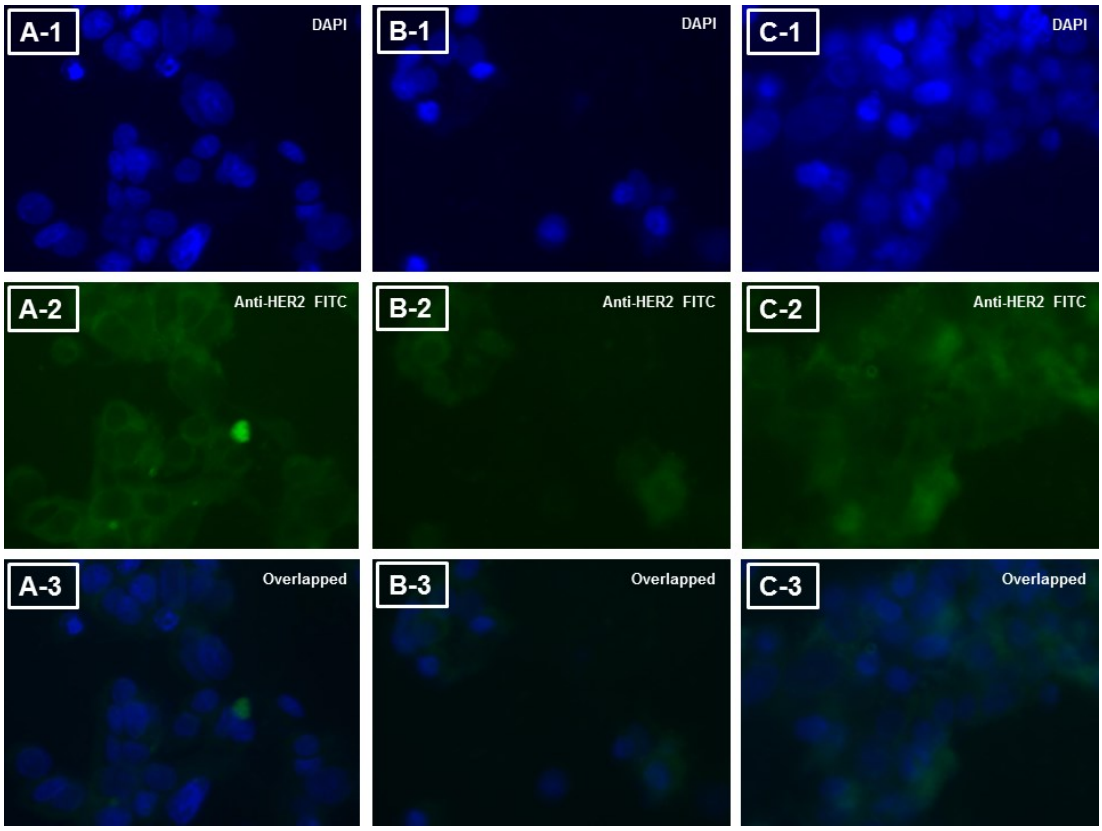

Figure-5.22: Fluorescent images of MCF-7 cells for HER2 expression levels after 48 hrs treatment with TmAb and TmAb modified Doc loaded NPs. HER2 receptor expression is shown in green (anti-HER2 FITC labeled) and nuclei in blue (DAPI stained): (A-series) untreated cells, (B-series) TmAb-250µg, and (C-series) Doc loaded TmAb modified NPs-

25µg equivalent. (A-1), (B-1), and (C-1) are shown for DAPI staining. (A-2), (B-2), and (C-2) are shown for anti-HER2 FITC staining. (A-3), (B-3), and (C-3) are shown for overlaying their respective DAPI and anti-HER2 FITC stained. Fluorescence images were obtained using Olympus fluorescence microscope with 40X objective lens

5.7.3.2. HER2 expression in SKBR-3 cells

In figure-5.23, fluorescence images for HER2 expression levels after 48 hrs treatment of SKBR-3 cells with TmAb and TmAb modified Doc loaded NPs were shown.

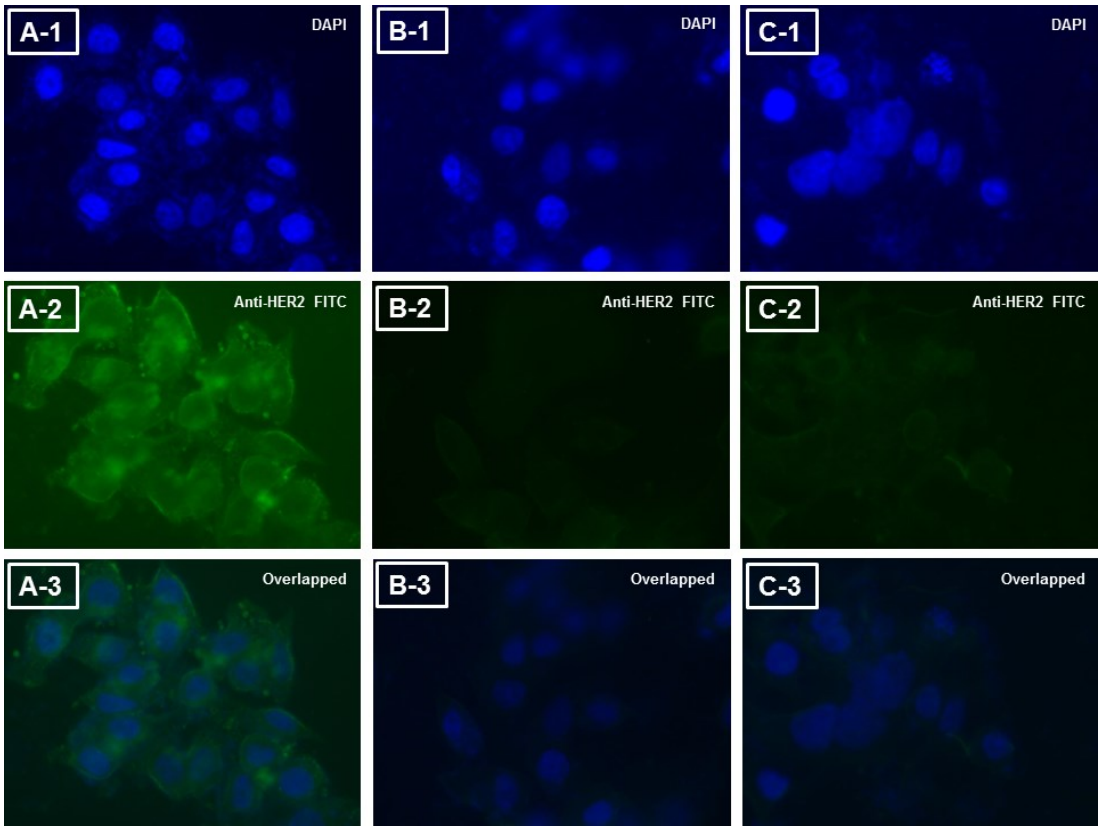

Figure-5.23: Fluorescent images of SKBR-3 cells for HER2 expression levels after 48 hrs treatment with TmAb and TmAb modified Doc loaded NPs. HER2 receptor expression is shown in green (anti-HER2 FITC labeled) and nuclei in blue (DAPI stained): (A-series) untreated cells, (B-series) TmAb-250µg, and (C-series) Doc loaded TmAb modified NPs-25µg equivalent. (A-1), (B-1), and (C-1) are shown for DAPI staining. (A-2), (B-2), and (C-2) are shown for anti-HER2 FITC staining. (A-3), (B-3), and (C-3) are shown for overlaying their respective DAPI and anti-HER2 FITC stained. Fluorescence images were obtained using Olympus fluorescence microscope with 40X objective lens.

5.8. Cell viability and toxicity studies

Staining of both cell types after nano-formulation treatments was performed using Annexin V-FITC/ PI to evaluate the cell death followed by apoptosis. Comparative percentages of cell viability, cell death, apoptosis, and necrosis were meant to evaluate how the chemotherapeutic response worked after receptor-mediated endocytosis of targeted and non-targeted nano-formulations into the cells cytoplasm. Relative gating on total cell population was considered based on the forward and side scattering histograms; and subsequently FACS data was analyzed based on the double staining of both cell types with Annexin V-FITC/PI.

5.8.1. Moderate HER2 expressed cells: MCF-7

In figure-5.24, the comparative percentages of live cells, cell death, necrosis and apoptosis data were represented in the dotplots upon respective treatments. Four uneven quadrants were considered to reflect the percentange of live cells in lower left, cell necrosis in upper left, cell early apoptosis in lower right, and cell death in upper right quadrants of the dotplots square.

Upon treating MCF-7 cells with different treatment groups, the percentage of live cells was found in a range from 56.26±5.59% to 81.46±0.93%. Early apoptotic cell percentage was varied from 4.16±0.38% to 27.10±4.23%, whereas cell death via late apoptosis was observed within 8.11±1.30% to 17.10±3.04% range. However, cell necrosis range varied from 3.15±0.12% to 14.55±4.01%.

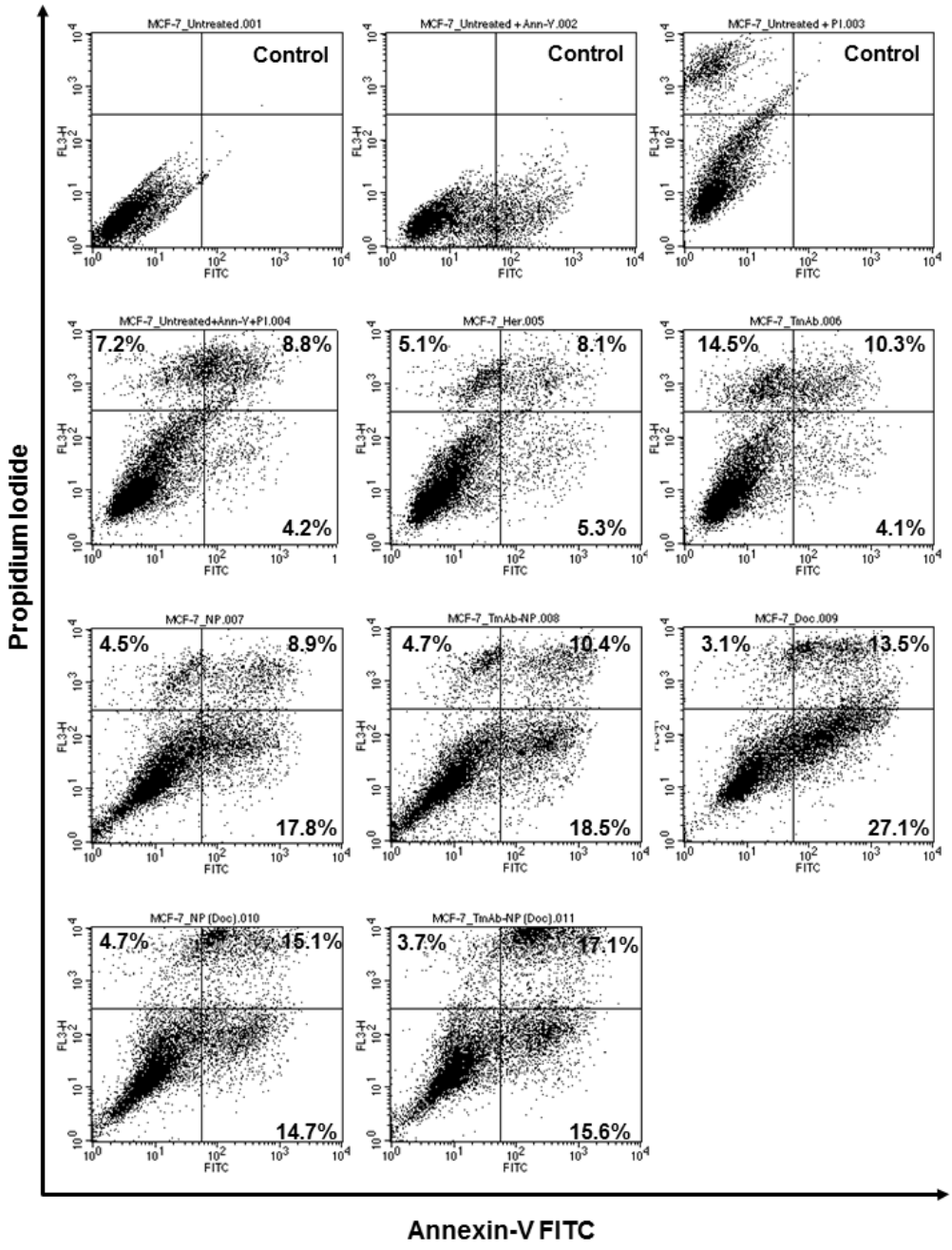

Figure-5.24: Evaluation of viability and toxicity in HER2 moderate expressed cells (MCF-7) by flow cytometry upon 48 hrs incubation with culture media (3 controls plus untreated cells+Ann-V+PI), Herceptin® (Her), TmAb, plain NPs (NP), TmAb modified plain NPs (TmAb-NP), free drug (Doc), drug loaded unmodified NPs [NP-(Doc)], TmAb modified drug loaded NPs [TmAb-NP(Doc)]

Figure-5.25 shows the relative evaluation of viability and toxicity in HER2 moderate expressed cells (MCF-7) by flow cytometry upon 48 hrs incubation with different treatment groups.

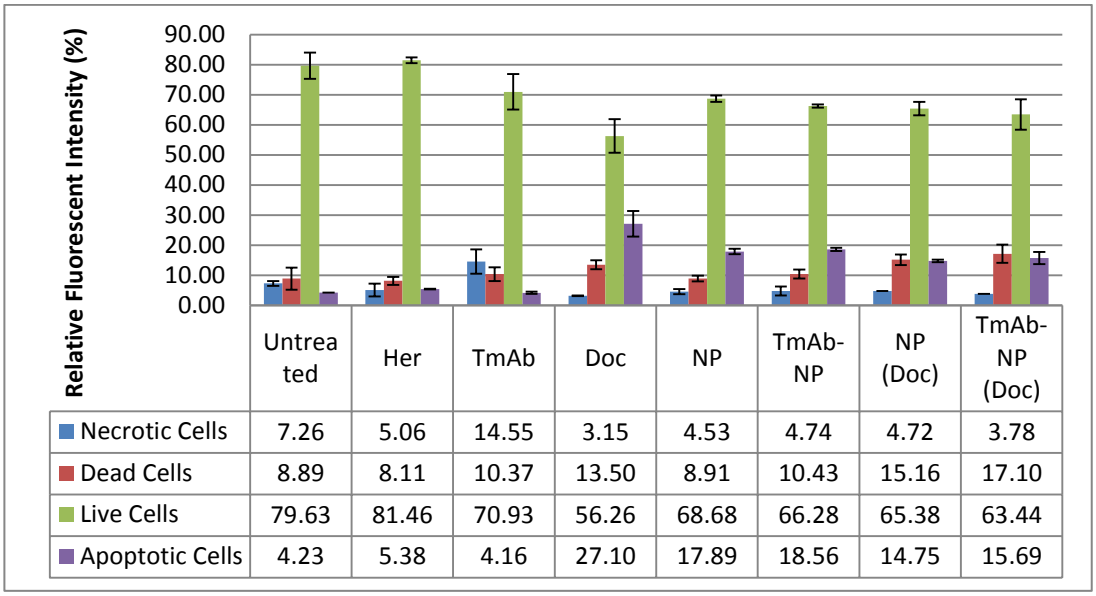

	Untreated	Her	TmAb	Doc	NP	TmAb-NP	NP (Doc)	TmAb-NP (Doc)
Necrotic Cells	7.26	5.06	14.55	3.15	4.53	4.74	4.72	3.78
Dead Cells	8.89	8.11	10.37	13.50	8.91	10.43	15.16	17.10
Live Cells	79.63	81.46	70.93	56.26	68.68	66.28	65.38	63.44
Apoptotic Cells	4.23	5.38	4.16	27.10	17.89	18.56	14.75	15.69

Figure-5.25: Relative evaluation of viability and toxicity in HER2 moderate expressed cells (MCF-7) by flow cytometry upon 48 hrs incubation with culture media (3 controls plus untreated cells+Ann-V+PI), Herceptin® (Her), TmAb, plain NPs (NP), TmAb modified plain NPs (TmAb-NP), free drug (Doc), drug loaded unmodified NPs [NP-(Doc)], TmAb modified drug loaded NPs [TmAb-NP(Doc)]

Upon treatment with different formulations after 48 hrs, MCF-7 cells showed a relative percentage of necrosis, death cells, early apoptosis, and live cell. The percentage necrotic cells for TmAb treatment was found higher compared to other treatments and untreated cells. The cell death and apoptotic cell percentages were found highest for the free drug. In addition, the early apoptosis was observed relatively higher with plain NPs and TmAb modified plain NPs compared to drug loaded unmodified and modified NPs. However, drug loaded TmAb unmodified and modified NPs showed relatively lower apoptotic rate than the drug free unmodified and modified NPs.

5.8.2. HER2 overexpressed cells: SKBR-3

Figure-5.26 shows the comparative percentage of live cells, cell death, necrosis and apoptosis data was represented in the dotplots upon respective treatments with HER2 overexpressed cells.

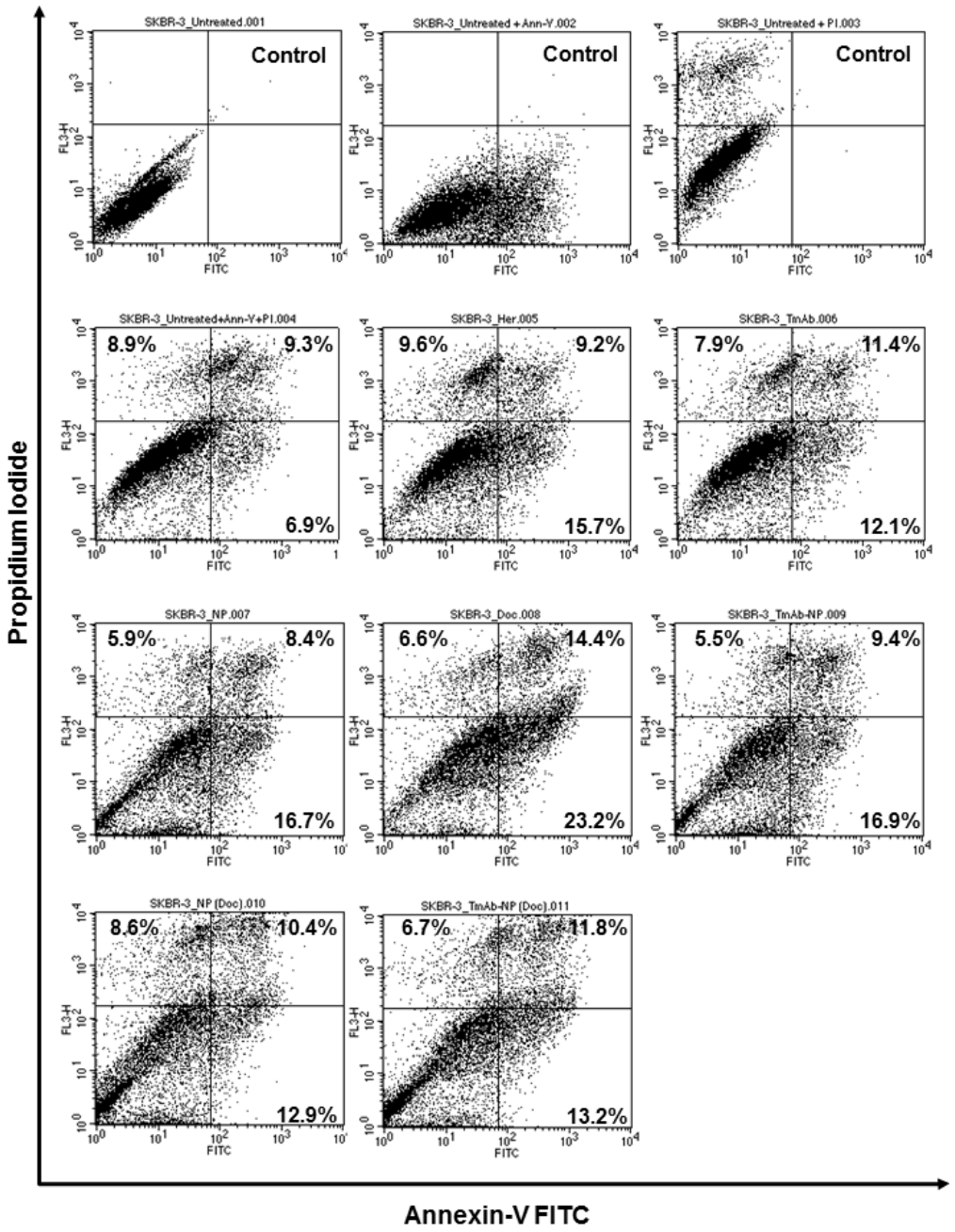

Figure-5.26: Evaluation of viability and toxicity in HER2 overexpressed cells (SKBR-3) by flow cytometry upon 48 hrs incubation with culture media (3 controls plus untreated cells+Ann-V+PI), Herceptin® (Her), TmAb, plain NPs (NP), TmAb modified plain NPs (TmAb-NP), free drug (Doc), drug loaded unmodified NPs [NP-(Doc)], TmAb modified drug loaded NPs [TmAb-NP(Doc)]

The percentage of live cells was found in a range from 5567±1.21% to 74.81% after treating SKBR-3 cells with different treatment groups. Early apoptotic cell percentage was varied from 6.98% to 23.24%, whereas cell death via late apoptosis was observed within 8.40±1.28% to 14.46±2.11% range. However, cell necrosis range varied from 5.53±1.54% to 9.63±2.95%.

Followed by 48 hrs incubation with different treatment groups, the relative evaluation for viability and toxicity in HER2 overexpressed cells (SKBR-3) was shown in figure-5.27.

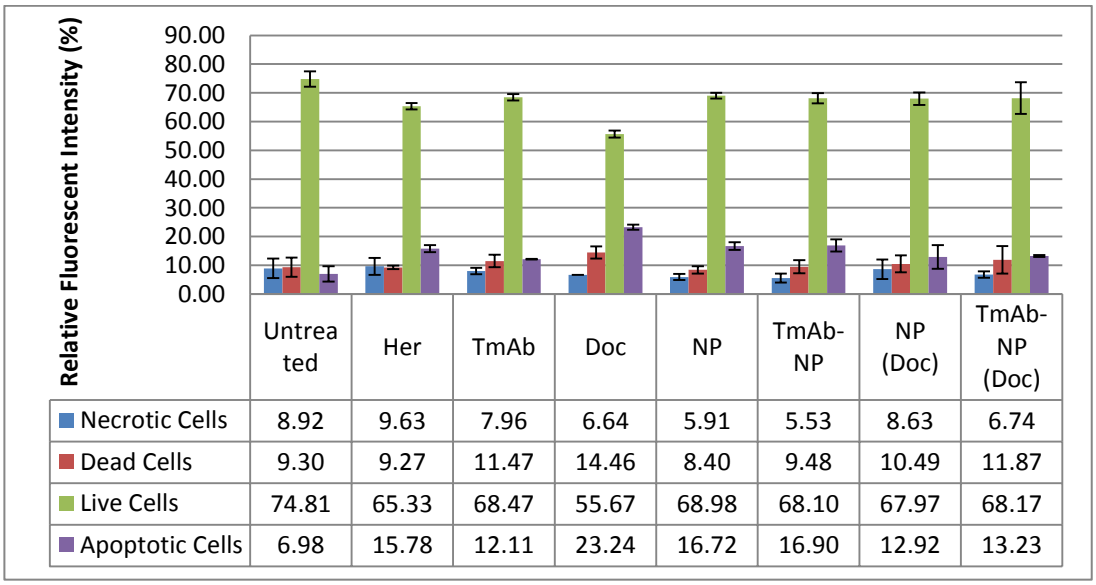

	Untreated	Her	TmAb	Doc	NP	TmAb-NP	NP (Doc)	TmAb-NP (Doc)
Necrotic Cells	8.92	9.63	7.96	6.64	5.91	5.53	8.63	6.74
Dead Cells	9.30	9.27	11.47	14.46	8.40	9.48	10.49	11.87
Live Cells	74.81	65.33	68.47	55.67	68.98	68.10	67.97	68.17
Apoptotic Cells	6.98	15.78	12.11	23.24	16.72	16.90	12.92	13.23

Figure-5.27: Relative evaluation of viability and toxicity in HER2 overexpressed cells (SKBR-3) by flow cytometry upon 48 hrs incubation with culture media (3 controls plus untreated cells+Ann-V+PI), Herceptin® (Her), TmAb, plain NPs (NP), TmAb modified plain NPs (TmAb-NP), free drug (Doc), drug loaded unmodified NPs [NP-(Doc)], TmAb modified drug loaded NPs [TmAb-NP(Doc)]

In summary, highest percentage of necrotic cells was observed for treating HER2 overexpressed cells with Herceptin® although not significantly different from necrotic cell percentages observed in the untreated cells and other treatment groups. The percentage of cell death and apoptosis was found higher with free drug treatment as followed similar trend in moderate expressed cells. Regardless of free drug treatment, TmAb alone and TmAb modified drug loaded NPs showed relatively higher percentage of dead cells than other controls. However, early apoptosis was observed relatively lower for drug loaded modified and unmodified NPs. In addition, the apoptosis rate was observed higher in plain NPs and TmAb modified plain NPs compared to drug loaded unmodified and modified NPs.

6. DISCUSSIONS

6.1. Size, PDI, and ZP

Getting therapeutic agents internalized into target cells is an important physicochemical criterion for efficient targeted drug delivery system prior to *in vivo* application. Among all internalization mechanisms, endocytosis plays an important role in targeted delivery. Endocytosis is the bulk active transport process to internalize small molecules following two main endocytic mechanisms such as phagocytosis and pinocytosis (97). Phagocytic cells (e.g. macrophages, neutrophils, dendritic cells etc.) mediated cellular internalization is mostly involved with NPs with larger size (98). Adsorption or receptor mediated internalization is the main mechanism of pinocytosis, which is more related to NPs uptake by the cells following different pathways such as macro pinocytosis, clathrin, caveolin dependent or independent pinocytosis (99). Size, PDI, and surface charge of polymeric NPs are likely the primary physicochemical variables, which govern the endocytosis dependent cellular uptake.

In this study, freeze-drying is the key step to produce dry NPs. Size of the NPs of all formulations was found to be larger after freeze-drying process compared to that of NPs before freeze-drying. Freeze-drying could be a reason to increase the size of NPs. The generation of freeze-drying stress is an important factor to be considered during freeze-drying process. The increase in size of NPs following freeze-drying could be attributed to the disruption of electrostatic repulsion between

the particles by freeze-drying stress. This can be responsible to yield higher particle-particle aggregations (Table-5.1). The high PDI value observed from freeze-dried NPs indicates the presence of higher aggregation tendency leading to poly-dispersed larger particles. The PDI of NPs is a number after cumulative analysis calculated from a simple two-parameter fit to the correlation data. The maximum value of PDI equal to 1 demonstrates that the sample is associated with a broad size distribution. The PDI of our nano-suspension was in a low to moderate range, which demonstrated a more uniform size distribution. The ZP values shifted towards more negative after freeze-drying in a range to be appropriate for a pharmaceutically stable formulation.

To minimize the particle-particle aggregations, 10% sucrose as cryoprotectant was used in the NP suspenstion. Utilizing cryoprotectant in the NP suspension offered NPs with a narrow size range and PDI, compared to the formulations without cryoprotectant before freeze-drying (Table-5.2). Similar trend was observed when these measurements were obtained after freeze-drying. The obtained lower average size and PDI values after freeze-drying is due to the addition of cryoprotectant in the NP suspension, which could possibly minimize the freeze-drying stress in order to create steric stabilization. In addition, ZP values were found to be less negative after using 10% sucrose as cryoprotectant in the plain NP formulations compared to the formulation freeze-dried with no cryoprotectant. However, no significant correlation could be made after statistical evaluation of ZP values using cryoprotectant between the plain NP formulations before and after freeze-drying.

BS3 is one of the main variable components of targeted NP formulations. In case of size measurement, no significant differences were found after inclusion of BS3 in all plain NP formulations when freez-dried with 10% cryoprotectant (Table-5.3). Similar PDI values were observed for the BS3 containing formulations before freeze-drying. ZP values of BS3 containing plain formulations with 10% cryoprotectant were observed to be less than -20mV. ZP values showed a more negative trend by increasing the amount of BS3 in NPs. However, using cryoprotectant in the BS3 included formulation was not found to interfere with the particle surface charge. Before and after freeze-drying, the ZP values of BS3 containing batches did not follow any order or consistency. Based on the results obtained, no statistically significant differences were observed for surface charge after incorporation of different amounts of BS3.

Doc loaded NPs were found to have a lower size compared to the plain NPs without drug loading; and size of the NPs was decreased with the increase in the concentrations of Doc initially used (Table-5.4). Both drug and PLGA polymer are hydrophobic in nature; and the hydrophobic interactions between them could condense the droplets during the NP preparation to yield a lower particle size. Precipitation of non-emulsified drug or polymer in aqueous phase during the solvent evaporation could be a probable reason to lessen the quantity of polymer or drug leading to lowering the yield of preparation or encapsulation efficiency, respectively (100). In Doc loaded NP formulations without BS3, the ZP values were stabilized towards more negative surface charge by higher concentration of the drug initially used to prepare the NPs. After freeze-drying the drug-loaded formulations with cryoprotectant, the surface charges shifted towards less negative compared to before

freeze-drying. This could be due to shielding of negative charges of drug (hydroxyl groups) by cryoprotectant and PLGA itself. However, no significant differences were found after statistical analysis.

Similar trend of decreasing size of Doc loaded NPs was also observed with increasing the initial concentration of drug used in the BS3 included formulations (Table-5.5). Addition of BS3 into the aqueous phase of the formulation could be a possible reason to lower the particle size since it could lead to more porous surface area of NPs. BS3 consists of an amine-reactive N-hydroxysulfosuccinimide (NHS) ester at each end of an 8-carbon spacer arm and is soluble up to ~100mM in water as it contains the hydrophilic sulfonyl moiety. Thus, BS3 could be able to lead the diffusion of drug and polymer from the matrix to either solvent during preparation or water during washing steps. Similar PDI values were observed for the BS3 containing formulations and NPs without BS3, which demonstrates that the presence of BS3 in the formulations does not interfere with the size distribution profile. Considering BS3 as an important variable for targeted NP formulations, ZP values of the BS3 containing drug-loaded formulations were observed to be slightly more negative compared to the formulations with no BS3 before freeze-drying. This could be accounted for the presence of residual sulfo-NHS (water soluble N-hydroxy sulfo-succinimide) in the nano-suspension and Doc itself.

A significant increase in the average hydrodynamic diameter of all NPs was observed after TmAb attachment, which was in the range of 300-450 nm depending on the formulation composition (Table-5.6). TmAb functionalization did not show any significant change in terms of PDI. However, a significant change in surface charge was observed for the NPs after TmAb attachment and the change shifted

towards more positive surface charge to nearly neutral. This result indicates the presence of positively charged Ab on the NP surface.

6.2. Drug loading and entrapment efficiency

Compared to theoretical amount of drug to be loaded per mg of NPs, practically loaded drug into the NPs was found very low (table-5.7 and table-5.8). Reduced size of the particle due to hydrophobic interactions between drug and polymer can also result in low drug loading. In addition, insufficient polymer or drug amount due to precipitation during solvent evaporation can also be involved in reduced encapsulation (100). Since Doc is associated with higher affinity for organic solvents, it could diffuse out of the polymer matrix of unstable emulsion droplets into the organic solvent during preparation. This could also be a possible reason for low entrapment efficiencies (101).

The loading of drug and EE are extensively correlated with one another (figure-5.1 and figure-5.2). By increasing the concentration of the drug, loading may increase but the entrapment efficiency may be reduced (102). The observation can be clarified by the fact that osmotic pressure gap between two phases (inner and outer) could be changed due to higher concentration of drug into the NPs. Some damage to the formed quasi-emulsion droplets could occur due to the change between two phases. This could be the reason for the escape of drug molecules from the inner phase of emulsion droplets to outer phase (103). Drug entrapment efficiency can be decreased since higher amount of initial drug content in the formulation may not be proportional to the higher amount of entrapped amounts of drug (104, 105). When the maximum loading capacity of NPs is achieved; further increase of initial drug concentration can reduce the entrapment efficiency (106). Taking into account these considerations, our results demonstrated similar trend when using higher concentration of drug in the formulations with and without BS3.

Besides, NPs were prepared following o/w emulsion technique where the drug is associated with poor water solubility. Poor water-soluble drug is supposed to favor the oil or organic phase during o/w emulsion procedure. Such higher affinity of poorly water-soluble drug to the inner or oil phase could favour higher loading compared to water soluble drugs (107).

6.3. TmAb quantification and attachment to the NPs

Higher TmAb attachment efficiency was observed with lowest amount of BS3 used in the formulations (table-5.9). However, TmAb attachment followed by adsorption method was also found higher, which was comparable with attached TmAb amount followed by covalent method. For further experiments, BS3 was applied at the amount of 1.5 mg per formulation since it showed the highest Ab attachment efficiency.

The results after using variable amounts of TmAb and BS3 pre-activated NPs showed a comparative TmAb attachment amount and attachment efficiency per mg of NPs (table-5.10). Relatively higher amount of TmAb was attached with higher amount of Ab initially used in the formulation. However, the attachment efficiencies upon treating different TmAb amounts did not show any significant difference. Reasonably, the loss of excess unbound TmAb was found higher when higher amount of TmAb used for the attachment.

Different incubation conditions also showed a relative TmAb attachment efficiency (table-5.11). Relatively higher TmAb attachment was observed when the conjugation was performed at room temperature compared to the conjugation at 4°C.

In conclusion, covalently attached TmAb modification for BS3 included plain NPs showed higher amount of Ab attachment compared to physically adsorbed TmAb modified NPs. However, physically adsorption method showed relatively higher percentage of attachment than covalently conjugated TmAb modified Doc loaded NPs in both incubation conditions. Non-specific elestrostatic interaction between the ligand and NP surface could be attributed to increase the TmAb attachment with plain NPs with no crosslinking agent. In addition, less TmAb

binding to the drug loaded NPs could be due to less amount of BS3 available on the surface of the drug loaded NPs. Since, the percentage of TmAb attachment efficiency was found higher at room temperature incubation, I decided to continue TmAb modification of NPs at room temperature for rest of the studies. Considering room temperature as a standard condition, the TmAb attachment among all the NP formulations followed this trend: TmAb-BS3-NP > TmAb-NP > TmAb-BS3-Doc(3)-NP > TmAb-BS3-Doc(0.75)-NP > TmAb-BS3-Doc(1.5)-NP. No significant difference was observed after assessing TmAb attachment levels with the respective NP formulations.

The structural modification of BS3 activated formulations with TmAb were confirmed by FTIR and SDS-PAGE studies (figure-5.3 and figure-5.4).

6.4. Targeting efficiency: Uptake studies

Doc itself is not fluorescent and Coum-6 was used as a dye to be loaded into the NPs to evaluate the targeting efficiency of TmAb modified NPs. The loading and EE of Coum-6 into the PLGA NPs were found comparatively higher than the drug loaded NP formulations (table-5.8 and table-5.12). The reason for higher loading of Coum-6 over Doc into the PLGA NPs could be attributed to the molecular weight difference, since the molecular weight of Coum-6 (350.43 g/mol) is about half of Doc (807.88 g/mol). In addition, the partition coefficient of drug and Coum-6 between internal and external phases in o/w emulsion could be different for the entrapment into the NPs. Because, the viscosity of the solution would be higher after dissolving high molecular weight drugs into the solvent, which might have reduced the diffusion rate of drug into the external aqueous phase of o/w emulsion. This slow extruding of solvent could result a slow precipitation of polymer to form a concrete external phase of emulsion droplet. Therefore, more time is required for the drug molecules to come into aqueous phase which ultimately results a reduced EE (64). Although these considerations might affect the loading, EE, and ultimately the release of the drug/Coum-6 from NPs they may not influence the purpose and outcome of our study, which is the investigation of NP uptake by the cells not the uptake of free drug or dye. Finally, two different NP treatment conditions were considered to evaluate the cell uptake studies in both cell types: one was without TmAb preincubation of cells and other was after TmAb preincubation of cells.

For the treatment of TmAb modified Coum-6 loaded NPs both cells with no TmAb preincubation, the shift in fluorescence was found relatively higher (right side) (figure-5.7 and figure-5.10). This is because these NPs consist of TmAb ligand,

which could better recognize the HER2 receptor for uptake. Covalently modified NPs showed comparatively higher uptake in both cell types compared to plain and physically adsorbed TmAb modified NPs, although physically absorbed NPs contained a high percentage of TmAb on the surface. However, covalent attachment of the ligand to the NPs was not found to significantly improve the cellular uptake in comparison to the NPs that were physically attached with the ligand. Despite the higher Ab incorporation after physical adsorption, the possible reason of lower uptake could be detachment of loosely attached Ab from the particle surface during the treatment process (91). This indicates the necessity of covalent conjugation for the targeted vehicle, which can maintain the intactness of desired drug delivery system. The overall uptake studies in both cell types with no TmAb pre-incubation indicated higher fold increase in MFI for TmAb functionalized nano-formulation compared to its plain or unmodified subtype. Thus, higher cellular uptakes confirmed the enhanced targeted receptor mediated cellular recognition and endocytosis.

Followed by TmAb preincubation of both cells with TmAb, non-specific cell uptake of TmAb free Coum-6 loaded NPs in both cells was found in a similar range after 24 hrs incubation as reported with NPs uptake without TmAb preincubation (figure-5.12 and figure-5.13). However, fold increases in MFI for both [TmAb-NP (Coum-6)] and [TmAb-BS3-NP (Coum-6)] were reduced significantly after preincubation of HER2 overexpressed cells with TmAb. This could be attributed to the lack of sufficient free binding sites of HER2 receptors available for TmAb-NPs, which may already be preoccupied during the TmAb preincubation. In contrast, HER2 moderate expressed cells showed comparatively higher uptake for physically

adsorbed and covalently attached TmAb modified Coum-6 loaded NPs compared to HER2 overexpressed cell lines. MCF-7 cells lack abundant HER2 receptors to bind with TmAb. Insufficient HER2 receptors on MCF-7 cell surface and nonspecific cellular binding could be the possible reasons for higher NPs uptake. In addition, the positive surface charge of [TmAb-NP (Coum-6)] formulations could provide the incentive aid for better interection with negatively charged cell membrane, leading to more NPs to be internalized (108) (109). However, the fold increases in MFI were found to be lower for both [TmAb-NP (Coum-6)] and [TmAb-BS3-NP (Coum-6)] after preincubation of MCF-7 cells with TmAb, compared to the condition without TmAb preincubation. It could be due to unavailable or preoccupied HER2 receptors for HER2 overexpressed cells as dicussed above. In case of both cell types, the overall binding efficacy between TmAb modified NPs and cells declined after preincubation with TmAb. However, similar binding trends (as mentioned earlier for without preincubation condition) were observed for TmAb free NPs after TmAb preincubation due to nonspecific binding. As a result of this investigation, it could be concluded that free targeting ligands could occupy the binding sites of the specific receptors leading to inhibition of targeted receptor mediated endocytosis.

CLSM images also confirm the the comparative NPs uptake in MCF-7 and SKBR-3 cells depending on the presence of TmAb in NP formulations. From the figure-5.14, it can be assumed that the fluorescence of Coum-6 loaded TmAb modified NPs (green) are localized around the cytoplasm, which indicates the binding of NPs to the cell surface for subsequent endocytosis. Fluorescent intensity is varied depending on the formulations. Fluresencent intensity of the cells uptaking the fluorescent NPs also depends on the concentration or amount of the dye used to

prepare the NPs, which maintained constant in all the formulations. The fluorescent NPs uptake into the cells is expressed as the intensity of the fluorescent dye and depends on the concentration used. In the CLSM image, non-specifice binding between unmodified Coum-6 loaded NPs to both cells was not visibly profound as indicated in flow cytometric analysis. In the literature, it has been stated that misinterpretation could occur for cellular uptake of fluorescent NPs because of leaching or dissociation of the dye into the cell suspension medium. This leaching in the cell suspension with improper washing steps could extrapolate an enhanced cellular uptake (3). However, a comparative fluorescent intensity of the Coum-6 can be visualized to comprehend the influence of ligand on NPs for receptor mediated binding to the cell surface.

6.5. Assessment of HER2 expression

HER2 antigen or receptor is a surface marker on breast cancer cells. Anti-HER2 FITC antibody can recognize and bind to stain the external domain of this protein (HER2) present on cell surface such as moderately expressing MCF7 and overexpressing SKBR-3 cell lines. To optimize the best incubation time for treating both cell types with different formulations, initially two different time points (24 and 48 hrs) were considered. In addition, the level of HER2 expression of untreated cells (control: stained with anti-HER2 FITC Ab) was also evaluated to support this time dependent factor after two different time periods since HER2 expression was found comparatively higher in both untreated cell types (control) after 48 hrs than 24 hrs (figure-5.15 and figure-5.16). In addition, a reduced HER2 expression was observed after 48 hrs for treating the cells with TmAb of different amounts (250 μg and 500 μg) and TmAb modified drug free NPs (25 μg TmAb equivalent amounts of NP). Depending on the results of this time dependent experiment, 48 hrs incubation times was considered for further investigation.

After 48 hrs incubation of MCF-7 cells, higher HER2 expressions and fluorescent cell percentages were found in case of the treatments with Doc, plain NPs and Doc loaded unmodified NPs compared to other treatments (figure-5.18). Although cytotoxic drug or it's delivery through NPs is designated to kill or stop the proliferation of cancer cells by interfering with microtubular functions in cytoplasm, still cancer cells are able to survive in different pathways. Multiple drug resistance, alternative cell signaling pathways might help cancer cells to stay alive and enhance further growth. In the results, Doc and Doc loaded unmodified NPs have been found to increase HER2 expression that could be attributed to the increased generation of

HER2 receptors for survival of MCF-7 cells. However, the percentage of cells showing HER2 expression was also higher which could be comparable with that of other treatment groups. Increased HER2 expression in MCF-7 cells observed for unmodified plain NPs could be further investigated although it was insignificant. The resulted reduced percentage of MCF-7 cells showing HER2 expression observed for both TmAb modified plain and TmAb docetaxel loaded NPs indicates a better cellular recognition as well as less free ligand binding sites or reduced HER2 receptors.

Followed by similar experiments (48 hrs incubation) in HER2 overexpressed SKBR-3 cells, a relatively higher HER2 expression along with high percentage of fluorescent cells was observed for Herceptin®, TmAb, and Doc compared to that of plain NPs, TmAb modified plain NPs, Doc loaded unmodified NPs, and Doc loaded TmAb modified NPs (figure-5.20). It was noted that neither Herceptin® nor filtered TmAb could reduce the significant HER2 expression although these are clinically recommended mAb therapy for HER2 positive breast cancer. However, plain NPs showed relatively less percentage of fluorescent cells compared to TmAb modified drug free NPs although their levels of HER2 expression were in similar range. Reasonably, drug loaded unmodified and modified NPs showed reduced HER2 expressions where modified one was found with more prominent reduction for HER2 expression than the unmodified one. It is important to notice that TmAb modified drug loaded NPs resulted the lowest percentage of cells which is also comparable with the reduced percentage of cells observed for plain and drug loaded unmodified NPs. Some explanations can be made for the reasons of reduced percentage of cells showing HER2 expression due to these respective treatments. For

TmAb modified drug loaded NPs, it was expected as it consists of targeting ligand that can better recognize overexpressed HER2 receptors for subsequent binding and endocytosis. In case of drug loaded unmodified NPs, the significant reduction of cell percentage could be related to the amount NPs excessively entrapped into the cells due to the size dependent cellular endocytosis. But, the resulted higher HER2 expression could be due to lack of targeting ligand in the respective NP formulation. Furthermore, the reduced HER2 expression resulted with TmAb modified and unmodified Doc loaded NPs could also be associated with chemotherapeutic responses after endocytosis due to initial release of drugs into cell cytoplasm.

In addition, the reason for reduced HER2 expression levels could be involved with the physicochemical characteristics of NPs such as size, surface charge, and the presence or absence of targeting ligand. This also because, the Ab modified NPs were almost double in size and positive to neutral in charge compared to the negatively charged unmodified NPs. If the size of NPs is high, it may inadequate for these to be internalized into the cells. However, electrostatic interaction may expedite the adherence of modified NPs to the cell surface. In addition, extracellular region of HER2 receptor involves four domains: two cysteine-rich regions (domain-II and -IV) and two ligand binding regions (domain-I and -III). Domain-I consists of amino-terminal that possesses positive charge in nature (110). Due to negative charges of unmodified NPs, nonspecific electrostatic interactions could be the possible mechanism to occupy the abundant positively charged terminal ends of the receptors in overexpressed SKBR-3 cells. As a result, the percentage of cells showing HER2 expression was found lower to be stained with anti-HER2 FITC Ab after treating the overexpressed cells with unmodified docetaxel loaded and plain

NPs. However, the flow cytometry studies demonstrated the enhanced ligand-receptor interaction with nanoparticulate system depending on the variables. After treating different formulations, the overexpressed HER2 cell lines showed a comparative reduction for HER2 expression than HER2 moderate expressed cells.

The overall Western blot studies revealed a declining trend of HER2 protein expression levels in cells treated with TmAb modified plain NPs (NP-TmAb), Doc loaded NPs (NP-Doc), and Doc loaded TmAb modified NPs (NP-Doc-TmAb) compared to other treatment groups and control (untreated cells). However, a significant decrease in HER2 protein level was found for the treatment of SKBR-3 cells with drug loaded Ab modified NPs. Although plain NPs showed a significant reduction of HER2 expression with both cells in flow cytometry studies, the opposite results were observed in western blot studies. It was somewhat higher or equivalent to relative HER2 protein levels observed in case of untreated cells. It could be attributed to the inertness or only masking of cells by the negative charged plain NPs due to electrostatic attachment. Due to masking of cells surrounded by the plain NPs or inadequate HER2 receptors due to shielding could be a reason to hinder the binding of fluorescent anti-HER2 FITC antibody to the extracellular HER2 receptors. But in western blot studies, only the protein of interest (HER2) was isolated and displayed for the level of its expression on the blotting membrane. In this case, no masking of cell surface or cell surface receptors by NPs was possible due to non-specific electrostatic or other possible interactions, as reported in flow cytometric analysis. As a result, actual protein expression level was determined for the efficacy of different NP treatment groups.

Similarly in the images from fluorescent microscope (figure-5.22 and figure-5.23), the cell membrane of both cell types with a comparatively lower HER2 expression was observed for TmAb modified Doc loaded NPs treatment compared to the untreated cells and TmAb treatment. This demonstrates the specific binding between the ligand and the available HER2 receptors on cell surface.

6.6. Evaluation of chemotherapeutic response

Apoptosis is a normal physiological process of a programmed cell death that involves tumor suppression (111). Ideally, assessing early or late apoptosis rate of tumor cells relative to their viability percentages was considered to evaluate the respective responses of treatment groups depending on the treating materials. Since Doc is a cytotoxic drug of choice, the chemotherapeutic responses of free drug and drug loaded NPs were also compared with other treatment options.

Figure-5.25 and figure-5.27 show the relative evaluation of viability and toxicity in HER2 moderate expressed (MCF-7) and overexpressed (SKBR-3) cells after treatment where the cell viability was higher for the untreated cells. However, the cell viability percentages went down for other treatment groups. Treatment of both cells with Doc was found with lowest cell viability. It could be attributed to the direct effects of cytotoxic drug in contact with cells. Almost similar cell viability percentages were observed for drug loaded unmodified NPs, TmAb modified plain NPs, TmAb modified drug loaded NPs respectively.

Upon treatment with different formulations, both cell types were observed for necrosis percentage. The percentage of necrotic cells for TmAb treatment was found to be extensively higher in MCF-7 cells compared to other treatments and untreated cells. TmAb was purified from the clinical formulation (Herceptin®) and the presence of impurities into the filtered TmAb could be a possible reason for more necrosis. However, the difference in necrosis was not significant. The highest necrotic cells were found in clinically recommended Herceptin® treatment with HER2 overexpressed cells although it was not significantly different from untreated cells and other treatment groups.

It is more important to observe the chemotherapeutic responses of different treatment groups in HER2 moderate expressed cells. The percentages of cell death and apoptosis may also be considered for evaluating the chemotherapeutic responses since considering the live cells only could not be an accurate evaluation. From analysis, the cell death and apoptotic cell percentages were found highest for the free drug.

In both cells, early apoptosis was observed relatively higher with plain NPs and TmAb modified plain NPs than drug loaded unmodified and modified NPs. Suitable size of the plain unmodified NPs for nonspecific binding as well as internalization into the cells could trigger the early apoptosis. In addition, nonspecific electrostatic interactions between positively charged TmAb modified plain NPs and negatively charged cell surface could contribute to higher percentage of apoptotic cells. However, drug loaded TmAb unmodified and modified NPs showed relatively lower apoptotic rate than the drug free unmodified and modified NPs. Inadequate release or access of drug from the NP matrix could be attributed to the reduced apoptosis compared to free drug treatment group. However, results for the treatments with drug free plain NPs may not be related to excessive toxicity to some extent (112).

7. CONCLUSION

The ester-ended drug loaded NPs with low molecular weight result in a desirable size range of 100-200 nm and is suitable for effective intracellular uptake (113). Fenestration or pore sizes in tumor microvasculature vary between 100 nm and 780 nm (89). Many studies have revealed that the suitable or effective size of nanocarriers below 400 nm was found to have a better extravasation and accumulation (114). Considerable increase in size of NPs was observed when NPs were redispersed after freeze-drying due to the aggregation of particles. Achieving such a higher size range of freeze-dried NPs following redispersion in any media is a major drawback in emulsification-solvent evaporation method. Our aim was to overcome this limitation using cryoprotectants in the drug loaded formulations. The results demonstrated the average size range below 400 nm after freeze-drying when 10% sucrose was used as a suitable cryoprotectant in the formulations. Addition of cryoprotectant not only protected NPs from strong aggregation but also reduced the energy required for the redispersion for further uses. Two possible mechanisms could attribute to: i) steric stabilization (formation of steric hindrance among particles) and ii) electrostatic stabilization (generation of higher repulsion forces between the dispersed particles). For sucrose, steric stabilization might be more dominant reason to yield less negative ZP after freeze-drying.

The ZP of the NPs before freeze-drying demonstrated more negative charge due to presence of PVA residues and drug exposed to the surface. Using

cryoprotectant may be able to neutralize those unwanted residues leading to desirable less negative ZP after freeze drying. Compared to very high positive and negative surface charge, NPs with moderate negative or neutral surface charge have been found with higher residence time in the tumor and with lower phagocytic rate during the circulatory system (115). Therefore, we decided to continue using cryoprotectant for future studies to benefit from both the suitable size and tumor uptake.

Drug loading efficiency was reached to 85% for certain drug loaded formulations; and amount of drug loaded per mg of NPs reached to 30%. TmAb modified NPs were found in a desired size range (below 400nm) with suitable PDI and ZP. Relatively less positive surface charges of modified NPs could be considered as neutral charged NPs, which may be able to avoid nonspecific electrostatic binding with the cells. Covalent attachment between NP and TmAb through cross-linking agent was found to be prominent. Using increased amounts of cross-linking agent in the formulation was unable to enhance the TmAb attachment with NPs. During emulsification process, aqueous phase could be saturated with maximum amount of BS3 (1.5 mg) and thus, excess amount of BS3 (over 1.5 mg) could be precipitated during solvent evaporation process. In addition, masking of BS3 may take place when excess amount of BS3 was used in the NP formulations. This may result in insufficient terminal spacer arms available to bind with TmAb. However, the maximum TmAb attachment efficiency was found in a range 50% to 60%.

HER2 overexpressed cells showed a promising cellular uptake of Coum-6 loaded NPs compared to HER2 moderate expressed cells. Targeting efficiency of

TmAb was evaluated by preincubating both HER2 dependent cells with TmAb before Coum-6 loaded NPs treatment. Confocal images confirmed the clear cellular localization of dye loaded NPs. Covalently attached TmAb modified NPs showed comparatively better cellular internalization compared to physically adsorped TmAb modified and TmAb free plain NPs.

Both HER2 dependent cell types after the treatment with different NP formulations showed different levels of HER2 expression and chemotherapeutic responses. The response was proportionally associated to the abundance of extracellular HER2 receptors on the cell types. A significant reduction for the level of HER2 expression was observed for targeted drug loaded NPs in HER2 overexpressed SKBR-3 cells. The level of HER2 expression upon NPs treatments was also visually investigated with the images obtained using fluorescence microscope.

The evaluation of chemotherapeutic responses upon treating both cells with different formulations was comparatively analyzed based on the percentages of cell viability, cell death, apoptosis, and necrosis. Both cell types showed higher percentage of cell death as well as early apoptosis for free drug treatment compared to other treatment groups. The cell viability was higher for the untreated cells in both cell types and was comparable with the treatment of cells with Herceptin® and the free TmAb. Compared to free drug treatment alone, drug loaded TmAb modified and unmodified NPs showed insignificant early apoptotic rate, which could be attributed to the lack of proper release of drug from the NP matrix. Notably, a clear chemotherapeutic effect was observed for the presence of TmAb in the NP formulations althouth the results were not significant.

Overall, the *in vitro* data using TmAb modified Doc loaded NPs have demonstrated a prospective potential to be applied as targeted chemotherapy against HER2 overexpressed breast cancer.

8. FUTURE DIRECTIONS AND RECOMMENDATIONS

The primary *in vitro* results shown above clearly indicate that the TmAb functionalized Doc loaded PLGA NPs are capable platforms for HER2 positive breast cancer treatment. Although such NPs showed a potential for targeted chemotherapy over the chemotherapeutic drug alone, some future directions and recommendations may be considered to achieve better outcomes.

1. The competency of biodegradable polymeric NPs for targeted delivery depends on the modification of size and surface charge of NPs. Surface functionalization of NPs with a suitable ligand tends to increase the size above the desired range, which could impede the internalization. To reduce the size of modified NPs, F_{ab} fragment or single chain F_{ab} (scF_{ab}) fragment could be functionalized avoiding the F_c fragment of whole mAb.
2. Structural integrity and retaining encoded action are important factors for targeting ligand. Here, TmAb was extracted from the clinical formulation Herceptin®. Although covalent conjugation between BS3 and TmAb was investigated and confirmed using FTIR and SDS-PAGE, it was not observed whether the extracted TmAb retained the similar structural integrity as it was formulated with other excipients in Herceptin®. New method could be considered to investigate this parameter before applying in further experiments.

3. In the study, the amount of TmAb attachment to the NPs was low, which could be attributed to the lack of sufficient crosslinking agents embedded onto the NP surface. To overcome this issue, other possible conjugation methods can be used to achieve higher Ab attachment. By enhancing the TmAb attachment, the amount of NPs can be reduced for the treatments with the cell lines.
4. Ester terminated PLGA was used to prepare the targeted NPs in this study. However, COOH terminated PLGA can be used for better TmAb attachment through EDC/NHS covalent conjugation process.
5. BS3 inclusion as crosslinking agent in the NP formulation was observed with low drug loading and reduced TmAb attachment efficiency. In this case, the TmAb attachment process can be changed to yield more conjugation efficiency such as electrostatic bond. Because, the isoelectric point of Herceptin® is 8.5 that is positive in charge at acidic pH. The surface charge of NPs is negative in charge. A strong electrostatic bond could be formed between positively charged TmAb and negatively charged NPs.
6. Treating cells with NP formulations with similar size and surface charge was not considered in this study. Maintaining similar size range and surface charge of all NP formulations could be served as better controls to assess the respective effects due to different treatment options.
7. Balance between TmAb and loaded drug amounts in NPs could be made for desired treatment concentration. Because, no controls could be considered to treat the cells with specific amounts of drug loaded NPs or or vice versa.
8. However, *in vivo* work should be undertaken to oberve the effects of whether our targeted chemotherapeutic NPs can efficiently reduce the size of tumor and

its HER2 expression with minimum side effects compared to free cytotoxic drug and TmAb. To evaluate its efficacy, evaluation of immune responses for this formulation and its related distribution throughout the body should be considered in future investigations.

9. REFERENCES

1. Kamaly N, Xiao Z, Valencia PM, Radovic-Moreno AF, Farokhzad OC. Targeted polymeric therapeutic nanoparticles: design, development and clinical translation. Chemical Society reviews. 2012 Apr 7;41(7):2971-3010. PubMed PMID: 22388185. Pubmed Central PMCID: 3684255.
2. Choi WI, Lee JH, Kim JY, Heo SU, Jeong YY, Kim YH, et al. Targeted antitumor efficacy and imaging via multifunctional nano-carrier conjugated with anti-HER2 trastuzumab. Nanomedicine : nanotechnology, biology, and medicine. 2014 Sep 28. PubMed PMID: 25262581.
3. Sun B, Ranganathan B, Feng SS. Multifunctional poly(D,L-lactide-co-glycolide)/montmorillonite (PLGA/MMT) nanoparticles decorated by Trastuzumab for targeted chemotherapy of breast cancer. Biomaterials. 2008 Feb;29(4):475-86. PubMed PMID: 17953985.
4. Fauzee NJ, Wang YL, Dong Z, Li QG, Wang T, Mandarry MT, et al. Novel hydrophilic docetaxel (CQMU-0519) analogue inhibits proliferation and induces apoptosis in human A549 lung, SKVO3 ovarian and MCF7 breast carcinoma cell lines. Cell proliferation. 2012 Aug;45(4):352-64. PubMed PMID: 22672263.
5. Irache JM, Esparza I, Gamazo C, Agueros M, Espuelas S. Nanomedicine: novel approaches in human and veterinary therapeutics. Veterinary parasitology. 2011 Aug 4;180(1-2):47-71. PubMed PMID: 21680101.
6. Manchanda R, Fernandez-Fernandez A, Nagesetti A, McGoron AJ. Preparation and characterization of a polymeric (PLGA) nanoparticulate drug delivery system with simultaneous incorporation of chemotherapeutic and thermo-optical agents. Colloids and surfaces B, Biointerfaces. 2010 Jan 1;75(1):260-7. PubMed PMID: 19775872.
7. Koopaei MN, Dinarvand R, Amini M, Rabbani H, Emami S, Ostad SN, et al. Docetaxel immunonanocarriers as targeted delivery systems for HER 2-positive tumor cells: preparation, characterization, and cytotoxicity studies. International journal of nanomedicine. 2011;6:1903-12. PubMed PMID: 21931485. Pubmed Central PMCID: 3173052.
8. Thamake SI, Raut SL, Ranjan AP, Gryczynski Z, Vishwanatha JK. Surface functionalization of PLGA nanoparticles by non-covalent insertion of a homo-bifunctional spacer for active targeting in cancer therapy. Nanotechnology. 2011 Jan 21;22(3):035101. PubMed PMID: 21149963.
9. Brannon-Peppas L, Blanchette JO. Nanoparticle and targeted systems for cancer therapy. Advanced drug delivery reviews. 2004 Sep 22;56(11):1649-59. PubMed PMID: 15350294.
10. Misra R, Acharya S, Sahoo SK. Cancer nanotechnology: application of nanotechnology in cancer therapy. Drug discovery today. 2010 Oct;15(19-20):842-50. PubMed PMID: 20727417.

11. Society AC. ACS Cancer Facts & Figures. 2012.
12. International Agency for Research on Cancer WHO. World Cancer Report. 2008.
13. Pupa SM, Tagliabue E, Menard S, Anichini A. HER-2: a biomarker at the crossroads of breast cancer immunotherapy and molecular medicine. Journal of cellular physiology. 2005 Oct;205(1):10-8. PubMed PMID: 15887236.
14. How is breast cancer diagnosed? American Cancer Society [Internet]. 2013. Available from: http://www.cancer.org/cancer/breastcancer/detailedguide/breast-cancer-diagnosis.
15. Miller E, Lee HJ, Lulla A, Hernandez L, Gokare P, Lim B. Current treatment of early breast cancer: adjuvant and neoadjuvant therapy. F1000Research. 2014;3:198. PubMed PMID: 25400908. Pubmed Central PMCID: 4224200.
16. Hadden JW. The immunology and immunotherapy of breast cancer: an update. International journal of immunopharmacology. 1999 Feb;21(2):79-101. PubMed PMID: 10230872.
17. Grobmyer SR, Iwakuma N, Sharma P, Moudgil BM. What is cancer nanotechnology? Methods in molecular biology. 2010;624:1-9. PubMed PMID: 20217585.
18. Egusquiaguirre SP, Igartua M, Hernandez RM, Pedraz JL. Nanoparticle delivery systems for cancer therapy: advances in clinical and preclinical research. Clinical & translational oncology : official publication of the Federation of Spanish Oncology Societies and of the National Cancer Institute of Mexico. 2012 Feb;14(2):83-93. PubMed PMID: 22301396.
19. Chidambaram M, Manavalan R, Kathiresan K. Nanotherapeutics to overcome conventional cancer chemotherapy limitations. Journal of pharmacy & pharmaceutical sciences : a publication of the Canadian Society for Pharmaceutical Sciences, Societe canadienne des sciences pharmaceutiques. 2011;14(1):67-77. PubMed PMID: 21501554.
20. Shapira A, Livney YD, Broxterman HJ, Assaraf YG. Nanomedicine for targeted cancer therapy: towards the overcoming of drug resistance. Drug resistance updates : reviews and commentaries in antimicrobial and anticancer chemotherapy. 2011 Jun;14(3):150-63. PubMed PMID: 21330184.
21. Gillet JP, Gottesman MM. Mechanisms of multidrug resistance in cancer. Methods in molecular biology. 2010;596:47-76. PubMed PMID: 19949920.
22. Hu CM, Zhang L. Therapeutic nanoparticles to combat cancer drug resistance. Current drug metabolism. 2009 Oct;10(8):836-41. PubMed PMID: 20214578.
23. Mitri Z, Constantine T, O'Regan R. The HER2 Receptor in Breast Cancer: Pathophysiology, Clinical Use, and New Advances in Therapy. Chemotherapy research and practice. 2012;2012:743193. PubMed PMID: 23320171. Pubmed Central PMCID: 3539433.
24. Pollock NI, Grandis JR. HER2 as a Therapeutic Target in Head and Neck Squamous Cell Carcinoma. Clinical cancer research : an official journal of the American Association for Cancer Research. 2014 Nov 25. PubMed PMID: 25424855.
25. Tai W, Mahato R, Cheng K. The role of HER2 in cancer therapy and targeted drug delivery. Journal of controlled release : official journal of the Controlled

Release Society. 2010 Sep 15;146(3):264-75. PubMed PMID: 20385184. Pubmed Central PMCID: 2918695.
26. Koutras AK, Evans TR. The epidermal growth factor receptor family in breast cancer. Onco Targets Ther. 2008;1:5-19. PubMed PMID: 21127748. Pubmed Central PMCID: 2994209.
27. Citri A, Yarden Y. EGF-ERBB signalling: towards the systems level. Nature reviews Molecular cell biology. 2006 Jul;7(7):505-16. PubMed PMID: 16829981.
28. Yarden Y, Sliwkowski MX. Untangling the ErbB signalling network. Nature reviews Molecular cell biology. 2001 Feb;2(2):127-37. PubMed PMID: 11252954.
29. Davoli A, Hocevar BA, Brown TL. Progression and treatment of HER2-positive breast cancer. Cancer chemotherapy and pharmacology. 2010 Mar;65(4):611-23. PubMed PMID: 20087739.
30. Thibault C, Khodari W, Lequoy M, Gligorov J, Belkacemi Y. HER2 status for prognosis and prediction of treatment efficacy in adenocarcinomas: a review. Critical reviews in oncology/hematology. 2013 Oct;88(1):123-33. PubMed PMID: 23566949.
31. Cirstoiu-Hapca A, Bossy-Nobs L, Buchegger F, Gurny R, Delie F. Differential tumor cell targeting of anti-HER2 (Herceptin) and anti-CD20 (Mabthera) coupled nanoparticles. International journal of pharmaceutics. 2007 Mar 1;331(2):190-6. PubMed PMID: 17196347.
32. ZHANG J, LAN CQ, POST M, SIMARD B, DESLANDES Y, HSIEH TH. Design of Nanoparticles as Drug Carriers for Cancer Therapy. Cancer Genomics - Proteomics. 2006 May 1, 2006;3(3-4):147-57.
33. Nishioka Y, Yoshino H. Lymphatic targeting with nanoparticulate system. Advanced drug delivery reviews. 2001 Mar 23;47(1):55-64. PubMed PMID: 11251245.
34. Cho K, Wang X, Nie S, Chen ZG, Shin DM. Therapeutic nanoparticles for drug delivery in cancer. Clinical cancer research : an official journal of the American Association for Cancer Research. 2008 Mar 1;14(5):1310-6. PubMed PMID: 18316549.
35. Poste G KR. Site–Specific (Targeted) Drug Delivery in Cancer Therapy. Nature Biotechnology. 1983;1:869-78.
36. Parveen S, Sahoo SK. Polymeric nanoparticles for cancer therapy. Journal of drug targeting. 2008 Feb;16(2):108-23. PubMed PMID: 18274932.
37. Salomon DS, Brandt R, Ciardiello F, Normanno N. Epidermal growth factor-related peptides and their receptors in human malignancies. Critical reviews in oncology/hematology. 1995 Jul;19(3):183-232. PubMed PMID: 7612182.
38. Schwechheimer K, Huang S, Cavenee WK. EGFR gene amplification--rearrangement in human glioblastomas. International journal of cancer Journal international du cancer. 1995 Jul 17;62(2):145-8. PubMed PMID: 7622287.
39. Danhier F, Ansorena E, Silva JM, Coco R, Le Breton A, Preat V. PLGA-based nanoparticles: an overview of biomedical applications. Journal of controlled release : official journal of the Controlled Release Society. 2012 Jul 20;161(2):505-22. PubMed PMID: 22353619.
40. Grislain L, Couvreur P, Lenaerts V, Roland M, Deprez-Decampeneere D, Speiser P. Pharmacokinetics and distribution of a biodegradable drug-carrier. International journal of pharmaceutics. 1983 7//;15(3):335-45.

41. Cengelli F, Maysinger D, Tschudi-Monnet F, Montet X, Corot C, Petri-Fink A, et al. Interaction of functionalized superparamagnetic iron oxide nanoparticles with brain structures. The Journal of pharmacology and experimental therapeutics. 2006 Jul;318(1):108-16. PubMed PMID: 16608917.
42. Davis ME, Chen ZG, Shin DM. Nanoparticle therapeutics: an emerging treatment modality for cancer. Nature reviews Drug discovery. 2008 Sep;7(9):771-82. PubMed PMID: 18758474.
43. Borghaei H, Smith MR, Campbell KS. Immunotherapy of cancer. European journal of pharmacology. 2009 Dec 25;625(1-3):41-54. PubMed PMID: 19837059. Pubmed Central PMCID: 2783916.
44. Spector NL, Blackwell KL. Understanding the mechanisms behind trastuzumab therapy for human epidermal growth factor receptor 2-positive breast cancer. Journal of clinical oncology : official journal of the American Society of Clinical Oncology. 2009 Dec 1;27(34):5838-47. PubMed PMID: 19884552.
45. Cho HS, Mason K, Ramyar KX, Stanley AM, Gabelli SB, Denney DW, Jr., et al. Structure of the extracellular region of HER2 alone and in complex with the Herceptin Fab. Nature. 2003 Feb 13;421(6924):756-60. PubMed PMID: 12610629.
46. Moore GL, Chen H, Karki S, Lazar GA. Engineered Fc variant antibodies with enhanced ability to recruit complement and mediate effector functions. mAbs. 2010 Mar-Apr;2(2):181-9. PubMed PMID: 20150767. Pubmed Central PMCID: 2840237.
47. Neve RM, Holbro T, Hynes NE. Distinct roles for phosphoinositide 3-kinase, mitogen-activated protein kinase and p38 MAPK in mediating cell cycle progression of breast cancer cells. Oncogene. 2002 Jul 4;21(29):4567-76. PubMed PMID: 12085235.
48. Xia W, Chen JS, Zhou X, Sun PR, Lee DF, Liao Y, et al. Phosphorylation/cytoplasmic localization of p21Cip1/WAF1 is associated with HER2/neu overexpression and provides a novel combination predictor for poor prognosis in breast cancer patients. Clinical cancer research : an official journal of the American Association for Cancer Research. 2004 Jun 1;10(11):3815-24. PubMed PMID: 15173090.
49. Yakes FM, Chinratanalab W, Ritter CA, King W, Seelig S, Arteaga CL. Herceptin-induced inhibition of phosphatidylinositol-3 kinase and Akt Is required for antibody-mediated effects on p27, cyclin D1, and antitumor action. Cancer research. 2002 Jul 15;62(14):4132-41. PubMed PMID: 12124352.
50. Asanuma H, Torigoe T, Kamiguchi K, Hirohashi Y, Ohmura T, Hirata K, et al. Survivin expression is regulated by coexpression of human epidermal growth factor receptor 2 and epidermal growth factor receptor via phosphatidylinositol 3-kinase/AKT signaling pathway in breast cancer cells. Cancer research. 2005 Dec 1;65(23):11018-25. PubMed PMID: 16322251.
51. Sabbatini P, McCormick F. Phosphoinositide 3-OH kinase (PI3K) and PKB/Akt delay the onset of p53-mediated, transcriptionally dependent apoptosis. The Journal of biological chemistry. 1999 Aug 20;274(34):24263-9. PubMed PMID: 10446202.
52. Le XF, Claret FX, Lammayot A, Tian L, Deshpande D, LaPushin R, et al. The role of cyclin-dependent kinase inhibitor p27Kip1 in anti-HER2 antibody-

induced G1 cell cycle arrest and tumor growth inhibition. The Journal of biological chemistry. 2003 Jun 27;278(26):23441-50. PubMed PMID: 12700233.
53. Le XF, Pruefer F, Bast RC, Jr. HER2-targeting antibodies modulate the cyclin-dependent kinase inhibitor p27Kip1 via multiple signaling pathways. Cell cycle. 2005 Jan;4(1):87-95. PubMed PMID: 15611642.
54. Lane HA, Motoyama AB, Beuvink I, Hynes NE. Modulation of p27/Cdk2 complex formation through 4D5-mediated inhibition of HER2 receptor signaling. Annals of oncology : official journal of the European Society for Medical Oncology / ESMO. 2001;12 Suppl 1:S21-2. PubMed PMID: 11521716.
55. Xia W, Liu LH, Ho P, Spector NL. Truncated ErbB2 receptor (p95ErbB2) is regulated by heregulin through heterodimer formation with ErbB3 yet remains sensitive to the dual EGFR/ErbB2 kinase inhibitor GW572016. Oncogene. 2004 Jan 22;23(3):646-53. PubMed PMID: 14737100.
56. Molina MA, Codony-Servat J, Albanell J, Rojo F, Arribas J, Baselga J. Trastuzumab (herceptin), a humanized anti-Her2 receptor monoclonal antibody, inhibits basal and activated Her2 ectodomain cleavage in breast cancer cells. Cancer research. 2001 Jun 15;61(12):4744-9. PubMed PMID: 11406546.
57. Izumi Y, Xu L, di Tomaso E, Fukumura D, Jain RK. Tumour biology: herceptin acts as an anti-angiogenic cocktail. Nature. 2002 Mar 21;416(6878):279-80. PubMed PMID: 11907566.
58. Pietras RJ, Fendly BM, Chazin VR, Pegram MD, Howell SB, Slamon DJ. Antibody to HER-2/neu receptor blocks DNA repair after cisplatin in human breast and ovarian cancer cells. Oncogene. 1994 Jul;9(7):1829-38. PubMed PMID: 7911565.
59. Pietras RJ, Pegram MD, Finn RS, Maneval DA, Slamon DJ. Remission of human breast cancer xenografts on therapy with humanized monoclonal antibody to HER-2 receptor and DNA-reactive drugs. Oncogene. 1998 Oct 29;17(17):2235-49. PubMed PMID: 9811454.
60. Le XF, Lammayot A, Gold D, Lu Y, Mao W, Chang T, et al. Genes affecting the cell cycle, growth, maintenance, and drug sensitivity are preferentially regulated by anti-HER2 antibody through phosphatidylinositol 3-kinase-AKT signaling. The Journal of biological chemistry. 2005 Jan 21;280(3):2092-104. PubMed PMID: 15504738.
61. Pietras RJ, Poen JC, Gallardo D, Wongvipat PN, Lee HJ, Slamon DJ. Monoclonal antibody to HER-2/neureceptor modulates repair of radiation-induced DNA damage and enhances radiosensitivity of human breast cancer cells overexpressing this oncogene. Cancer research. 1999 Mar 15;59(6):1347-55. PubMed PMID: 10096569.
62. Acharya S, Sahoo SK. PLGA nanoparticles containing various anticancer agents and tumour delivery by EPR effect. Advanced drug delivery reviews. 2011 Mar 18;63(3):170-83. PubMed PMID: 20965219.
63. Mattheolabakis G, Rigas B, Constantinides PP. Nanodelivery strategies in cancer chemotherapy: biological rationale and pharmaceutical perspectives. Nanomedicine. 2012 Oct;7(10):1577-90. PubMed PMID: 23148540.
64. Dinarvand R, Sepehri N, Manoochehri S, Rouhani H, Atyabi F. Polylactide-co-glycolide nanoparticles for controlled delivery of anticancer agents. International

journal of nanomedicine. 2011;6:877-95. PubMed PMID: 21720501. Pubmed Central PMCID: 3124394.
65. Mundargi RC, Babu VR, Rangaswamy V, Patel P, Aminabhavi TM. Nano/micro technologies for delivering macromolecular therapeutics using poly(D,L-lactide-co-glycolide) and its derivatives. Journal of controlled release : official journal of the Controlled Release Society. 2008 Feb 11;125(3):193-209. PubMed PMID: 18083265.
66. Kocbek P, Obermajer N, Cegnar M, Kos J, Kristl J. Targeting cancer cells using PLGA nanoparticles surface modified with monoclonal antibody. Journal of controlled release : official journal of the Controlled Release Society. 2007 Jul 16;120(1-2):18-26. PubMed PMID: 17509712.
67. Faraji AH, Wipf P. Nanoparticles in cellular drug delivery. Bioorganic & medicinal chemistry. 2009 Apr 15;17(8):2950-62. PubMed PMID: 19299149.
68. Makadia HK, Siegel SJ. Poly Lactic-co-Glycolic Acid (PLGA) as Biodegradable Controlled Drug Delivery Carrier. Polymers. 2011 Sep 1;3(3):1377-97. PubMed PMID: 22577513. Pubmed Central PMCID: 3347861.
69. Wang JJ, Zeng ZW, Xiao RZ, Xie T, Zhou GL, Zhan XR, et al. Recent advances of chitosan nanoparticles as drug carriers. International journal of nanomedicine. 2011;6:765-74. PubMed PMID: 21589644. Pubmed Central PMCID: 3090273.
70. Grabnar PA, Kristl J. The manufacturing techniques of drug-loaded polymeric nanoparticles from preformed polymers. Journal of microencapsulation. 2011;28(4):323-35. PubMed PMID: 21545323.
71. Zhao P, Astruc D. Docetaxel nanotechnology in anticancer therapy. ChemMedChem. 2012 Jun;7(6):952-72. PubMed PMID: 22517723.
72. Takimoto C, Beeram M. Microtubule Stabilizing Agents in Clinical Oncology. In: Fojo T, editor. The Role of Microtubules in Cell Biology, Neurobiology, and Oncology. Cancer Drug Discovery and Development: Humana Press; 2008. p. 395-419.
73. Youm I, Yang XY, Murowchick JB, Youan BB. Encapsulation of docetaxel in oily core polyester nanocapsules intended for breast cancer therapy. Nanoscale research letters. 2011;6(1):630. PubMed PMID: 22168815. Pubmed Central PMCID: 3292599.
74. Fox BA, Schendel DJ, Butterfield LH, Aamdal S, Allison JP, Ascierto PA, et al. Defining the critical hurdles in cancer immunotherapy. Journal of translational medicine. 2011;9(1):214. PubMed PMID: 22168571. Pubmed Central PMCID: 3338100.
75. Fumoleau P, Seidman AD, Trudeau ME, Chevallier B, Ten Bokkel Huinink WW. Docetaxel: a new active agent in the therapy of metastatic breast cancer. Expert opinion on investigational drugs. 1997 Dec;6(12):1853-65. PubMed PMID: 15989586.
76. Byrne JD, Betancourt T, Brannon-Peppas L. Active targeting schemes for nanoparticle systems in cancer therapeutics. Advanced drug delivery reviews. 2008 Dec 14;60(15):1615-26. PubMed PMID: 18840489.
77. Lu JM, Wang X, Marin-Muller C, Wang H, Lin PH, Yao Q, et al. Current advances in research and clinical applications of PLGA-based nanotechnology.

Expert review of molecular diagnostics. 2009 May;9(4):325-41. PubMed PMID: 19435455. Pubmed Central PMCID: 2701163.
78. Liu Y, Li K, Liu B, Feng SS. A strategy for precision engineering of nanoparticles of biodegradable copolymers for quantitative control of targeted drug delivery. Biomaterials. 2010 Dec;31(35):9145-55. PubMed PMID: 20864169.
79. Nobs L, Buchegger F, Gurny R, Allemann E. Current methods for attaching targeting ligands to liposomes and nanoparticles. Journal of pharmaceutical sciences. 2004 Aug;93(8):1980-92. PubMed PMID: 15236448.
80. Lutsiak ME, Robinson DR, Coester C, Kwon GS, Samuel J. Analysis of poly(D,L-lactic-co-glycolic acid) nanosphere uptake by human dendritic cells and macrophages in vitro. Pharmaceutical research. 2002 Oct;19(10):1480-7. PubMed PMID: 12425465.
81. Han R, Zhu J, Yang X, Xu H. Surface modification of poly(D,L-lactic-co-glycolic acid) nanoparticles with protamine enhanced cross-presentation of encapsulated ovalbumin by bone marrow-derived dendritic cells. Journal of biomedical materials research Part A. 2011 Jan;96(1):142-9. PubMed PMID: 21105162.
82. Elamanchili P, Diwan M, Cao M, Samuel J. Characterization of poly(D,L-lactic-co-glycolic acid) based nanoparticulate system for enhanced delivery of antigens to dendritic cells. Vaccine. 2004 Jun 23;22(19):2406-12. PubMed PMID: 15193402.
83. Wuang SC, Neoh KG, Kang ET, Pack DW, Leckband DE. HER-2-mediated endocytosis of magnetic nanospheres and the implications in cell targeting and particle magnetization. Biomaterials. 2008 May;29(14):2270-9. PubMed PMID: 18289668. Pubmed Central PMCID: 2312094.
84. Zou W, Liu C, Chen Z, Zhang N. Studies on bioadhesive PLGA nanoparticles: A promising gene delivery system for efficient gene therapy to lung cancer. International journal of pharmaceutics. 2009 Mar 31;370(1-2):187-95. PubMed PMID: 19073241.
85. Bandyopadhyay A, Fine RL, Demento S, Bockenstedt LK, Fahmy TM. The impact of nanoparticle ligand density on dendritic-cell targeted vaccines. Biomaterials. 2011 Apr;32(11):3094-105. PubMed PMID: 21262534.
86. Rafiei P, Michel, D. and Haddadi, A. Application of a Rapid ESI-MS/MS Method for Quantitative Analysis of Docetaxel in Polymeric Matrices of PLGA and PLGA-PEG Nanoparticles through Direct Injection to Mass Spectrometer. American Journal of Analytical Chemistry. 2015;6(2):164-75.
87. Pabari RM, Ryan B, Ahmad W, Ramtoola Z. Physical and structural stability of the monoclonal antibody, trastuzumab (Herceptin(R)), intravenous solutions. Current pharmaceutical biotechnology. 2013;14(2):220-5. PubMed PMID: 23360264.
88. Pabari RM, Ryan B, McCarthy C, Ramtoola Z. Effect of microencapsulation shear stress on the structural integrity and biological activity of a model monoclonal antibody, trastuzumab. Pharmaceutics. 2011;3(3):510-24. PubMed PMID: 24310594. Pubmed Central PMCID: 3857080.
89. Steinhauser I, Spankuch B, Strebhardt K, Langer K. Trastuzumab-modified nanoparticles: optimisation of preparation and uptake in cancer cells. Biomaterials. 2006 Oct;27(28):4975-83. PubMed PMID: 16757022.

90. Yu ZG, Wang Q, Li K, Li YQ, Gao XX. Determination and pharmacokinetics of 6,7-dimethoxycoumarin in rat plasma after intragastric administration of different decoctions of yinchenhao tang. Journal of chromatographic science. 2007 Sep;45(8):544-8. PubMed PMID: 18019567.
91. Ghotbi Z, Haddadi A, Hamdy S, Hung RW, Samuel J, Lavasanifar A. Active targeting of dendritic cells with mannan-decorated PLGA nanoparticles. Journal of drug targeting. 2011 May;19(4):281-92. PubMed PMID: 20590403.
92. Miyano T, Wijagkanalan W, Kawakami S, Yamashita F, Hashida M. Anionic amino acid dendrimer-trastuzumab conjugates for specific internalization in HER2-positive cancer cells. Molecular pharmaceutics. 2010 Aug 2;7(4):1318-27. PubMed PMID: 20527783.
93. Brown GD, Nazarali AJ. Matrix metalloproteinase-25 has a functional role in mouse secondary palate development and is a downstream target of TGF-beta3. BMC developmental biology. 2010;10:93. PubMed PMID: 20809987. Pubmed Central PMCID: 2944159.
94. Smith TM, Wang X, Zhang W, Kulyk W, Nazarali AJ. Hoxa2 plays a direct role in murine palate development. Developmental dynamics : an official publication of the American Association of Anatomists. 2009 Sep;238(9):2364-73. PubMed PMID: 19653318.
95. Sampath M, Lakra R, Korrapati P, Sengottuvelan B. Curcumin loaded poly (lactic-co-glycolic) acid nanofiber for the treatment of carcinoma. Colloids and surfaces B, Biointerfaces. 2014 May 1;117:128-34. PubMed PMID: 24646452.
96. Kountz SL. The effect of bioscience and technological momentum on the surgical treatment of chronic illness. Surgery. 1975 Jun;77(6):735-40. PubMed PMID: 1145439.
97. Conner SD, Schmid SL. Regulated portals of entry into the cell. Nature. 2003 Mar 6;422(6927):37-44. PubMed PMID: 12621426.
98. Zhao F, Zhao Y, Liu Y, Chang X, Chen C, Zhao Y. Cellular uptake, intracellular trafficking, and cytotoxicity of nanomaterials. Small. 2011 May 23;7(10):1322-37. PubMed PMID: 21520409.
99. Wang J, Byrne JD, Napier ME, DeSimone JM. More effective nanomedicines through particle design. Small. 2011 Jul 18;7(14):1919-31. PubMed PMID: 21695781. Pubmed Central PMCID: 3136586.
100. Vicari L, Musumeci T, Giannone I, Adamo L, Conticello C, De Maria R, et al. Paclitaxel loading in PLGA nanospheres affected the in vitro drug cell accumulation and antiproliferative activity. BMC cancer. 2008;8:212. PubMed PMID: 18657273. Pubmed Central PMCID: 2519087.
101. Layre AM, Gref R, Richard J, Requier D, Chacun H, Appel M, et al. Nanoencapsulation of a crystalline drug. International journal of pharmaceutics. 2005 Jul 25;298(2):323-7. PubMed PMID: 15899561.
102. Shi W, Zhang ZJ, Yuan Y, Xing EM, Qin Y, Peng ZJ, et al. Optimization of parameters for preparation of docetaxel-loaded PLGA nanoparticles by nanoprecipitation method. Journal of Huazhong University of Science and Technology Medical sciences = Hua zhong ke ji da xue xue bao Yi xue Ying De wen ban = Huazhong keji daxue xuebao Yixue Yingdewen ban. 2013 Oct;33(5):754-8. PubMed PMID: 24142732.

103. Kakran M, Sahoo NG, Antipina MN, Li L. Modified supercritical antisolvent method with enhanced mass transfer to fabricate drug nanoparticles. Materials science & engineering C, Materials for biological applications. 2013 Jul 1;33(5):2864-70. PubMed PMID: 23623107.
104. Keum CG, Noh YW, Baek JS, Lim JH, Hwang CJ, Na YG, et al. Practical preparation procedures for docetaxel-loaded nanoparticles using polylactic acid-co-glycolic acid. International journal of nanomedicine. 2011;6:2225-34. PubMed PMID: 22114486. Pubmed Central PMCID: 3215163.
105. Song X, Zhao Y, Hou S, Xu F, Zhao R, He J, et al. Dual agents loaded PLGA nanoparticles: systematic study of particle size and drug entrapment efficiency. European journal of pharmaceutics and biopharmaceutics : official journal of Arbeitsgemeinschaft fur Pharmazeutische Verfahrenstechnik eV. 2008 Jun;69(2):445-53. PubMed PMID: 18374554.
106. Lamprecht A, Ubrich N, Hombreiro Perez M, Lehr C, Hoffman M, Maincent P. Influences of process parameters on nanoparticle preparation performed by a double emulsion pressure homogenization technique. International journal of pharmaceutics. 2000 Mar 10;196(2):177-82. PubMed PMID: 10699713.
107. Feng L, Wu H, Ma P, Mumper RJ, Benhabbour SR. Development and optimization of oil-filled lipid nanoparticles containing docetaxel conjugates designed to control the drug release rate in vitro and in vivo. International journal of nanomedicine. 2011;6:2545-56. PubMed PMID: 22072889. Pubmed Central PMCID: 3205148.
108. Mei L, Sun H, Jin X, Zhu D, Sun R, Zhang M, et al. Modified paclitaxel-loaded nanoparticles for inhibition of hyperplasia in a rabbit arterial balloon injury model. Pharmaceutical research. 2007 May;24(5):955-62. PubMed PMID: 17372684.
109. Bhardwaj V, Ankola DD, Gupta SC, Schneider M, Lehr CM, Kumar MN. PLGA nanoparticles stabilized with cationic surfactant: safety studies and application in oral delivery of paclitaxel to treat chemical-induced breast cancer in rat. Pharmaceutical research. 2009 Nov;26(11):2495-503. PubMed PMID: 19756974.
110. Bazley LA, Gullick WJ. The epidermal growth factor receptor family. Endocrine-related cancer. 2005 Jul;12 Suppl 1:S17-27. PubMed PMID: 16113093.
111. Wong RS. Apoptosis in cancer: from pathogenesis to treatment. Journal of experimental & clinical cancer research : CR. 2011;30:87. PubMed PMID: 21943236. Pubmed Central PMCID: 3197541.
112. Haddadi A, Elamanchili P, Lavasanifar A, Das S, Shapiro J, Samuel J. Delivery of rapamycin by PLGA nanoparticles enhances its suppressive activity on dendritic cells. Journal of biomedical materials research Part A. 2008 Mar 15;84(4):885-98. PubMed PMID: 17647224.
113. Musumeci T, Ventura CA, Giannone I, Ruozi B, Montenegro L, Pignatello R, et al. PLA/PLGA nanoparticles for sustained release of docetaxel. International journal of pharmaceutics. 2006 Nov 15;325(1-2):172-9. PubMed PMID: 16887303.
114. Hobbs SK, Monsky WL, Yuan F, Roberts WG, Griffith L, Torchilin VP, et al. Regulation of transport pathways in tumor vessels: role of tumor type and microenvironment. Proceedings of the National Academy of Sciences of the United

States of America. 1998 Apr 14;95(8):4607-12. PubMed PMID: 9539785. Pubmed Central PMCID: 22537.
115. Xiao K, Li Y, Luo J, Lee JS, Xiao W, Gonik AM, et al. The effect of surface charge on in vivo biodistribution of PEG-oligocholic acid based micellar nanoparticles. Biomaterials. 2011 May;32(13):3435-46. PubMed PMID: 21295849. Pubmed Central PMCID: 3055170.